NIST Technical Note 2076
NTIA Joint Report JR-20-549

Channel Sounder Measurement Verification: Conducted Tests

Jeanne Quimby, Jeffrey A. Jargon, Rod Leonhardt, Jacob D. Rezac, Paul D. Hale, Kate A. Remley
National Institute of Standards and Technology, Communications Technology Laboratory

Amanda Koepke, Sarah Streett
National Institute of Standards and Technology, Information Technology Laboratory

Robert T. Johnk, Chriss Hammerschmidt, Paul McKenna, Irena Stange, Mike Chang, Nicholas DeMinco
National Telecommunications and Information Administration, Institute for Telecommunication Sciences

Joseph E. Diener, Richard Chad Smith, Christopher Hoyt, Sofia Springer
Affiliates, National Institute of Standards and Technology

April 2020

NIST
National Institute of Standards and Technology
U.S. Department of Commerce

NTIA
National Telecommunications and Information Administration
U.S. Department of Commerce

Contents

Figures

Tables

Executive Summary

Channel modeling often provides a basis for the design and deployment of wireless technology. Engineers design systems to operate under certain expected channel conditions. Channel models are typically based on the statistics of a collection of many measurements performed by channel sounders in nominally similar radio-propagation environments. Channel sounders measure characteristics of a radio propagation channel such as path gain, decay time, and angular dispersion, among other channel model metrics. The models developed from these measurements are typically the first step in standardizing a new wireless technology. While many such models currently exist, wireless technology for new use cases is constantly under development, necessitating continued development of new and improved channel models. For example, in the 3550 MHz to 3650 MHz ("3.5 GHz") band, rules for spectrum sharing and systems for implementing those rules are being developed based on specific channel models. Success of the spectrum sharing systems will, in part, depend on the accuracy of those models. As another example, new wireless systems will operate in the millimeter-wave bands; developing new channel models will be of paramount importance due to the significantly different impact of the propagation phenomena at these higher frequencies. At both microwave and millimeter-wave frequencies, separating measurement uncertainty from channel variations provides rigor for channel-model development and validation. Such measurement uncertainties can be caused by systematic hardware nonidealities, system noise, and the repeatability and reproducibility of the measurements, as well as user error.

In 2016, researchers at the US Department of Commerce National Institute of Standards and Technology (NIST) and the National Telecommunications and Information Administration Institute for Telecommunication Sciences (ITS) began a collaboration to conduct a series of channel sounder verifications to identify sources of uncertainty due to systematic and random effects in channel sounder hardware. Channel sounders operating in the 3.5 GHz frequency band, but having three significantly different architectures, were studied.

For the VNA measurements, propagation of the uncertainties to the channel sounder metric of interest was possible using NIST's Microwave Uncertainty Framework software. A key feature of our approach was to shift the VNA reference plane to align directly to the individual channel sounder's reference plane to allow for comparisons of the channel sounder's performance with the VNA performance. The random components of uncertainty of the channel sounding systems were also studied over various timescales of relevance to channel measurements, including repeated measurements conducted between rapid succession and a hour-scale timeframe, and measurements reproduced over several days.

The work reported here consisted of conducted-channel measurements designed to focus on errors within the channel sounding hardware, as opposed to antenna and channel variations, as a baseline test of the channel sounder's performance. Here, two simulated propagation channels were studied. The first propagation channel consisted of a length of cable and an attenuator to simulate a pure line-of-sight channel. The second added a pair of coaxial power splitters joined by coaxial cables of different lengths to simulate a multipath environment. Repeat measurements and an analysis of the random components of uncertainty were performed. For path gain, all three channel sounders agreed with the VNA measurements to within 0.6 dB.

The work concludes with guidance and best-practice procedures with the intent of allowing users to perform similar verifications of their channel sounders. The mention of brand names does not imply an endorsement by NIST or NTIA. Other products may work as well or better.

List of Acronyms and Definitions

Acronyms	Definitions
$\boldsymbol{\sigma_D^2}$	Component of variance due to day
$\boldsymbol{\sigma^2}$	Component of variance due to error
ANOVA	Analysis of variance
AWG	Arbitrary waveform generator
BPF	Band-pass filter
BPSK	Binary phase shift keying
CS	Channel sounder
CTL	Communications Technology Laboratory
CW	Continuous wave
DUT	Device under test
DPDT	Double-pole, double-throw transfer switch
ITS	Institute for Telecommunication Sciences
LO	Local oscillator
LRM	Line-reflect-match calibration method
MSD	Mean-squared error associated with SSD
MSE	Mean-squared error associated with SSE
MUF	Microwave uncertainty framework
NIST	National Institute of Standards and Technology
OATS	Open area test site
OSLT	Open-short-load-thru calibration method
PA	Power amplifier
PDP	Power delay profile
PN-sequence	Pseudo-Noise sequence
PPS	Pulse per second
RAID	Redundant array of independent discs
RH	Relative humidity
RSS	Root-sum-of-squares
RTO	Real-time oscilloscope
RX	Receiver
S-parameters	Scattering parameters
SP4T	Single-pole, four-throw switch
SPDT	Single-pole, double-throw switch
SSD	Sums of squares between days
SSE	Sums of squares due to error within a day
TCXO	Temperature compensated crystal oscillator
TRL	Multiline thru-reflection-line calibration method
TX	Transmitter
VSA	Vector signal analyzer
VST	Vector signal transceiver

1 Introduction

A revolution in emerging wireless technologies has placed a major demand on our limited radio spectrum. This has made it paramount for new wireless systems to have high spectral efficiency [1]–[4] and to be able to dynamically share spectrum with other wireless systems. As well, there is a need to provide our spectrum policy makers and regulators with well-informed and accurate propagation-channel models to insure optimal and trouble-free use of the radio spectrum. A key component of accurate channel modeling and wireless-device performance prediction is accurate propagation measurement data obtained with channel sounders.

Channel sounders may be placed on a sound metrological foundation by use of well-established laboratory verification methods coupled with modern waveform metrology tools [5]–[7]. Much of the prior work on channel sounder performance verification compares channel model metrics to simulated or computational models such as map-based or ray-tracing models. Assumptions about the reflective characteristics of the environment and the antenna characteristics of the channel sounder may increase uncertainty in the estimate of the channel sounder's performance.

To provide channel sounder hardware verification, we have developed a program of propagation measurements, modeling, and computations. Taking an incremental approach, we have started with measurements of deterministic conducted channels, and plan to progress with a program of increasing complexity to open area test site (OATS) channels. This will allow us to first identify the intrinsic sources of error and determine the variability due to random effects in the channel measurement equipment and to verify simple (short-range) channel models. When we move to more complicated and stochastic channels, we will be able to separate channel variations from equipment-caused variability, giving a rigorous basis for channel-model development and validation. Throughout, guidance and best-practice procedures will be provided with the intent of allowing users to perform similar comparisons and/or verifications of their channel sounders.

The series of verifications reported here is based on controlled, conducted-channel measurements to establish the channel sounders' performance and isolate hardware effects. We used both a single cable in series with an attenuator to simulate a pure line-of-sight channel and power splitters joined to cables of different lengths to simulate a multipath environment. This gives two stable and repeatable environments in which to compare channel sounder hardware performance to a reference measurement provided by a vector network analyzer (VNA).

Repeat measurements and uncertainty analyses were performed for each channel sounder: the Correlation-Based channel sounder, Direct-Pulse channel sounder, and Scanning-Probe channel sounder. The reference VNA measurement has an uncertainty analysis which includes components due to both systematic and random effects to provide a reference to which the channel sounder performances could be compared.

The uncertainty due to random effects for the channel sounder measurements was estimated using a random effects model. We provide an investigation of the channel sounder path gain measurements to ensure that they are independent and identically distributed, as assumed under the random effects model. Here, identically distributed means that our measurement system is stable and that all repeat measurements are measuring the same quantity (path gain of the channel sounder under the same conditions) with some variability. This variability had different time scales from an hour-scale timeframe to several days.

We focused on the identification of hardware non-idealities of three types of channel sounding systems using path gain and/or power delay profile (PDP) [8] as the metric. Path gain is a measure of attenuation an electromagnetic field can experience as it propagates through space. PDP is a derived from the

measurement of the channel's complex impulse response. In this report, we have slightly modified this definition to include propagation through a conducted cable. Throughout the course of this report, path gain refers to the attenuation experienced by the electromagnetic field as it propagates through a conducted cable.

We compared measurements of a stable and repeatable conducted channel made by the channel sounders to measurements of the same channel made with the VNA. That is, the verification of a channel sounder occurs against the VNA and never against another channel sounder. The VNA measurements of the channels were post-processed to shift the measurement reference plane to the specific channel sounder's reference plane, allowing for direct comparison of measurements of the same physical channel. Also, the frequency range of the VNA was adjusted to match the frequency range of the specific channel sounder for accurate comparison of path gain. The three channel sounders and the reference VNA all had different architectures, providing a broad range of topologies to illustrate the channel sounder verification methodology.

The ability to verify measurements from multiple channel sounders can give insight into the error sources in each of the sounders giving a more robust validation of each. The different sounders also provide several different "views" of the same channel, ultimately providing a more in-depth understanding of the channel's characteristics, which enables the development of more robust channel models.

In Section 2, we provide an overview of the test set-up used for the channel sounder/VNA comparisons. The measurement location on the Boulder Labs site is described and the configuration of the hardware, including the channel sounders and simulated channels, is presented.

Section 3 contains the descriptions of the reference VNA and channel sounders:

- Reference NIST VNA (Section 3.1)
- NIST Correlation-Based Channel Sounder (Section 3.2)
- ITS Scanning-Probe Channel Sounder (Section 3.3)
- NIST Direct-Pulse Channel Sounder (Section 3.4)

In Section 4, we provide a description of the random and systematic measurement errors prevalent in channel sounder hardware, and we define the random effects model. This model is used to describe the channel sounder's random components of uncertainty. While only the VNA has a complete uncertainty analysis, in this study, we characterized the channel sounders' random uncertainties associated with repeatability, reproducibility, and drift.

Section 5 presents our measured channel sounders' result including the random components of uncertainty with comparison to the VNA's results. Both our pre-characterization tests and the results of the measurements are described, and representative data are shown. We provide sufficient detail so that these tests can be reproduced. Such detail is helpful when considering best practices for future channel sounder comparison activities, wherever they may be performed. Path gain was either computed from a very narrow band of frequencies, as was done for the Institute for Telecommunication Sciences (ITS) Scanning-Probe channel sounder data or by taking an average across a range of frequencies as was done for the Correlation-Based and Direct-Pulse channel sounder data. The frequency ranges of the channel sounders are provided in Section 5.

Section 6 presents best practices to channel sounder comparisons such as those discussed here. In Section 7, we discuss future plans for the comparisons. Several Appendices follow with detailed information on the measurements and the complete summary of data.

2 Description of the Conducted-Channel Measurement Campaign

2.1 Channel Sounder Verification Methodology

This report provides verification of three distinct channel sounder architectures:

- NIST Correlation-Based channel sounder and Reference VNA (Section 5.1.3)
- ITS Scanning-Probe channel sounder and Reference VNA (Section 5.2.3)
- NIST Direct-Pulse channel sounder and Reference VNA (Section 5.3.4)

The verification consists of quantitative assessments of the differences between measurements of path gain and/or power delay profile for the various channel sounders as compared individually to the reference VNA. Specifically, the path gain or power delay profile measured by a single channel sounder is compared to the reference VNA measurements. The VNA's frequency range is changed to be identical to the individual channel sounder's frequency range. The VNA's reference plane is shifted to the channel sounder's reference plane during the post-processing of the measurement data. These re-alignments of the VNA measurement data enable informative comparisons of the individual channel sounder measurements of the channel. This re-alignment removes the effects of the adapters, switches, and cabling.

2.2 Laboratory Set-up and Fixtures for the Channel Sounder Verification

2.2.1 Description of Test Set-up for Conducted Tests

The Correlation-Based, Scanning-Probe, and Direct-Pulse channel sounders and VNA were co-located where they could easily access the hardware used to simulate the conducted channels. The room layout for the tests appears in Fig. 2-1. It consists of tables in a T shape with the channel sounders locations. A key set-up feature was the two switch matrices to sequentially connect the channel sounders to the channel. These switches removed the need for connecting or disconnecting the coaxial cables eliminating the connection repeatability as a source of measurement uncertainty and allowing the channel measurement within a short timeframe under nearly identical conditions.

Each sounder was switched sequentially between the same channel input and channel output ports, as shown in the schematic of the set-up in Fig. 2-2. The direct-path-only channel used a coaxial cable and attenuators to simulate free space propagation environment. The direct-and-bounce-path channel used two cables and coaxial power splitters to simulate a ground bounce propagation environment. Note the additional attenuators placed in both the direct-path-only (i.e. free space propagation) and direct-and-bounce-path (ground bounce propagation) channels. These attenuators provide a variable-attenuation channel and protect the input of the receivers from accidental high-power connections.

The channel sounders were configured so that each transmitter provided approximately 0 dBm or +30 dBm at the reference plane labeled as P*, depending on the measurement. The VNA output power was either -5 dBm or 0 dBm depending on the experiment. Due to the potential for high conducted power being directed in an unknown direction, great care was used to protect equipment and personnel. An initial investigation of all hardware equipment and its damage limits or potential for reduction of power was carried out. Safety guidelines were implemented when it was determined that the transmitter (TX) switch matrix could lead to damage of the transmit channel sounders. Potential damage to the hardware could occur if the TX switch matrix was switched to a new channel sounder while the previous channel sounder's power amplifier was operating. Therefore, the power amplifiers were always placed in stand-by prior to switching to a new channel sounder. Note that the power amplifiers (PAs) and band-pass filters (BPFs, if used) were considered part of the channel sounder system and therefore appear behind the Instrument Reference Plane.

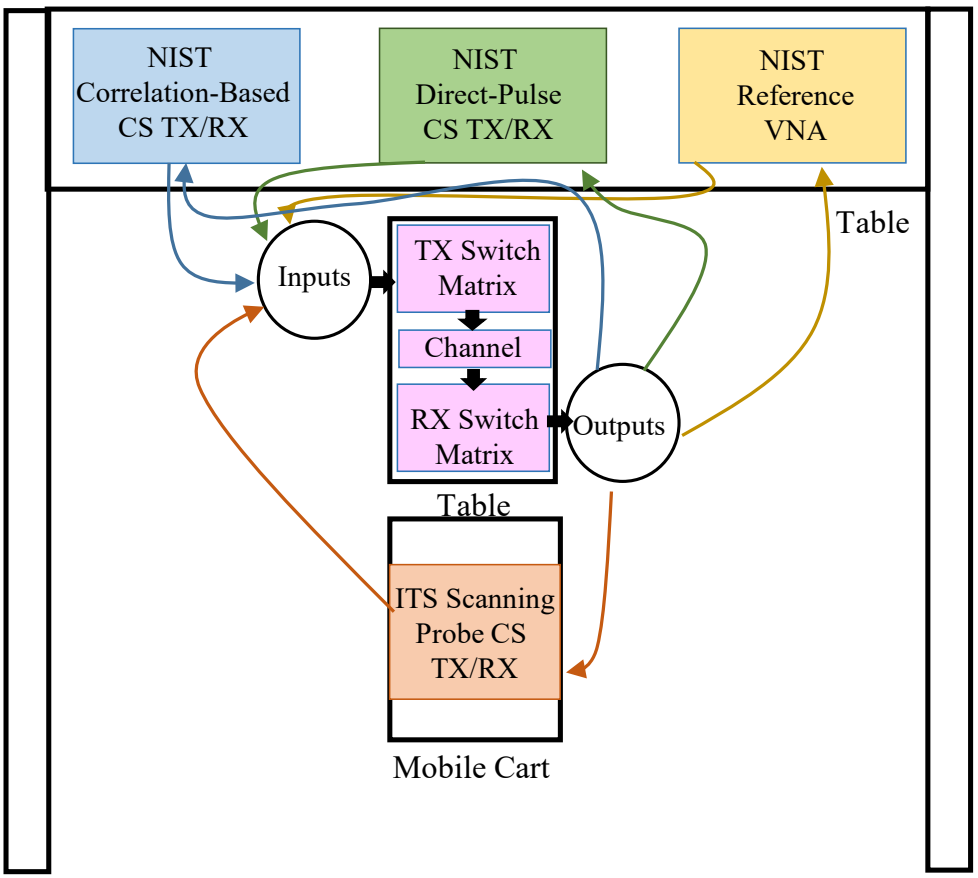

Fig. 2-1: Room configuration for conducted channel tests.

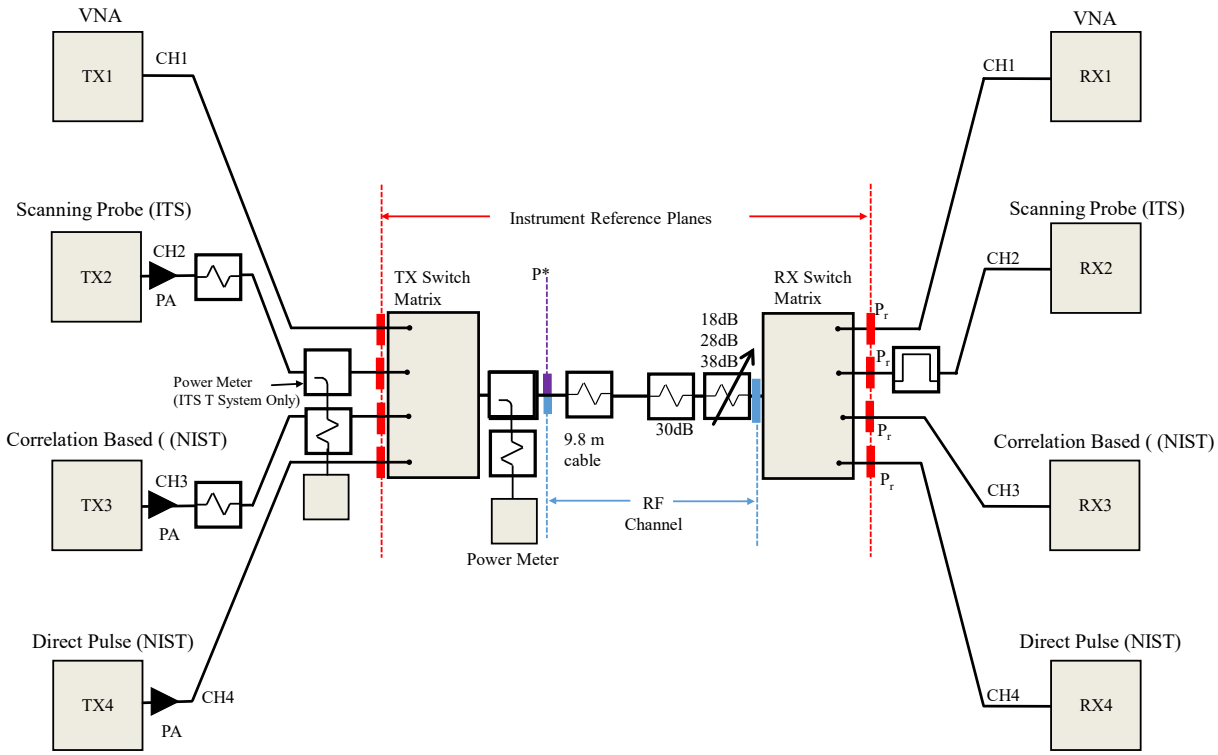

(a)

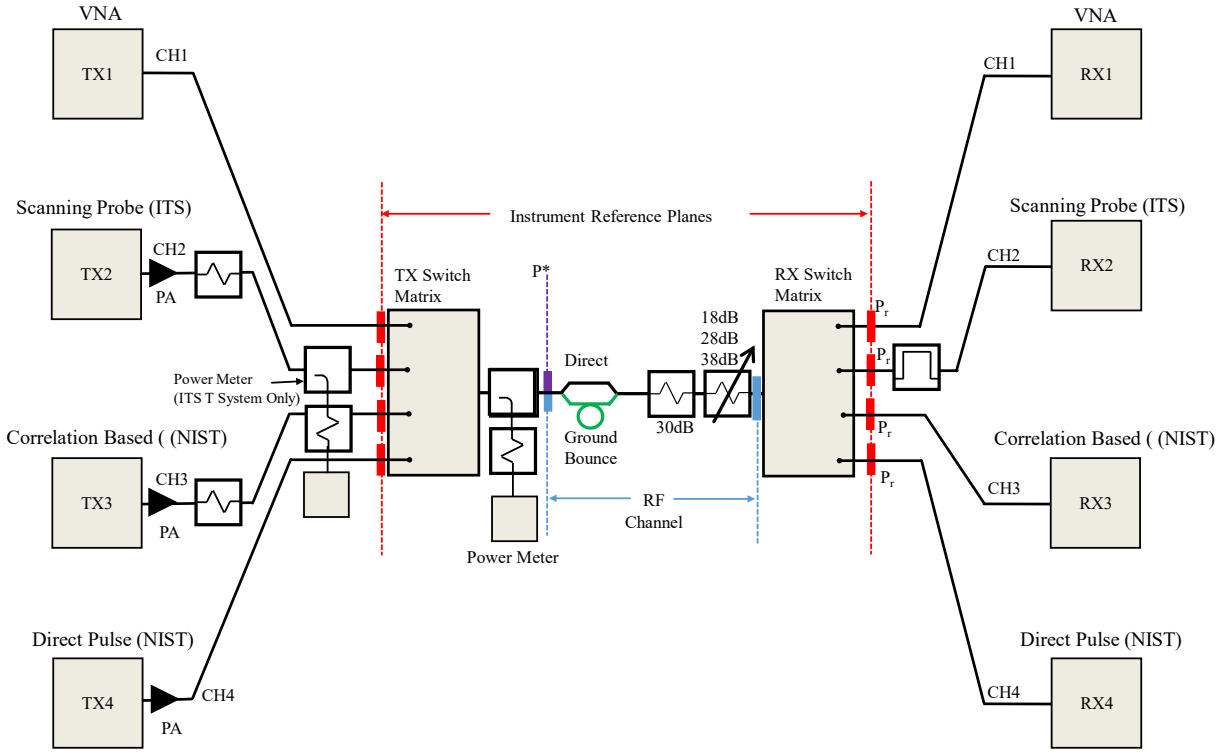

(b)

Fig. 2-2: Schematic diagram of the comparison set-up for (a) the direct-path-only channel and (b) direct-and-bounce-path channel. See Section 2.3 for further details.

The simulated RF channel input and output ports are shown by the blue vertical lines in Fig. 2-2. The direct-path-only channel is shown in (a), and the direct-and-bounce-path channel is shown in (b). The Instrument Reference Planes shown by the red vertical lines indicate the comparison reference planes. The VNA reference plane was shifted to match the reference plane for each of the other channel sounders. The common point where each channel sounder's output power was measured is labeled P*.

2.2.2 Transmit and Receive Switch Matrices

The verification of the channel sounders requires that the simulated channel be stable and repeatable over the course of the measurement campaign. Using switches helps to establish this type of channel by eliminating issues arising from the continuous multiple connecting and disconnecting of cables to the channel sounders and VNA. In addition, we wanted to be able to measure the channel sequentially for all of the channel sounders and VNA. If a single channel sounder is verified using a VNA, a simpler switch design may be used.

The switch matrix on the transmit side of the set-up consisted of three double-pole, double-throw (DPDT) transfer switches and one single-pole, double-throw (SPDT) switch, all electronically controlled. The multiple switch set-up connected all inactive transmitters to 50 Ω loads. The switch on the receive side of the set-up consisted of one manually controlled single-pole, four-throw (SP4T) switch. Additional information is contained in Appendix B.

2.3 Description of the Stable Repeatable Conducted Channels

The conducted channels utilized attenuators and cables to form the direct-path-only and the direct-and-bounce-path channels. The choice to use attenuators came from a desire to compare measurements well within dynamic range of the channel sounder and measurements near the noise floor of some of the channel sounders.

2.3.1 Direct-path-only Channel Tests

The direct-path-only channel used a single 9.8 m coaxial cable, as shown in Fig. 2-2(a). The attenuators were a part of the channel. The settings of the three variable attenuators are given in Table 2-1.

Table 2-1: Attenuator settings for direct-path-only channel tests.
Note: attenuation due to other losses in the channel such as cable losses is not included in this table.

Channel Description Test Name	Approximate Attenuation Setting (dB)	Attenuator 1 Setting (dB)	Attenuator 2 Setting (dB)
DirectPath_1	48	30	18
DirectPath_2	58	30	28
DirectPath_3	68	30	38

2.3.2 Direct-and-bounce-path Channel Tests

The direct-and-bounce-path channel used two lengths of coaxial cables (9.8 m and 15.2 m) connected by power dividers and combiners at the input and output ports, respectively, as shown in Fig. 2-3. The different lengths of the two coaxial cables simulate the magnitude and time delay, allowing channel sounders to resolve the individual peaks corresponding to the short and longer physical paths. The settings of the variable attenuators are given in Table 2-2.

Table 2-2: Attenuator settings for direct-and-bounce-path tests.
Note: attenuation due to other losses such as cable losses in the channel is not included in this table.

Channel Description Test Name	Approximate Attenuation (dB)	Attenuator 1 Setting (dB)	Attenuator 2 Setting (dB)
DirectBouncePath_1	48	30	18
DirectBouncePath_2	58	30	28
DirectBouncePath_3	68	30	38

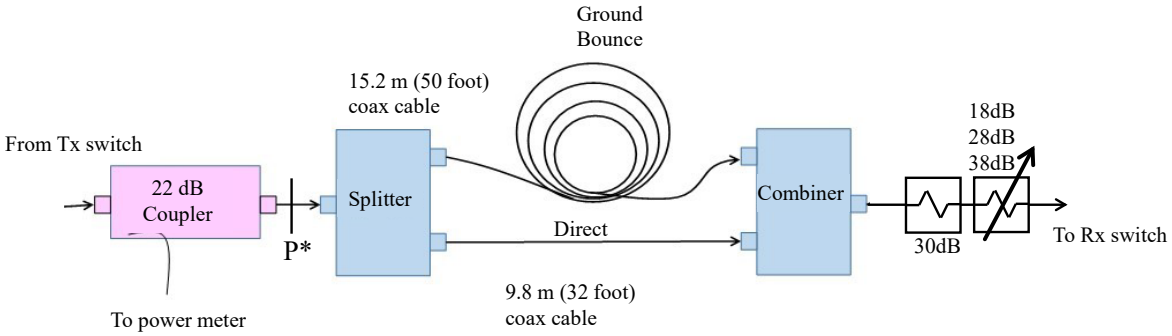

Fig. 2-3: Direct-and-bounce-path channel tests use two power splitters/combiners, a thru connection, 9.8 m coaxial cable and a 15.2 m coaxial cable to simulate a ground bounce propagation loss environment.

2.4 Laboratory Test Environment

The conducted-cables testing was carried out in a laboratory environment known as Lab 1-1207 on the NIST Boulder campus. This was a temperature stabilized lab, with the temperature values provided in Appendix C for the entire measurement campaign.

2.4.1 Ambient Environment Measurements

During the measurement campaign, we tracked different ambient environmental parameters including

- Temperature (ºC)
- Humidity (%)
- Barometer (mmHg)

The temperature drifted by up to four degrees Celsius during the direct-path measurements and up to three degrees Celsius for the direct-and-bounce-path measurements. Humidity was observed to drift over a range of 20 % to 50 % over the course of the measurements. Barometric pressure readings that showed the ambient pressure over the course of the tests are provided in Appendix C.

2.4.2 Environmental Effects

2.4.2.1 Environmental Chamber and Linear Component Tests

To support our uncertainty analyses, the effect of temperature on the 15.2 m cable was pre-characterized in the NIST environmental chamber. The temperature range was varied from 6 °C to 49 °C, where 23 °C corresponds to approximately normal room temperature. The effect of the temperature on the transmission scattering parameter S_{21} is shown in Fig. 2-4. The difference in cable loss between 6 ºC to 49 ºC at 1.5 GHz is approximately 0.06 dB and at 3.5 GHz is approximately 0.19 dB. See Appendix D for more details.

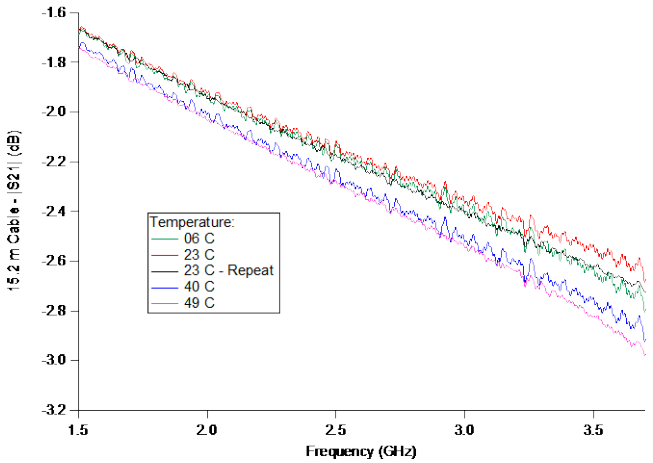

Fig. 2-4: Measurements of a 15.2 m coaxial cable for four temperatures: 6 ºC (green line), 23 ºC (red and black lines), 40 ºC (blue line), and 49 ºC (pink line).

2.4.2.2 Channel Sounder Power Draw

Using a commercially available, consumer-grade in-line power monitoring device, the wall-plug power-draw values shown in Table 2-3 were measured.

It was important to determine these values to ensure that circuit breakers were not overloaded for the experiment. From Table 2-3 information, we determined that all the channel sounders could run off a single 20 A circuit.

Table 2-3: Power draw of channel sounder systems.

Channel Sounder	Approximate Power Draw (W)	
	TX	**RX**
VNA	325	--
Scanning-Probe channel sounder	600	400
Correlation-Based channel sounder	810	230
Direct-Pulse channel sounder	450	650

2.4.3 Power Amplifier Effects

All of the channel sounders used a power amplifier. The amplifiers were measured prior to the measurement campaign. To do this, the channel sounder was connected to the power amplifier. A power sensor with a 50 dB dynamic range, protected by 50 dB of attenuation, was used to measure the output power from the amplifier. Figure 2-5 shows the results of this test for the Correlation-Based channel sounder. From this figure, it can be seen that saturation of the power amplifier approaches 1-dB compression at approximately -4 dBm input power and 42 dBm output power.

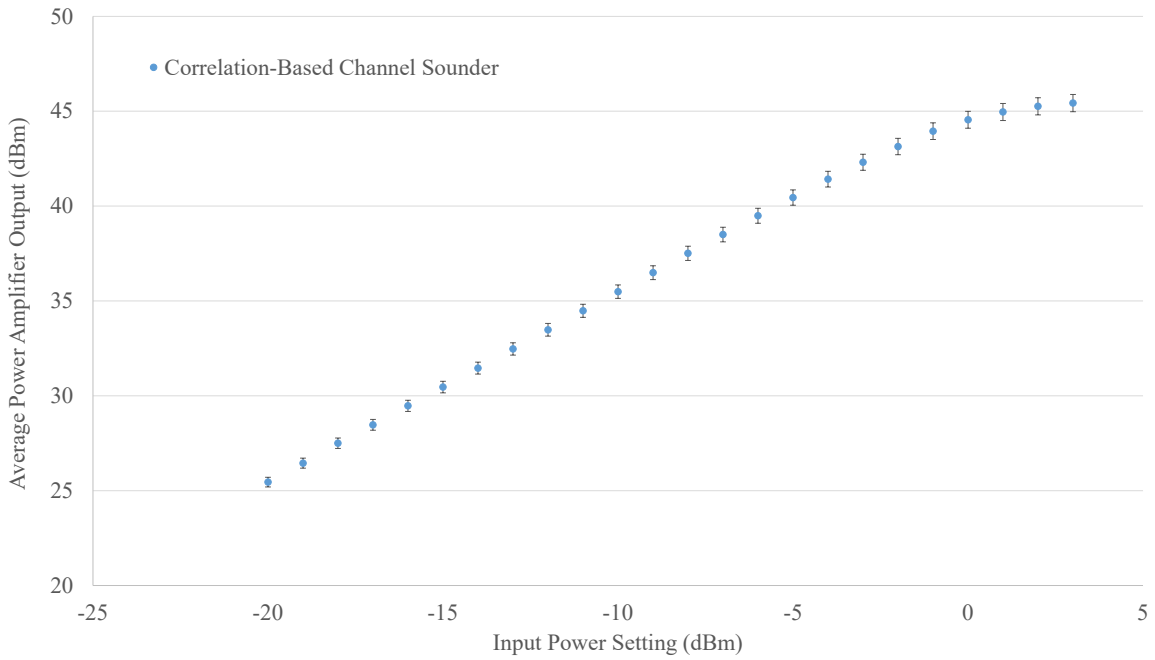

Fig. 2-5: Correlation-Based channel sounder power amplifier.

2.5 Measurement Campaign Description of Roundabouts Procedure

In order to apply the random effects model, we performed multiple measurements using a "roundabout format" over multiple days.

Prior to the start of a roundabout, the VNA was calibrated using a mechanical open-short-load-thru (OSLT) technique. While the VNA was being calibrated, the Correlation-Based channel sounder's transmitter was connected to its receiver using a previously-measured fixed attenuator and coaxial cable. This configuration is known as a back-to-back measurement. The attenuator protects the channel sounder receiver from damage during this measurement. Upon completion of the VNA calibration and back-to-back measurement of the Correlation-Based channel sounder, both systems were connected to the switch matrices. Once all the systems were connected to the switch matrix, a roundabout began.

A roundabout is a sequence of measurements of a single channel set-up for all of the channel sounders and the VNA. An example of a single channel set-up would be the Direct-Path-Only channel using attenuation of 48 dB. Fig. 2-6(a) illustrates the general concept of a roundabout. The VNA would perform one measurement of the channel set-up. Next, the Scanning-Probe channel sounder (CS) would measure 458,881 waveforms of the same channel set-up. The Correlation-Based channel sounder would be the next instrument to measure the channel set-up. It would measure 4,000 waveforms of the channel. Finally, the Direct-Pulse channel sounder would measure 8,192 waveforms of the channel set-up. We define this sequence of VNA and channel sounder measurements of a single channel set-up as a roundabout.

To provide insight into the hardware stability and uncertainties associated with random effects over both the short term and long term, we chose to do five roundabouts a day for a single channel set-up, as shown in Fig. 2-6(b). With this roundabout format, we measure a single channel set-up for five days as illustrated in Fig. 2-6(c). We needed sufficient data to quantify the uncertainty associated with the various random effects. Section 4 will provide more detailed information on this random component of uncertainty. We used this procedure for all attenuation levels for the direct-path-only and direct-and-bounce-path channel tests.

Upon completion of all roundabouts for the day, the VNA was re-calibrated to estimate any VNA system drift, and final back-to-back measurements of the Correlation-Based and Direct-Pulse channel sounders were performed. All data were copied from the instruments to the NIST server as raw data.

A description of the verification set-up and components is provided in Table 2-4. Additional details may be found in the appendices listed.

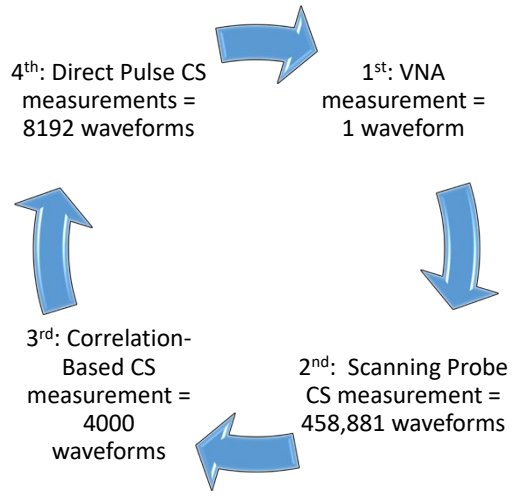

(a) Single roundabout.

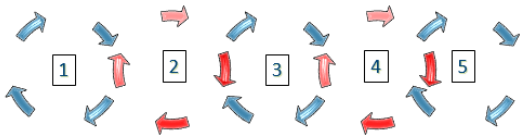

(b) Five Roundabouts per day

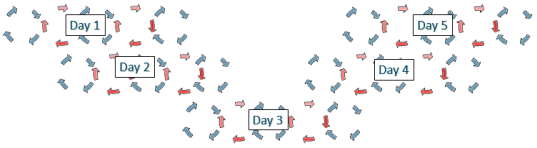

(c) Five days of roundabouts.

Fig. 2-6: Measurement campaign roundabout procedure.

Table 2-4: Description of verification set-up, components and appendices.

Measurement	Conditions	Appendix	Comments
Comparison set-up	Laboratory 1207	A	Detailed component listing of channels
Switch Matrix	Laboratory 1207	B	Detail switch matrixes list of components
Test Environment	Laboratory 1207	C	Environmental conditions in laboratory
Cable for Conducted channels	Environmental Chamber	D	Cable used in synthetic channel tests
Random Effects Model Technical Approach		E	Analysis procedure for random component of uncertainty
Software Script for Two-Tiered ANOVA		F	Two-tiered ANOVA software code
Test Schedule for Roundabouts		G	The test schedule used during the measurements.

3 VNA and Channel Sounder Descriptions

3.1 Vector Network Analyzer Description

The channel sounder verification process described here uses a VNA as a reference instrument. All measurements made by the VNA were calibrated with uncertainties propagated through the calibration and post processing to the channel metrics of path gain and PDP.

A VNA is an instrument used to measure complex scattering parameters (S-parameters). It does this by sampling the incident and reflected waves at both ports of a device under test (DUT), and then forming ratios that are directly related to the reflection and transmission coefficients of the device. See Fig. 3-1 for details regarding the definitions of two-port S-parameters. The VNA steps through the frequency range to obtain S-parameters over a band of interest. Directional couplers behind each test port are used to sample the incident and reflected waves with the source switched to one port while the other port is virtually terminated by an ideal load, as illustrated in Fig. 3-2.

During the measurement campaign, we calibrated the VNA at the beginning and end of the day to account for systematic imperfections such as impedance mismatch, loss in the cables and connectors, frequency response of the source and receiver, and directivity and cross talk due to signal leakage. This is not to say that calibrations account for all possible sources of error. For example, calibrations do not account for system drift, repeatability in the switches and connectors, instrument noise, or errors in the calibration standards.

There are a wide variety of calibration methods available to VNA users, most of which can be classified into one of three groups depending on the type of calibration standards used. The thru-reflect-line (TRL) calibration is perhaps the most fundamental and accurate VNA calibration for coaxial circuits. Multiline TRL calibrations measure the propagation constant of multiple transmission-line standards so that the characteristic impedance can be transformed to a selected reference impedance, and offer high-bandwidth and accuracy. However, a set of coaxial lines, some relatively long, is required to obtain a wide-band measurement. Coaxial airlines also require considerable care to ensure good connections without damaging the standards. Furthermore, a set of lines can be costly, and measurements are time-consuming. Other types of VNA calibrations make use of compact, lumped-element standards, the most common being open-short-load-thru (OSLT) and line-reflect-match (LRM) methods. They provide calibration procedures that are easier to perform, often at the cost of lower accuracy.

In this measurement campaign, we made use of an OSLT calibration kit with Type-N coaxial connectors. Physical models of the calibration standards were developed and validated using a TRL calibration within the NIST Microwave Uncertainty Framework (MUF) [9]. This software tool utilizes parallel sensitivity and Monte-Carlo analyses, and enables us to capture and propagate the S-parameter measurement uncertainties and statistical correlations between them. By identifying and modeling the physical error mechanisms in the calibration standards, we can determine the statistical correlations among the S-parameters. These uncertainties, which are due to systematic effects, can then be propagated to measurements of the DUT or the channel. For the tests shown here, the uncertainties were propagated through the entire channel sounder verification method to the computation of the channel metrics while maintaining the correlated uncertainty mechanisms throughout the process.

Prior to collecting data, several parameters must be entered on the front panel of the VNA, including the frequency grid, power level, IF bandwidth, and dwell time..

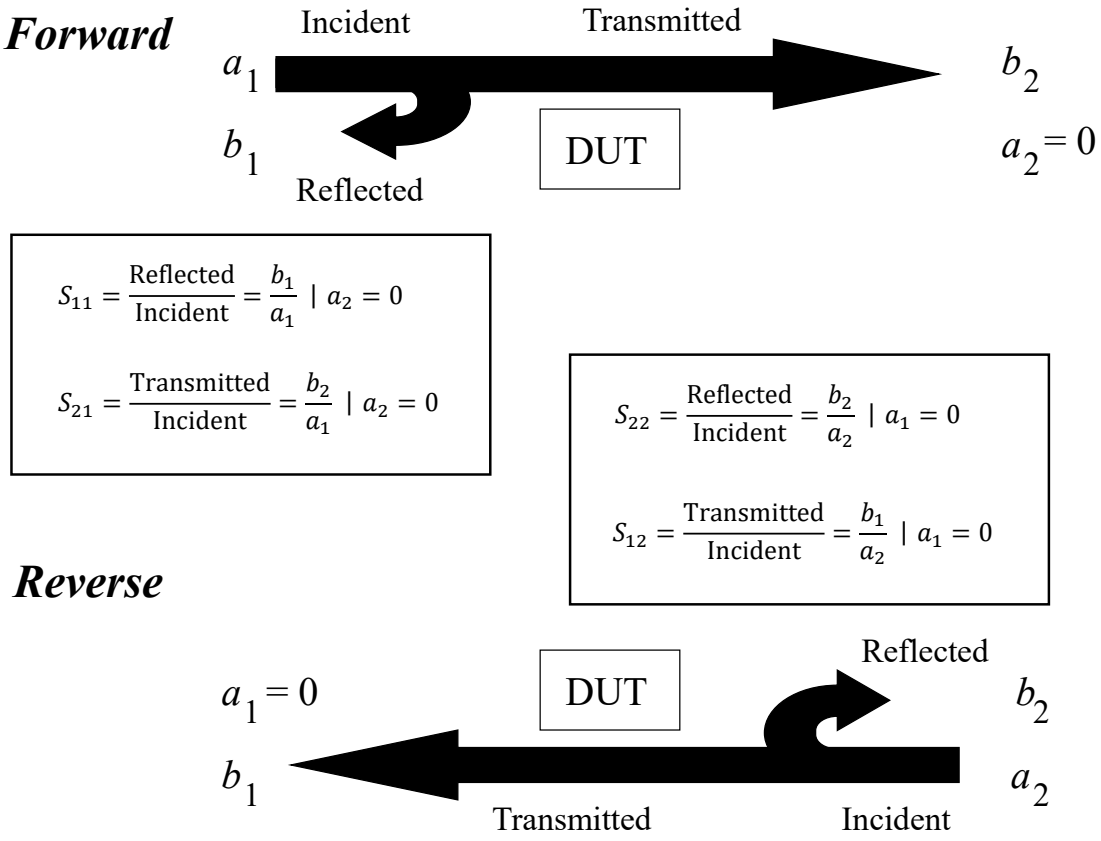

Fig. 3-1:Definition of VNA scattering parameters in terms of incident and reflected waves.

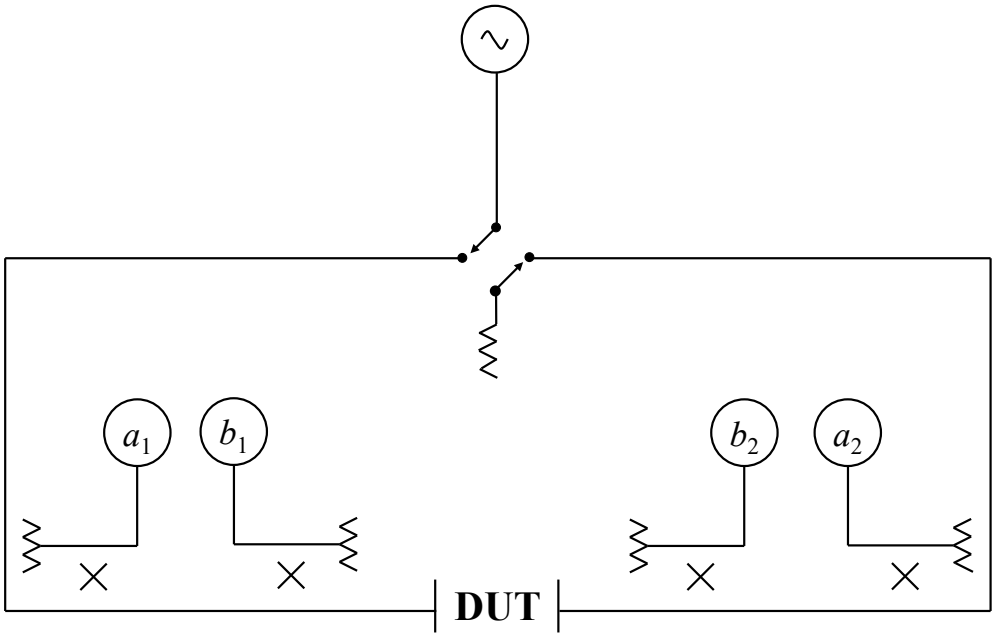

Fig. 3-2: Simplified schematic diagram of a four-sampler vector network analyzer.

3.1.1 Analysis of Vector Network Analyzer Uncertainties due to Systematic Effects

To determine the uncertainties due to systematic effects for our calibrated VNA measurements, the NIST MUF was employed to construct models for the Type-N OSLT calibration standards. The four standards (open, short, load, and thru) were modeled with the values and uncertainties listed in Table 3-1. We modeled the load standard as a simple 50 Ω resistor after observing that the magnitudes of the measured reflection coefficients for both the male and female connectors were less than -30 dB at most frequencies. The offset lengths of the open and short standards were estimated from the respective phase delays measured with the multiline TRL calibration as described in detail in reference [10]. Other values and distributions of the uncertainties come from a variety of sources, including manufacturers' specifications and an IEEE standard [11].

Once the models of the OSLT calibration standards were developed, they were validated by measuring verification devices using both OSLT and multiline TRL calibrations, and comparing the calibrated devices' values and uncertainties. Note that the values we determined for the Type-N calibration kit are valid only for our specific standards, and should not be utilized with other OSLT calibration kits.

Table 3-1: Physical error mechanisms of the Type-N OSLT standards.

Mechanism (units)	Value ± Uncertainty (Distribution)
Inner Conductor Diameter (mm)	3.04 ± 0.0026 (Rectangular)
Outer Conductor Diameter (mm)	7.0 ± 0.0051 (Rectangular)
Pin Diameter (mm)	1.651 ± 0.0127 (Rectangular)
Pin Depth (mm)	0.051 ± 0.051 (Rectangular)
Metal Conductivity (S/m)	$7.9\times10^6 \pm 4\times10^6$ (Rectangular)
Relative Dielectric Constant	1.000535 ± 0
Dielectric Loss Tangent	0 ± 0
Male Open Offset Length (mm)	6.504 ± 0.005 (Rectangular)
Female Open Offset Length (mm)	1.944 ± 0.005 (Rectangular)
Open Conductance (1/Ω)	0 ± 0
Open Capacitance (pF)	0 ± 0
Male Short Offset Length (mm)	5.321 ± 0.005 (Rectangular)
Female Short Offset Length (mm)	0.000 ± 0.005 (Rectangular)
Short Resistance (Ω)	0 ± 0
Short Inductance (nH)	0 ± 0
Load Resistance (Ω)	50.0 ± 0.1 (Rectangular)
Load Inductance (nH)	0.0 ± 0.1 (Rectangular)

3.1.2 Computing Path Gain from VNA Measurements

Path gain may be calculated from the reference VNA measurements. Prior to computing this metric, the VNA software and hardware settings were chosen with consideration of the conducted channel and the channel sounder. The IF bandwidth of the VNA was set to 20 Hz to ensure a high dynamic range in the VNA measurements. Next, the VNA frequency range was set to 3.3–3.7 GHz, which was the largest range used by any of the channel sounders. A dwell time of 1 ms was applied to the VNA measurements to ensure proper settling of the VNA while taking measurements. Finally, the number of points, N_{VNA}, for the VNA was computed from the spatial resolution of the channel sounder, as described in the following paragraphs.

The remainder of this section describes how to calculate the path gain and PDP from S-parameter measurements. We first calculate the PDP and then the path gain.

The effective time step, ΔT_{VNA}, derived from the VNA measurements is dependent upon the frequency range, BW

$$\Delta T_{\mathrm{VNA}} = {}^{1}/_{BW}. \tag{3.1}$$

The effective maximum time resolution for the VNA measurement will be equal to the number of VNA points and ΔT_{VNA}.

In order to compare channel sounder and VNA measurements, we are interested in setting the maximum time resolution of the VNA equal to the maximum detectable delay of the channel sounder $T_{\mathrm{max}}^{\mathrm{CS}}$, thus determining the number of points for the VNA measurements, N_{VNA}. The multipath time resolution, ΔT_{CS}, for a given channel measurement may be computed from

$$\Delta T_{\mathrm{CS}} = {}^{2}/_{Sample\ Rate}. \tag{3.2}$$

The sample rate of the channel sounder equals the symbol rate multiplied by the samples per symbol. The maximum detectable delay, $T_{\mathrm{max}}^{\mathrm{CS}}$, of the channel sounder is then

$$T_{\mathrm{max}}^{\mathrm{CS}} = N_{\mathrm{CS}} \Delta T_{\mathrm{CS}}, \tag{3.3}$$

where N_{CS} equals the PN sequence code length for a Correlation-Based channel sounder or number of pulses for the Direct-Pulse channel sounder. The number of points, N_{VNA}, for the VNA is then chosen to equal the time resolution of the channel sounder

$$N_{\mathrm{VNA}} = {T_{\mathrm{max}}^{\mathrm{CS}}}/{\Delta T_{\mathrm{VNA}}}. \tag{3.4}$$

Inspection of the above formula shows the number of VNA points will rise with either increasing channel sounder maximum detectable delay or increasing VNA frequency range. Therefore, choosing a frequency range that is the same as that of the channel sounder will minimize the number of points the VNA must measure.

Using the above settings, the calibrated VNA measurements of the channel are used to compute the PDP and path gain. We compute the VNA-measured impulse response, $h_{\mathrm{VNA}}(t)$, of the channel by taking an average of S_{12} and S_{21} assuming the channel is reciprocal

$$|h_{\mathrm{VNA}}(t)| = \left| IFFT\left(\frac{S_{12}(f)+S_{21}(f)}{2}\right)\right|. \tag{3.5}$$

$$PDP_{\mathrm{VNA}}(t) = |h_{\mathrm{VNA}}(t)|^2. \tag{3.6}$$

Channel metrics such as the initial time of arrival, RMS delay spread, 90% delay window, noise threshold, and delay interval may be computed from the PDP.

The VNA channel path gain, PG_{VNA}, can be computed by averaging over the frequency-domain data. Note that the channel path gain in this work does not include antenna gains since the channel included only coaxial cables and attenuators. For a single VNA measurement, the path gain may be computed from the calibrated channel response in the frequency domain as

$$PG_{\mathrm{VNA}} = \left(\frac{1}{N_{\mathrm{VNA}}} \sum_{n=1}^{N_{\mathrm{VNA}}} \left| \frac{S_{12}(f) + S_{21}(f)}{2} \right|^2 \right)^{1/2}, \tag{3.7}$$

$$PG_{\mathrm{VNA}}(dB) = 5 \log_{10} \left(\frac{1}{N_{\mathrm{VNA}}} \sum_{n=1}^{N_{\mathrm{VNA}}} \left| \frac{S_{12}(f) + S_{21}(f)}{2} \right|^2 \right). \tag{3.8}$$

The summation is over the number of points in the frequency range.

3.1.3 Shifting the VNA's Reference Plane for Channel Sounder Verification

The *S*-parameters of the switch matrix were measured to enable the shifting of the VNA's reference planes. Using de-embedding and embedding procedures, the reference plane of the VNA was shifted to the other channel sounder's reference plane. Thus, a direct comparison of the VNA data could be made with any channel sounder's measurement data. The reference plane shifting procedure was performed using the MUF, but the general approach consists of converting *S*-parameters to transmission matrices [12], multiplying by appropriate matrix inversions, and then converting back to *S*-parameters to obtain the new reference plane. This process is used to compare the individual channel sounder measurements of their unique channel with the VNA measurements of the same channel. Note that our goal is not to characterize the channel itself. Rather, we focus solely on identifying hardware non-idealities by comparing the channel sounder's measurements of the channel to those of the VNA.

3.2 Correlation-Based Channel Sounder Description

The NIST Correlation-Based channel sounder system [13]–[15] consists of a single transmitter (TX) and a single receiver (RX) synchronized with two rubidium clocks, as shown in Fig. 3-3. The clocks ensure that drift between samples is small enough for accurate resolution of the delay spread and allows for measuring the absolute timing between TX and RX. Our system uses commercial hardware and software[1] for data acquisition, with NIST-written programs used for post-processing.

The channel sounder's TX contains a vector signal transceiver (VST) generator that generates a pseudo-noise (PN) code sequence. This transceiver modulates the RF carrier with a binary phase shift keying (BPSK) signal. The TX VST that we used is specified to have a maximum output power of +10 dBm with a -161 dBm/Hz noise floor. The waveform corresponding to each PN sequence was configured to oversample by a factor of four, providing, in the work presented here, 8188 samples with a 5 ns/symbol sampling rate. Therefore, a single record of 400 PN sequences (or "code words") had a duration of 16.37 milliseconds.

The channel sounder's TX repetitively transmits a maximum-length PN sequence of order 11. The average power transmitted, as seen in Fig. C-4, was maintained through the continuous transmission of the signal. The RF signal was transmitted at an operating frequency of 3.5 GHz through an amplifier and a matched filter to reduce the harmonics. The amplifier was connected to the conducted RF channels. The signal then was transmitted either through an attenuator for a back-to-back measurement or through the conducted channel to the RX. The entire TX system except for the monitor, keyboard, and power amplifier was contained in a single chassis.

[1] The mention of brand names does not imply an endorsement by NIST or NTIA. Other products may work as well or better.

The channel sounder's RX downconverts and digitizes the received signal. Correlation processing of the measured signal is performed in post-processing to obtain the channel's complex time-domain impulse response. This system exploits correlation processing gains proportional to the time-bandwidth product of the PN sequence. From the time-domain impulse response, the PDP can be computed along with other channel parameters such as RMS delay spread, number of multipath components, and initial time of arrival. With the processing gain, this channel sounder can achieve higher dynamic range than with a simple wideband measurement system such as the Direct-Pulse channel sounder. The RX is also based upon a VST. The RX transceiver demodulates the BPSK signal from the impaired channel to obtain a measurement of the received signal, S_{meas}. The RX has an internal computer to run the NIST-developed software and to save data to an NI HDD-8260 redundant array of independent disks (RAID) hard drive, a data storage unit located in the RX chassis.

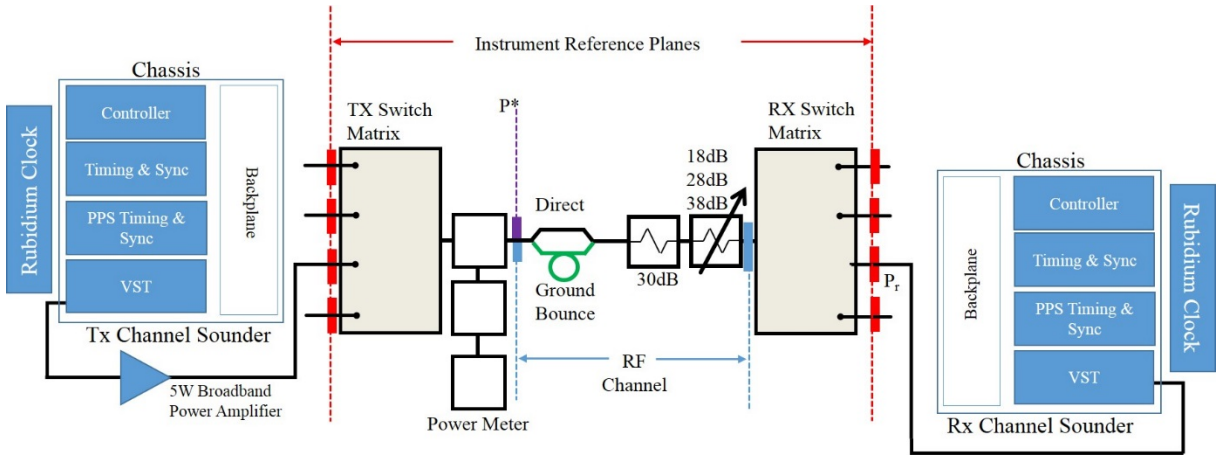

Fig. 3-3: Correlation-based channel sounder system block diagram as connected to the direct-and-bounce path channel.

The timing system is crucial for the synchronization between the transmit and receive sections of the channel sounder when they are disconnected from one another. The TX system is tied directly to a 10 MHz rubidium clock using a timing synchronizer. This unit shares clocks and triggers between the multiple modules in the chassis see **Error! Reference source not found.**. A timing synchronization unit generates the triggers from the Pulse Per Second (PPS) signal from the rubidium clock and disciplines its temperature-compensated crystal oscillator (TCXO) to the rubidium clock. The rubidium clock's PPS signal is used to create a reference trigger to coherently initiate signal generation in the TX and acquisition in the RX. With this approach, the trigger timing and the local oscillator (LO) RF up- and down- conversion are locked and synchronized. This use of the rubidium clock for both triggering and frequency conversion from the LO minimizes the jitter, phase and time drift.

Collected data, consisting of the measured channel sounder impulse response, are stored as "records." The length of a record equals the length of the ideal PN sequence, PN_{ideal}, times the number of samples/symbol (*e.g.*, a 2047-point ideal PN sequence times four samples/symbol equals 8188). We term a collection of records an "acquisition." The number of records in an acquisition is a user-defined number specified in the TX control software. We chose 4000 waveforms per record for this measurement campaign. A "file" is made up of a user-defined number of acquisitions. Multiple files may be created during a measurement run. These collected data are then processed to obtain the I/Q data of the channel measurement.

3.3 Scanning-Probe Channel Sounder Description

The ITS Scanning-Probe channel sounder measures the power of a continuous-wave (CW) signal after it has propagated through an RF channel, allowing the determination of path loss. By measuring CW signal

power at several adjacent frequencies, the frequency dependence of the channel may be measured. This channel sounder's scanning capability occurs when the channel sounder moves through the measurement campaign's propagation channels. Due to the nature of the verification approach presented in this report, the scanning capability of this channel sounder was not investigated. A full description of the ITS channel sounder as it is used in mobile channel measurements is provided in references [16]–[24].

The conducted test set-up for the ITS channel-sounder system is shown in Fig. 3-4. The auxiliary spectrum analyzer and associated GPS RX were not present in this test set-up since we were not performing geolocation in the benchtop conducted tests. The system parameters and hardware were configured to approximate those used in actual mobile channel measurements in the field.

The transmitting side of the system [20] consists of a synthesizer that generates a CW signal and a power amplifier that boosts the signal to a suitable power level. A 10 MHz rubidium clock is used to provide a frequency reference for the CW synthesizer. The output of the amplifier is fed into a low-pass filter to minimize interference at harmonics of the transmit frequency. The output of the filter is fed into a directional coupler which has a power-meter/sensor combination connected to the coupled port. This enables us to measure the total microwave power delivered to the TX switch matrix. The TX switch matrix routes the signal to the conducted channel.

The channel output is fed to the RX switch matrix which, in turn, directs the signal to the channel-sounder's receiving system through a bandpass (BP) filter that suppresses adjacent-channel interference. The BP filter output is connected to a vector signal analyzer (VSA) which is the heart of the measurement system. It takes the received signal and downconverts it to a discrete baseband time series of complex in-phase and quadrature samples. A second 10 MHz rubidium clock is used to provide a precise frequency reference for the VSA. This clock has a voltage-variable fine frequency adjustment to permit frequency alignment of the RX with the TX. The VSA typically acquires I-Q data at sampling rates in the range of 1−5 kHz. We selected a sampling rate of f_s = 3.840 KHz which is the value that ITS uses in mobile channel measurements. The sampling rate was selected for a mobile channel measurement at 3.5 GHz and a maximum speed of 29.5 m/s (60 mph). This results in a maximum Doppler shift of approximately 315 Hz. In order to ensure maximum measurement fidelity and to adequately sample abrupt channel transitions, we oversampled the signal by a factor of 10. The resulting sampling rate that we used was 3,840 Hz which results from selecting a 3 kHz bandwidth on the VSA. The measured time series of I-Q samples is then transferred to the computer for both post processing and data analysis using ITS-developed MATLAB® scripts.

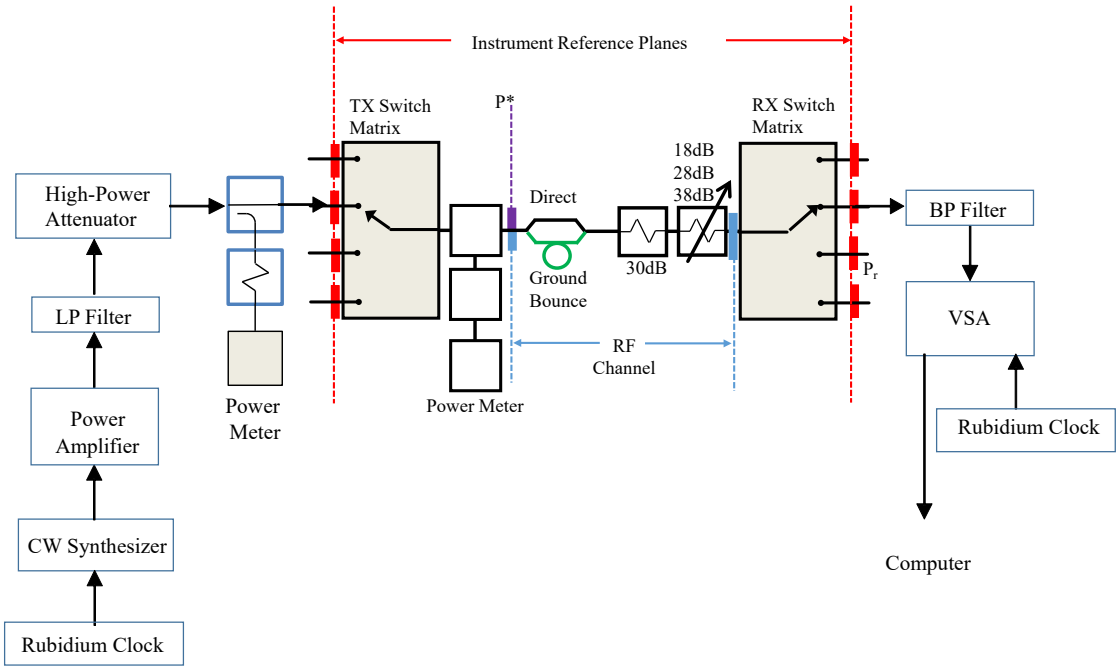

Fig. 3-4: Scanning-Probe channel sounder connected to the direct-and-bounce-path channel.

3.4 Direct-Pulse Channel Sounder Description

The Direct-Pulse channel sounder system consists of an arbitrary waveform and a 43 dB gain amplifier on the TX side and a real-time oscilloscope (RTO) on the RX side, as shown in Fig. 3-5. The arbitrary waveform generator (AWG) is enabled to continuously generate the sinc pulses. After the transmitted signal travels through the test channel, the received signal is detected and measured every other pulse event with the RTO, recording an arbitrary choice of 8192 waveforms. The RTO was configured for the waveform trigger sequence and captured every N^{th} pulse to measure various channel properties as they change in time, thereby taking snapshots of the channel as it evolves. The Fourier transform of this pulse train is a uniformly-spaced set of tones with equal amplitude in the frequency domain. Additional details of the Direct-Pulse channel sounder can be found in Section 5.3.2.

The Direct-Pulse channel sounder is controlled by custom software programs written by NIST staff. The software program is initiated with the necessary parameters and instructs the RTO to acquire a programmed number of waveforms and download the waveforms to an external hard drive for post-processing. Current post-processing includes calculation of median channel path gain over a set of frequencies.

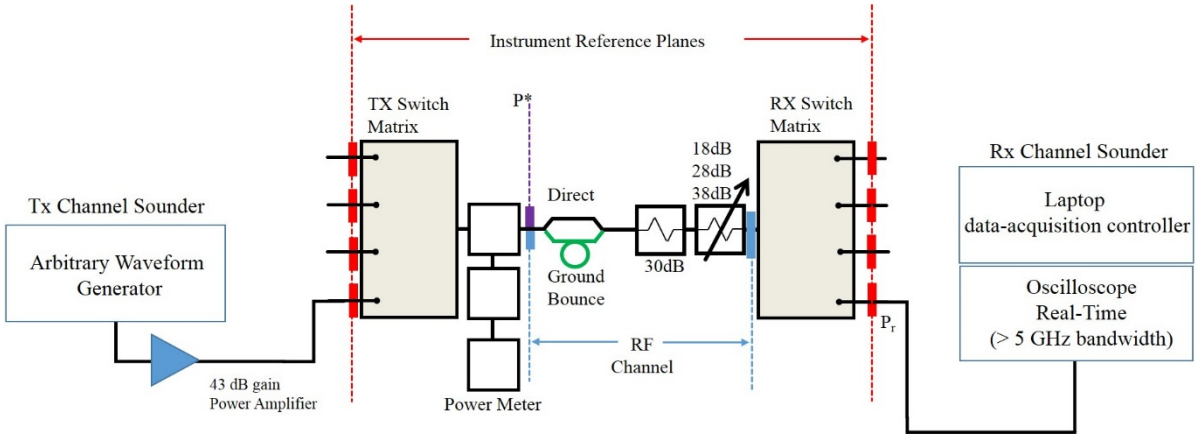

Fig. 3-5: Direct-pulse channel sounder system block diagram connected to the direct-and-bounce-path channel.

3.5 Summary of Channel Sounders Advantages and Disadvantages

The various channel-sounder architectures have a range of advantages and disadvantages. We have outlined a few of them in Table 3-2.

Table 3-2: Advantages and disadvantages of various channel-sounder systems.

Channel-Sounder	Advantages	Disadvantages	Application
NIST Vector Network Analyzer	• Very accurate (traceability path) • Very high dynamic range • Wideband • Time information (phase between TX and RX maintained)	• Not mobile (tethered) • Slow acquisition • Static channel only	• Static channel • Used to verify other systems • Small-scale fading and large-scale path gain • RMS delay spread, etc.
NIST Correlation-Based channel sounder	• Mobile (untethered) • Time information • Doppler	• Lower dynamic range (can recover with processing gain)	• Mobile communications for behavior of channel over modulation BW • Small-scale fading and large-scale path gain • RMS delay spread etc. • Doppler
ITS Scanning-Probe channel sounder	• Mobile (untethered) • Doppler • Low complexity hardware • High dynamic range	• No time information • Slow acquisition	• Mobile communications for power-like behavior (narrowband) • Large-scale path gain • “Clutter” and shadowing • Doppler
NIST Direct-Pulse channel sounder	• Traceability path established • Time information	• Lower dynamic range • Prone to jitter and drift	• Used to verify other systems • Small-scale fading and large-scale path gain • RMS delay spread, etc.

4 Channel-Sounder Error and Uncertainty Description

Random and systematic measurement errors are prevalent in channel-sounder hardware implementations and measurements [25]–[29]. While in the present work we only consider random measurement errors, we provide a brief description of potential systematic measurement errors for the reader's benefit. Definitions of random measurement errors and systematic measurement errors are given below in Sections 4.1 and 4.2, respectively. Complete uncertainty analyses involving all components of each channel sounder system are planned for future work. We also describe a statistical model used to quantify the variability in measurements due to random effects on different timescales.

4.1 Discussion of Random Measurement Error

According to the International Vocabulary of Metrology [25], random measurement error is the "component of measurement error that in replicate measurements varies in an unpredictable manner." For the channel-sounder measurement verification procedure described here, the uncertainty due to the random component of our measurement error will be estimated by (1) repeat measurements within a roundabout (2) multiple roundabouts within a day and (3) day-to-day measurements. Note that systematic errors in the non-VNA instruments have not been accounted for and will not be captured by this analysis.

4.1.1 Quantifying Uncertainty

We model the measured path gain with a random effects model [31]. This model quantifies the mean path gain, G, and the variability in the measurements occurring over different time scales. We investigated two random effects models, which we will refer to as Model 1 (Eq. 4.1) and Model 2 (Eq. 4.2). Under the Model 1, we assume that our measured channels are stable and that all measurements are of the same quantity (G, path gain of the channel) with some variability due to day, roundabout, and measurement error. A repeat is defined as a measurement within a single roundabout. For example, for the Correlation-Based channel sounder the variability due to repeat is related to the variation in the 4000 waveforms seen in Fig. 2-6. Similarly, the variability due to roundabout is related to the variation in Scanning-Probe channel sounder measurements made during different roundabouts. This model assumes that variability due to day is the same for all days. This assumption also applies to the variability due to roundabout and measurement error.

We also modeled our path-gain measurements using Model 2, which combines the repeat measurements within a roundabout, leaving only variance components attributable to day and roundabout. While Model 1 partitions the variance into more components (due to day, roundabout, and measurement error within a roundabout), it also places stronger statistical assumptions on the measured data. For example, even though thermal noise is typically considered to be a random effect within an electrical measurement, if data are collected over a very short time window, autocorrelation [38] may exist between samples. Upon checking the assumptions required for Model 1 using exploratory data analysis and autocorrelation function plots, detailed in Appendix E, we found that the path gain measurements taken within a roundabout were strongly autocorrelated for all of the channel sounders, meaning that the other sources of uncertainty dominated over each system's white noise. Therefore, we instead implemented Model 2 for the quantification of the mean path gain, G, and the variance components. *Important to note: channel sounder measurements do have variability due to measurement error within a roundabout and labs may wish to characterize this variability using Model 1. Because our measurement data as recorded violated the assumptions of Model 1, we chose not use it to quantify this variance component.*

4.1.2 Hierarchical Random Effects Model 1 Description

Model 1 allows us to estimate the imperfections in the expected value of the path gain and the components of variance from the path gain measurements taken over the course of the Conducted-

Channel measurement campaign. The analysis we perform here allows us to estimate separately the variability in measurements due to differences between days and between roundabouts. Other sources of variability—such as from instrumentation or measurement error within a roundabout—are considered together as a single source of variability. We assume the data may be represented with the random effects model [31]

$$X_{ijk} = G + D_i + R_{j(i)} + \epsilon_{k(ij)}, \tag{4.1}$$

where the expected value of the path gain for channel-sounder measurements X_{ijk} is given by G, D_i is an effect due to day, and $R_{(i)j}$ is an effect due to roundabout. D_i, $R_{j(i)}$ and $\epsilon_{k(ij)}$ are independent random variables with expectations 0 and variance σ_D^2, σ_R^2 and σ^2, respectively, for $i = 1, \dots, I$ (I =number of days), $j = 1, \dots, J$ (J =number of roundabouts in a day), and $k = 1, \dots, K$ (K = number of measurements within a roundabout). The notation *j*(*i*) indicates that roundabout is nested within day.

The model accounts for variability in the measurements due to their collection over different days as well as over multiple roundabouts each day. These effects are considered random since we are interested in the effect of roundabouts and days in general, rather than for these days in particular. The remaining error is captured by the $\epsilon_{k(ij)}$ term. The variance components σ_D^2, σ_R^2, and σ^2 represent the variability due to day, roundabout, and measurement error.

4.1.3 Hierarchical Random Effects Model 2 Description

The exploratory data analysis presented in Appendix E revealed that the measured data do not meet the statistical assumptions required to apply Model 1. There are data processing and statistical techniques to partially account for this, but they could lead to a different analysis method for each of the channel sounders. To have a common statistical method for analyzing all of the channel sounders, we chose to use Model 2:

$$Y_{ij} = G + D_i + \epsilon_{ij}, \tag{4.2}$$

where $Y_{ij} = \frac{1}{K}\sum_{k=1}^{K} X_{ijk}$ for $i = 1, \dots, I$ and $j = 1, \dots, J$ is equal to the mean over the measurement errors for each roundabout. As before, D_i is an effect due to day while ϵ_{ij} is the remaining error. Both D_i and ϵ_{ij} are assumed to be independent random variables with expectations 0 and variance σ_D^2 and σ^2, respectively.

Use of the well-known analysis of variance (ANOVA) method allows us to estimate the variance of the overall mean of our measurements (across all days) as well as the components of variance due to day and error [32]–[34]. These results are provided in Appendix E. The variance component estimates are presented in Section 5.

4.2 Discussion of Potential Systematic Measurement Errors

In this section, we describe some of the expected sources of systematic measurement errors for the channel sounders. From the International Vocabulary of Metrology, the definitions of systematic measurement error [25] and repeatability condition of a measurement [30] are:

- *Systematic measurement error*: Component of measurement error that in replicate measurements (under repeatability conditions) remains constant or varies in a predictable manner.
- *Repeatability condition of a measurement*: Condition of measurement, out of a set of conditions that includes the same measurement procedure, same operators, same measurement system, same

operating conditions, same location, and replicate measurements on the same or similar objects over a short period of time.

A quantitative analysis of the systematic errors of any of the channel sounders used in this study lies outside of the scope of this document. Systematic errors in channel sounding measurements are predominantly related to errors in characterizing the transmitted and received signals, signal distortion in coupling the signal between components, and the invasiveness of the physical measurement system in the channel. Most of these effects vary with time and temperature and may also vary with humidity. Some systematic effects commonly seen in channel sounder measurements are provided below.

4.2.1 Potential Systematic Measurement Errors in Channel-Sounder Transmitters

The signal produced by the channel-sounder TX is usually fed into a power amplifier. The resulting signal might be characterized with a power meter, digitizer, or VNA, all of which are subject to systematic calibration errors. An attenuator or coupler might be used to protect the signal measurement instrument from saturation, and the estimated value of attenuation may be slightly different than the true value; when this estimate is applied to the calculated transmitter power, the results have a systematic error. The amplifier, attenuator, and measurement instrument all have some impedance mismatch at their cable interfaces that result in standing wave effects. Such impedance mismatches alter the signal level that is ultimately incident on the measurement instrument. For example, these standing wave effects change when the amplifier is connected to an antenna for a channel measurement versus to an attenuator for a back-to-back measurement, causing the measured power to differ between these two measurement configurations. If these differences are not corrected, the estimated transmitted power during a measurement campaign has a systematic error due to the different load impedances.

The signal generator itself will generate a distorted version of the intended signal. The distortion might be random and noise-like or it might be systematic, such as frequency response errors in amplitude and phase or spurious harmonics. If an AWG is used, the errors might include interleave errors, quantization errors, and discontinuities between the beginning and end of a transmitted waveform.

4.2.2 Potential Systematic Measurement Errors in Channel-Sounder Receivers

The received signal might be amplified by a low-noise amplifier and then detected with a VST, VSA, or digitizer. Again, mismatch effects can establish standing waves and cause errors in the signal that are coupled into the measurement instrument. The measurement instrument can also have frequency-dependent calibration errors, the low-noise amplifier can have nonlinear distortion, and, in a digitizer-based RX, interleave errors and quantization errors may occur. In addition, timing errors and frequency deviation may cause poor synchronization, which can mimic Doppler broadening.

4.3 Operator Error

Differences in measurement technique, mal-functioning cables or connectors, and blunders are common occurrences and may contribute to both random and systematic measurement errors. These can include not following standard measurement procedures, different positioning of cables or antennas, incorrectly recording instrument settings or readings, and incorrectly implementing post processing computer code. Care should be taken to simplify and automate measurement procedures to minimize the chance of human error. Good note-taking practices should be observed. Data should also be checked for outliers that might be explained by human error. However, outliers should be carefully considered before discarding, as they may be an indication of unexpected behavior of the measurement equipment or the channel.

5 Comparison of Channel-Sounder and VNA Measurements

The channel-sounder measurements, with uncertainty due to random effects, are compared to the reference VNA's measurements, with uncertainty due to random and systematic effects. The set-up parameters and measurement steps are provided for Correlation-Based, Scanning-Probe, and Direct-Pulse channel sounders.

5.1 Correlation-Based Channel Sounder Results

5.1.1 Correlation-Based Channel Sounder Set-up Parameters

The Correlation-Based channel sounder was set-up as in Fig. 5-1 using the parameters listed in Table 5-1(a). Measurements were performed according to the steps listed in Table 5-1(b). Table 5-2 shows the power levels that we measured for different transmitted output powers.

Table 5-1: Correlation-Based channel sounder (a) set-up parameters and (b) measurement steps.

(a)

Set-up Parameters	
Sampling bandwidth	200 MHz
Center Frequency	3.5 GHz
PN Sequence	11
Number of measurements per roundabout	4000
TX Oversampling	4

(b)

Measurement Steps	
1	Perform a back-to-back measurement between each roundabout
1a	Turn on power amplifier and put it in stand-by mode for 1 hour (at the start of day only). Using coaxial cables, place a 60 dB attenuator between the TX and RX.
1b	Take power amplifier off of stand-by mode
1c	Collect back-to-back data using channel sounder's RX
1d	Put power amplifier back onto stand-by mode
1e	Disconnect the coaxial cables and connect the channel sounder to the transmit and receive matrices
2	Perform conducted-channel measurements for each roundabout (4000 measurements per roundabout) during the roundabout sequence
2a	Take power amplifier off of stand-by mode
2b	Collect channel data using channel sounder's RX
2c	Put power amplifier back onto stand-by mode
2d	At end of the day after all the roundabouts, ensure that the power amplifier is in stand-by mode

5.1.2 Correlation-Based Channel Sounder Post–Processing

The Correlation-Based channel sounder measures a set of complex data, $S_{meas}(\tau)$, which can be used to generate path gain values for the measured channel. These raw data are corrected to estimate the path gain of the channel. The calibration involves a back-to-back measurement, $S_{meas}^{B2B}(\tau)$, of the channel system to remove hardware effects. $S_{cal}(\tau)$ is the calibrated version of uncalibrated channel response, $S_{meas}(\tau)$:

$$S_{cal}(\tau) = \mathcal{F}^{-1}\left\{\mathcal{F}[w(\tau)] \times \frac{\mathcal{F}[S_{meas}(\tau)]}{\mathcal{F}[S_{meas}^{B2B}(\tau)]/A}\right\}. \quad (5.1)$$

where $\mathcal{F}$ is the Fourier transform, $w(\tau)$ is a windowing filter, and A is the attenuator used during the back-to-back measurement. Note: A may have a frequency dependence.

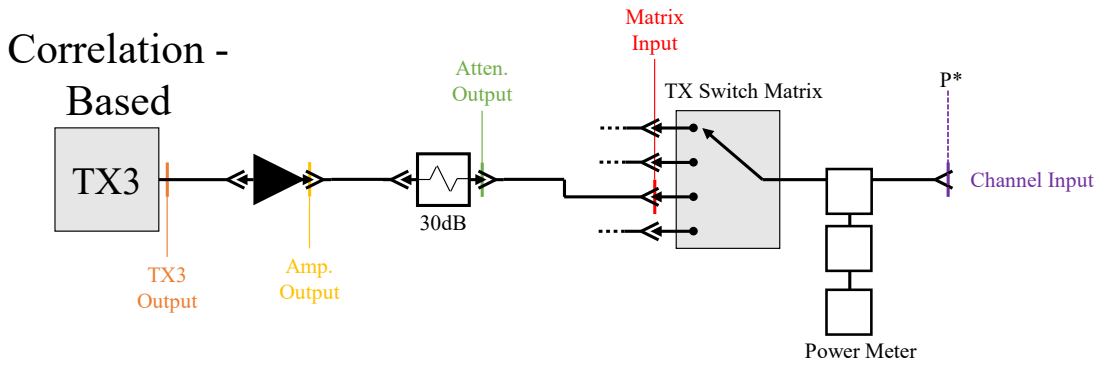

Fig. 5-1: Schematic for the Correlation-Based channel sounder up to *P**.

Table 5-2: Power budget for the Correlation-Based channel sounder. The power budget shows approximate power levels at various points in Fig. 5-1 with standard deviation of 0.02 dB

TX3 Output (dBm)	Amplifier Output (dBm)	Atten. Output (dBm)	Matrix Input (dBm))	Channel Input (dBm)
-25	21.01	-10.83	-12.37	-13.74
-24	22.2	-9.82	-11.39	-12.77
-23	23.16	-8.83	-10.43	-11.81
-22	24.18	-7.82	-9.41	-10.84
-21	25.16	-6.84	-8.43	-9.87
-20	26.14	-5.87	-7.44	-8.89
-19	27.14	-4.74	-6.47	-7.91
-18	27.4	-3.78	-5.45	-6.91

Eq. 5.1 results in a division by noise due to the $\mathcal{F}[S_{meas}^{B2B}(\tau)]$ in the denominator. Since the noise found in $S_{meas}(\tau)$ is a very small value, this leads to amplification at the band edges. We handled this challenge by use of the windowing filter, $w(\tau)$, to remove this amplified noise from $S_{cal}(\tau)$ and to reduce the resulting sidelobes due to the truncation of the measured spectrum. We use this approach here.

It is important to keep in mind that $S_{cal}(\tau)$ is only an estimate of the channel response. This is true not only because of the presence of noise, but also because of the additional filtering imposed on $S_{cal}(\tau)$ by the filter $w(\tau)$. One common implementation of $w(\tau)$ comes from the PN sequence used in the channel sounder TX. $PN_{ideal}(\tau)$ is the oversampled PN sequence used by the TX where N is the maximum length sequence order of the PN code of 11 and divided by $2 \times \sqrt{N}$ to obtain unity gain for $w(\tau)$:

$$w(\tau) = \mathcal{F}^{-1}\left\{\mathcal{F}\left[\frac{PN_{ideal}(\tau)}{2\times\sqrt{N}}\right]\mathcal{F}^{*}\left[\frac{PN_{ideal}(\tau)}{2\times\sqrt{N}}\right]\right\}. \quad (5.2)$$

A reduction of the magnitude of the received signal occurs when the filter, $w(\tau)$, is applied. To rescale the magnitude of the $S_{cal}(\tau)$, we applied an Area Sum scaling [13] to achieve a calibrated and scaled solution, $S_{cal}^{Scale}(\tau)$. This scaling is implemented as

$$S_{\text{cal}}^{\text{Scale}}(\tau) = S_{\text{cal}}(\tau) \frac{\sqrt{N}}{\sqrt{\sum_{n=1}^{N} |\mathcal{F}[w(\tau)]|^2}}. \tag{5.3}$$

The summation in Eq. 5.3 is over the *N* frequency components. It results in a scalar value. The value of the scale factor may be taken in the time or frequency domain, depending upon the desired implementation of the post-processing.

The average path gain over the frequency range may be computed from the calibrated and scaled channel response. The PDP [13] is used for this purpose. The PDP is computed from the magnitude squared of the calibrated and scaled channel response. In the time domain, the PDP equals

$$PDP(\tau) = \frac{N}{\sum_{n=1}^{N} |\mathcal{F}[w(\tau)]|^2} \left| \mathcal{F}^{-1} \left\{ \frac{\mathcal{F}[w(\tau)] \times \mathcal{F}[S_{\text{meas}}(\tau)]}{\mathcal{F}[S_{\text{meas}}^{\text{B2B}}(\tau)]/\mathcal{F}[A]} \right\} \right|^2. \tag{5.4}$$

While the channel path gain, G, can be computed in the time domain, we can also compute it by averaging over the frequency-domain data. For a single record, the path gain may be computed from the calibrated and scaled channel response in the frequency domain as

$$G = \frac{1}{N} \sum_{n=1}^{N} \frac{N}{\sum_{n=1}^{N} |\mathcal{F}[w(\tau)]|^2} \left| \frac{\mathcal{F}[w(\tau)] \times \mathcal{F}[S_{\text{meas}}(\tau)]}{\mathcal{F}[S_{\text{meas}}^{\text{B2B}}(\tau)]/\mathcal{F}[A]} \right|^2. \tag{5.5}$$

The summation is over the frequency range of the record. The number of points in the frequency range equals the length of the PN sequence. For purposes here, we use the path gain averaged over the measurement frequency range. To compute the average for an acquisition, we average the path gain, G_{Avg}, over the number of records, N_{rec}, within the acquisition using:

$$G_{\text{Avg}} = \frac{1}{N_{\text{rec}}} \sum_{p=1}^{N_{\text{rec}}} G(p). \tag{5.6}$$

5.1.3 Correlation-Based Channel Sounder Measurement Results, Path Gain

The Correlation-Based channel sounder path gains were measured during the roundabout sequence for the direct-only and direct-and bounce channels. Table 5-3 contains the path gains as measured by the Correlation-Based channel sounder and the VNA. The standard uncertainties accompanying the VNA measurements include components due to both systematic and random effects, while the standard uncertainties for the Correlation-Based channel sounder only include components due to random effects. For comparison purposes, the differences are also tabulated along with the root-sum-of-squares (RSS) of the uncertainties. The data show the differences are less than 0.28 dB for all cases, and the path gains as measured by the Correlation-Based channel sounder are always slightly higher.

We list in Table 5-4 the variance components from the hierarchical random effects model of Eq. 4.2 of the Correlation-Based channel sounder for both the direct-only and direct-and-bounce channels. Variability due to error and roundabout is $\hat{\sigma}_{dB}^2$. Variability due to day is $\hat{\sigma}_{\text{D,dB}}^2$. The largest variance component occurs for DirectBouncePath_2 at 0.18 dB due to day. This variance component was consistently larger than the variability due to error and roundabout. These terms are defined in Appendix E.

5.1.4 Correlation-Based Channel Sounder Measurement Results, PDP

A comparison between the Correlation-Based channel sounder and VNA PDPs provides insight into the channel-sounder's hardware performance. Fig. 5-2 and Fig. 5-3 show PDPs from the correlation-based channel sounder and the VNA measurements for the Direct Path 3 and Direct Bounce Path 1, respectively.

While there are many channel model metrics that may be derived from a PDP [29], two quantities of interest are the time of arrival of the signal and signal level further out in time (ex. 250 ns). For the Direct Path 3 and Direct Bounce Path 1, the time of arrival for the pulses and power levels are shown in Table 5-5. Referring to the figures, the peaks are aligned within 2 dB within the 5 ns resolution. Meanwhile, the signal level of the channel sounder is considerably higher than the signal level of the VNA PDPs. At 150 ns, the difference between the signal levels is approximately 36 dB for the direct path case and 13 dB for the direct-bounce case. Note that the VNA has a larger dynamic range than the Correlation-Based channel sounder due to the choice of the VNA's IF bandwidth of 50 Hz.

Table 5-3: Correlation-based channel sounder: comparison of path gain with VNA.

Direct Only Channel		Path Gain (dB) ± Std. Unc. (dB)	Difference (dB) ± Unc. (dB)
DirectPath_1	VNA	-53.52 ± 0.06	0.14 ± 0.08
	Correlation-based CS	-53.38 ± 0.05	
DirectPath_2	VNA	-63.38 ± 0.02	0.25 ± 0.07
	Correlation-based CS	-63.13 ± 0.07	
DirectPath_3	VNA	-73.43 ± 0.05	0.16 ± 0.07
	Correlation-based CS	-73.27 ± 0.05	
Direct and Bounce Channel		**Path Gain (dB) ± Std. Unc. (dB)**	**Difference (dB) ± Unc. (dB)**
DirectBouncePath_1	VNA	-60.63 ± 0.06	0.24 ± 0.09
	Correlation-based CS	-60.39 ± 0.07	
DirectBouncePath_2	VNA	-70.56 ± 0.04	0.14 ± 0.10
	Correlation-based CS	-70.42 ± 0.09	
DirectBouncePath_3	VNA	-80.58 ± 0.06	0.25 ± 0.06
	Correlation-based CS	-80.33 ± 0.10	

Table 5-4: Correlation-Based channel sounder: variance components from Eq. E.19.

Correlation-Based CS	$\widehat{\sigma}^2_{dB}$	$\widehat{\sigma}^2_{D,dB}$
DirectPath_1	0.07	0.13
DirectPath_2	0.11	0.15
DirectPath_3	0.06	0.09
DirectBouncePath_1	0.12	0.15
DirectBouncePath_2	0.13	0.18
DirectBouncePath_3	0.09	0.28

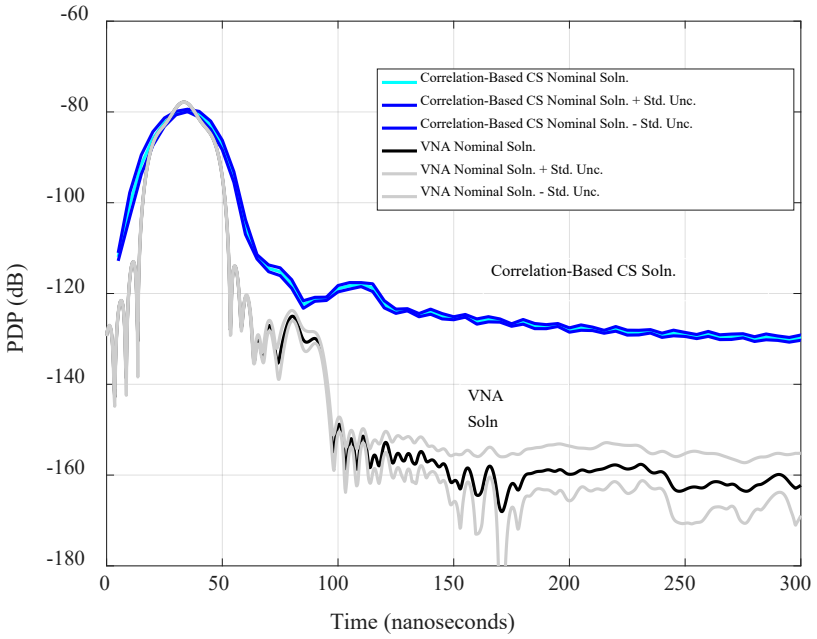

Fig. 5-2: Correlation-Based channel sounder's power delay profile for DirectPath_3.

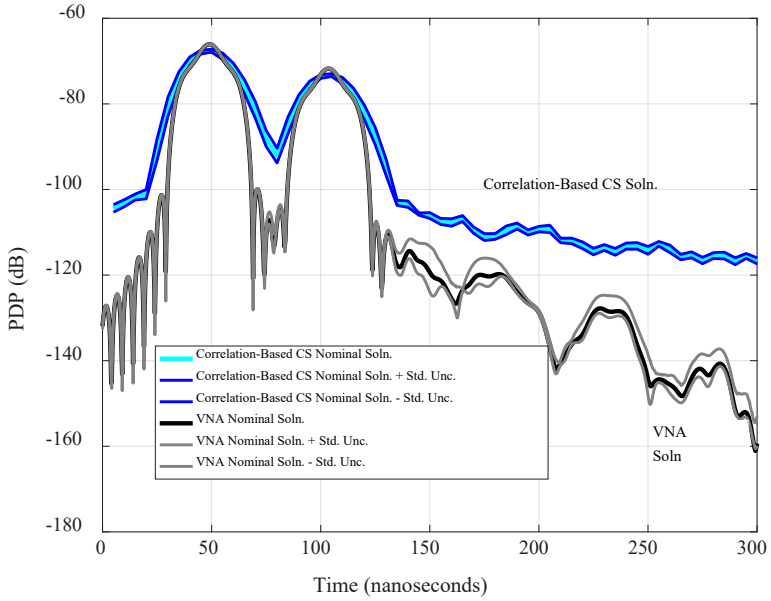

Fig. 5-3: Correlation-Based channel sounder's power delay profile for DirectBouncePath_1.

Table 5-5: Correlation-Based channel sounder: time of arrival and power levels.

	1st peak		2nd peak		Signal level	
	Time (ns)	Power (dB)	Time (ns)	Power (dB)	At Time (ns)	Power (dB)
CS: DirectPath_3	35	-79.68 ± 0.28	-	-	150	-125.5 ± 0.3
CS: DirectBouncePath_1	50	-67.91 ± 0.34	105	-73.27 ± 0.32	150	-106.1 ± 0.7
VNA: DirectPath_3	33.5	-77.83 ± 0.09	-	-	150	-161.3 ± 7.1
VNA: DirectBouncePath_1	49	-66.07 ± 0.1	103.8	-71.77 ±0.17	150	-119.4 ± 6.1

5.2 Scanning-Probe Channel Sounder Results

5.2.1 Scanning-Probe Channel Sounder Set-up Parameters

The set-up for the Scanning-Probe channel sounder is shown in Fig. 5-4 using the parameters listed in Table 5-6(a). The measurements were conducted according to the steps listed in Table 5-6(b). The different calculated power levels are shown in Table 5-7 for different transmitted output powers.

Table 5-6: Scanning-Probe channel sounder (a) set-up parameters and (b) measurement steps.

(a)

Set-up parameters	
Bandwidth, BW	3.0 kHz
Sampling Rate, f_s	3.840 Hz
Center Frequency	3.5 GHz
Record Duration	120 seconds
Number of measurements/roundabout	458,881

(b)

Measurement Steps	
1	Turn on power amplifier for a thirty-minute warm-up time
2	Recall stored synthesizer and VSA configurations
3	Turn on synthesizer and set power to appropriate level
4	Perform fine frequency voltage adjustment of VSA rubidium clock to align with TX
5	Record input power-meter level
6	Initiate 120 s data record capture on VSA
7	Store I-Q data for subsequent processing and analysis
8	Record input power meter level—drift check
9	Switch synthesizer to standby

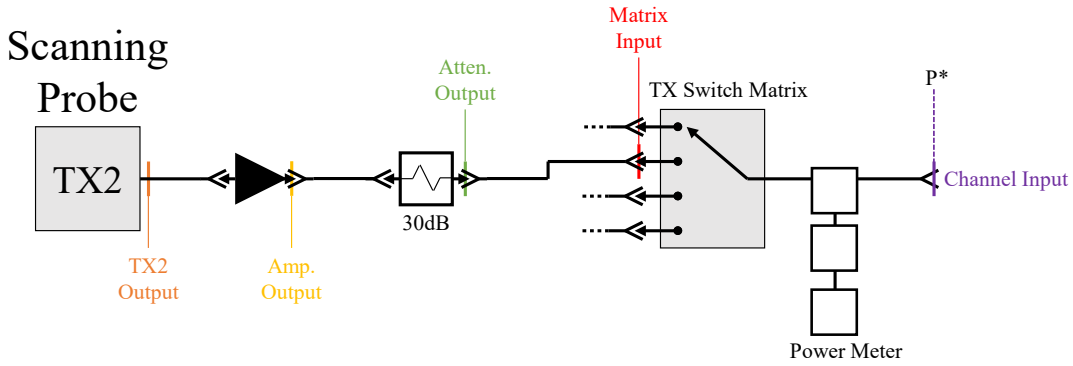

Fig. 5-4: Schematic for the Scanning-Probe channel sounder up to *P**.

Table 5-7: Power Budget Scanning-Probe Channel Sounder. The power budget shows approximate power levels at various points in Fig. 5-4 derived from a power measurement at *P** with a standard deviation of 0.02 dB.

TX2 Output (dBm)	Amplifier Output (dBm)	Atten. Output (dBm)	Matrix Input (dBm)	Channel Input (dBm)
-25	21.01	-10.83	-12.37	-13.74
-24	22.2	-9.82	-11.39	-12.77
-23	23.16	-8.83	-10.43	-11.81
-22	24.18	-7.82	-9.41	-10.84
-21	25.16	-6.84	-8.43	-9.87
-20	26.14	-5.87	-7.44	-8.89
-19	27.14	-4.74	-6.47	-7.91
-18	27.4	-3.78	-5.45	-6.91

5.2.2 Scanning-Probe Channel Sounder Post-Processing

The Scanning-Probe channel sounder measurements are post-processed to obtain path gain. A block diagram of the processing for the conducted channel-sounder measurements is shown in Fig. 5-5. Referring to Fig. 5-5, the path gain is computed by subtracting the measured power at the VSA from the transmitted power.

To measure the transmit power, we use a microwave power meter in conjunction with a calibrated directional coupler to directly measure the input power at the Scanning-Probe channel-sounder reference plane. We add a measured correction factor to the power meter reading that accounts for both the coupler characteristics and the associated cable losses to obtain the transmit power at the scanning-probe channel-sounder input reference plane.

To obtain the received power level at the output instrument reference plane, we both window and average the VSA I-Q data and then apply a correction factor that accounts for cable and filter losses to obtain the received power. Averaging the measured signal is important in measurement campaigns in order to reduce the peak-to-peak variations (i.e. fast fading). In Fig 5-6, this small variation of (< 0.008 dBV) does not necessitate averaging, but it is essential, for validation purposes, to maintain a similar configuration to a measurement campaign out in the field.

Fig. 5-6 shows a combination of VSA output and an associated window-averaged result. The raw I-Q envelope exhibits small, but rapid, variations which are caused by system noise. A sliding window is then applied to the I-Q data to compute an average envelope voltage which we refer to as the “local mean” voltage. This processing is used in ITS mobile channel measurements to reduce the effects of fast fading and is described in detail in [18], [19]. The windowing reduces the effects of system noise, and the results

are smoother with reduced variations. In Fig. 5-6, we use a 0.5 s window which has been widely used in ITS mobile channel measurements at 3.5 GHz and driving speeds of 8.94 m/s (20 mph). We next compute the local mean power by squaring the smoothed I-Q envelope then dividing by 100 (for a 50 Ω system). Thus, the path gain is given by

$$G\ (dB) = P_T - P_{LM} - L_T - L_R, \tag{5.7}$$

where P_T and P_{LM} are the transmitting and window-averaged received (local mean) power levels in dBm. The coupler/cable loss correction factor on the transmit side is L_T and the corresponding correction factor on the receive side is L_R.

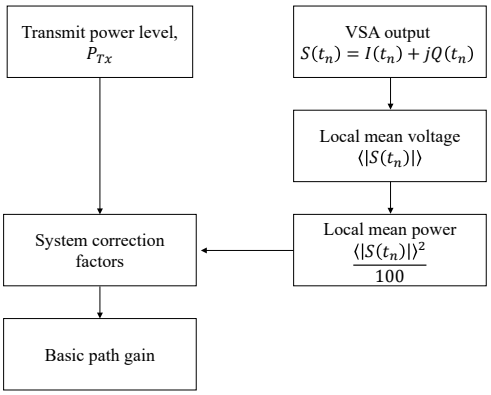

Fig. 5-5: Post-processing for the Scanning-Probe channel sounder. The brackets < > denote a windowed average.

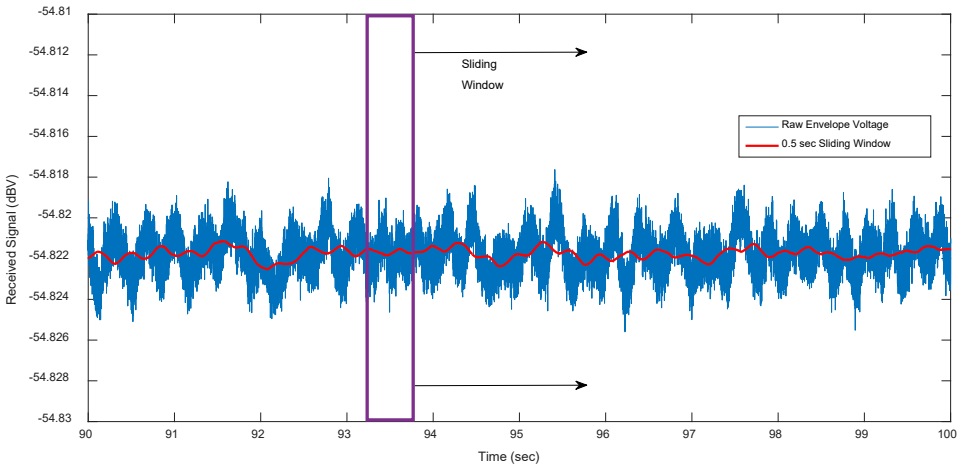

Fig. 5-6: Raw I-Q envelope and averaged envelope using a 0.5 sec wide centered sliding window obtained from the VSA. Note that the vertical scale has a range of 0.02 dB.

5.2.3 Scanning-Probe Channel Sounder Measurement Result

The Scanning-Probe channel sounder measurements of path gain are given in Table 5-8. This table has path-gain values for the channel-sounder and the VNA measurements of the direct-only channels and the direct-and-bounce channels. As previously described, the uncertainties accompanying the VNA measurements include components due to both systematic and random effects, while the uncertainties for the Scanning-Probe channel sounder only include components due to random effects. We provide the

RSS of the uncertainties in the tables. The data show the differences are less than 0.77 dB for all cases, and the path gains are always slightly higher than the path gain as measured by the VNA.

Table 5-9 lists the variance components of the scanning-probe channel sounder for both the direct-only and direct-and-bounce channels. Here, $\hat{\sigma}_{dB}^2$ refers to the variability due to error and roundabout, and $\hat{\sigma}_{\mathrm{D,dB}}^2$ refers to the variability due to day. All variance components were less than 0.13 dB.

Table 5-8: Scanning-Probe channel sounder: channel comparison of path gain with VNA.

Direct Only Channel		Path Gain (dB) ± Std. Unc. (dB)	Difference
DirectPath_1	VNA	-53.54 ± 0.11	0.40 ± 0.07
	Scanning Probe CS	-53.14 ± 0.05	
DirectPath_2	VNA	-63.41 ± 0.06	0.39 ± 0.03
	Scanning Probe CS	-63.02 ± 0.01	
DirectPath_3	VNA	-73.45 ± 0.07	0.37 ± 0.04
	Scanning Probe CS	-73.08 ± 0.02	
Direct and Bounce Channel		**Path Gain (dB) ± Std. Unc. (dB)**	**Difference**
DirectBouncePath_1	VNA	-58.24 ± 0.11	0.24 ± 0.07
	Scanning Probe CS	-58.00 ± 0.04	
DirectBouncePath_2	VNA	-68.17 ± 0.12	0.23 ± 0.08
	Scanning Probe CS	-67.94 ± 0.05	
DirectBouncePath_3	VNA	-78.17 ± 0.11	0.20 ± 0.08
	Scanning Probe CS	-77.97 ± 0.05	

Table 5-9: Scanning-Probe channel sounder: variance components from Eq. E.19..

Scanning Probe CS	$\hat{\sigma}_{dB}^2$	$\hat{\sigma}_{D,dB}^2$
DirectPath_1	0.10	0.13
DirectPath_2	0.03	0.04
DirectPath_3	0.02	0.06
DirectBouncePath_1	0.050	0.10
DirectBouncePath_2	0.01	0.045
DirectBouncePath_3	0.03	0.10

5.3 Direct-Pulse Channel Sounder Results

5.3.1 Direct-Pulse Channel Sounder Set-up Parameters

The Direct-Pulse channel sounder set-up is shown in Fig. 5-7. The parameters are listed in Table 5-10(a). The steps for the measurements are listed in Table 5-10(b).

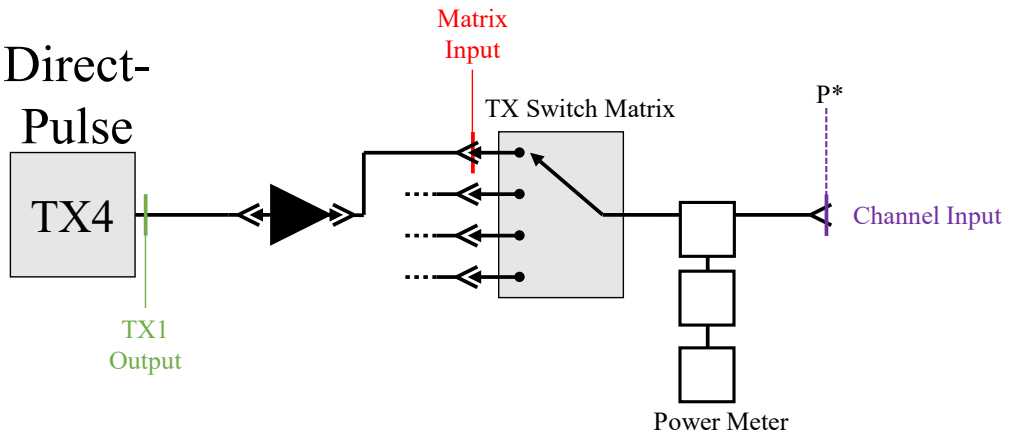

Fig. 5-7: Schematic for the Direct-Pulse channel sounder up to *P**.

The AWG is programmed to generate a train of sinc-function-like pulses in the time domain with a 100 kHz repetition rate and a pulse duration of 25 ns. The Fourier transform of these pulses is a uniformly-spaced set of tones with equal amplitude in the frequency domain extending from 3.3 to 3.7 GHz.

Table 5-10: Direct-Pulse channel sounder (a) set-up parameters and (b) measurement steps.

(a)

Set-up parameters	
Sampling bandwidth	400 MHz
Center Frequency	3.5 GHz
Number of measurements	8192

(b)

Measurement Steps	
1	Conduct a back-to-back reference measurement.
1a	Turn on RTO and warm-up > 1 hour.
1b	Set-up AWG software with the correct measurement parameters and enable AWG output.
1c	Turn on amplifier and warm-up > 30 minutes.
1d	Before the switch matrix, configure test cables to measure pulsed waveform with a 30 dB attenuator on the RTO input to protect the instrument.
1e	Measure received reference waveform with the RTO and download for later processing.
2	Conduct a roundabout measurement.
2a	Reconfigure measurement cables to route pulsed signal to the channel sounder switch matrix. Remove 30 dB attenuator from the RTO input. Route channel sounder output cable to RTO input.
2b	Check connections!
2c	Set-up AWG software program with the correct measurement parameters and enable AWG output.
2d	Perform measurement run, and download data from RTO to hard drive for later post-processing.
2e	Stop AWG output, and disengage amplifier power supply to put in standby mode.
3	Turn off AWG

Depending on the signal level required for testing, a separate amplifier may be configured between the AWG source and the channel input, as indicated in Table 5-11. The time-domain pulse is transmitted through the standard channel configuration and the output routed to the RTO with a measurement bandwidth of 5 GHz.

A single measurement run consists of the RTO acquiring 8192 time-domain waveforms, each consisting of one received pulse which was transmitted through the standard channel. The waveform data are downloaded via a laptop running an acquisition software program and saved on a portable hard drive for post-processing.

The RTO is set to measure every other pulse event but can be configured for arbitrary event spacing. We chose every other pulse collection to avoid extensive data collection and download during the roundabout measurements. This allows multiple snapshots of the channel response as the channel fluctuates over time, which will be useful for studies of time-varying channels. The pulse repetition period is set at 10 μs (and can be set lower). An example of a calibration and a single waveform capture are shown in Figs. 5-8 and 5-9. The yellow trace shows the sinc-like pulse transmitted through the direct-and-bounce path channel and the blue waveform is the synchronous waveform that is used for triggering the RTO. The full duration of the time record is 1 μs. The bottom trace in yellow shows the Fourier transform of the yellow trace in the upper graph.

Table 5-11: System configuration to achieve nominal power at P*

Target power, dBm	AWG amplitude, mV	Amplifier required?
0	1900	No
30	400	Yes

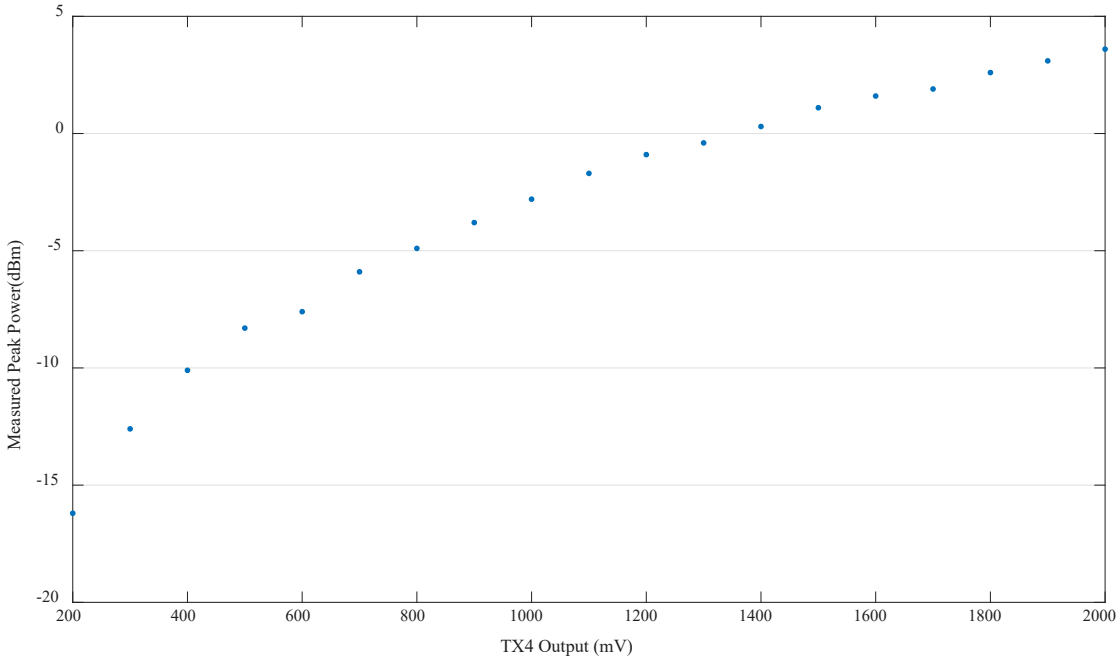

Fig. 5-8: Calibration data for output peak power of arbitrary waveform generator for various pulse amplitude settings.

Fig. 5-9: Screen shot of the Direct-Pulse channel sounder for the direct-and-bounce-path channel. The mention of brand names does not imply an endorsement by NIST or NTIA. Other products may work as well or better.

5.3.2 Direct-Pulse Channel Sounder Post-Processing

The Direct-Pulse channel sounder measures time-dependent data. We estimate the path gain of the conducted channels for each roundabout per day during the measurement campaign. Note that most of the processing will be done in the Fourier domain. We use capital letters to indicate the Fourier transform of the corresponding lower-case letter—e.g., for some time-dependent function $x(t)$, $\mathcal{F}\big(x(t)\big) \coloneqq X(f)$.

5.3.2.1 Back-to-back measurement using Direct-Pulse Channel Sounder

We performed a back-to-back measurement using a known attenuator. Since the same signal is transmitted by the AWG through the same amplifier as in the channel measurement, we obtain an estimate of signal coming from the power amplifier during this back-to-back measurement. Specifically, a signal $x_{AWG}(t)$ is transmitted by the AWG through an amplifier with system response function $g_{\text{amp}}(t)$ and an attenuator with system response function $a(t)$ before being measured by the RTO as shown in Fig. 5-10. The back-to-back measurement, denoted by $Y_{\text{ref}}(f)$, which is the Fourier transformation of $y_{\text{ref}}(t)$, is

$$Y_{\text{ref}}(f) = X_{\text{ref}}(f)A(f)\,, \tag{5.8}$$

where $X_{\text{ref}}(f) = X_{\text{AWG}}(f)G_{\text{amp}}(f)$ is the signal due to the AWG and power amplifier. Each day, a set of 8192 repeat measurements were made of $y_{\text{ref}}(t)$. To reduce noise, and hence improve signal-to-noise (SNR), we averaged over these 8192 repeat measurements when estimating $x_{\text{ref}}(t)$. Note that this means there was a different estimate of $x_{\text{ref}}(t)$ used for each day's data, but within a day the estimate was fixed.

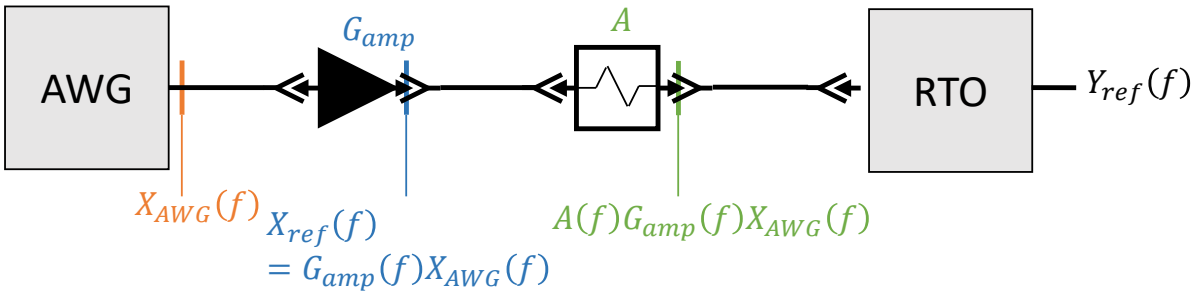

Fig. 5-10: Schematic for the back-to-back measurement of the Direct-Pulse channel sounder. The expressions in orange, yellow, and green indicate the modeled value of the Fourier transform of the signal.

5.3.2.2 Channel measurement using Direct-Pulse Channel Sounder

We transmitted the AWG signal through the conducted channels and measured the signal on the RTO. This signal also travels through two cables outside of the switch matrices: one cable with system response function $r(t)$ between the AWG and the TX side of the switch matrix and another cable, with system response function $s(t)$, between the RX side of the switch matrix and the RTO. Using the signal measured by the RTO, the channel's path gain can be determined by comparing the estimate of the back-to-back signal to the calibrated measurement data. Following the schematic in Fig. 5-11, the measurement channel data, $y_{\mathrm{ch}}(t)$, are computed using

$$Y_{\mathrm{ch}}(f) = X_{\mathrm{ch}}(f)R(f)C(f)S(f)\,, \tag{5.9}$$

where the channel, cable R, and cable S has a frequency-domain system response function denoted by $\mathrm{C}(f), R(f), S(f)$ respectively and where $X_{\mathrm{ch}}(f) = X_{\mathrm{AWG}}(f)G_{\mathrm{amp}}(f)$ is the signal due to the AWG and power amplifier.

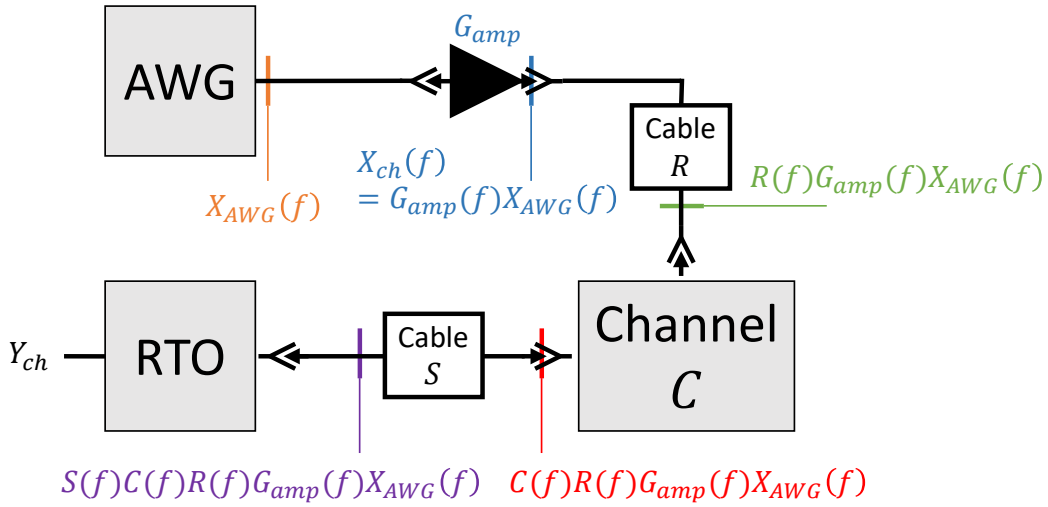

Fig. 5-11: Direct-Pulse channel sounder schematic for channel measurements. The expressions in orange, yellow, green, blue, and purple indicate the modeled value of the Fourier transform of the signal at the specified point in the system.

We assume that the AWG consistently generates the same pulse and so take $X_{\mathrm{ch}}(f) = X_{\mathrm{ref}}(f)$. Hence, using (5.8) and (5.9), an estimate of the channel may be computed using

$$C(f) = \left(\frac{Y_{\mathrm{ch}}(f)}{Y_{\mathrm{ref}}(f)}\right)\left(\frac{A(f)}{R(f)S(f)}\right). \tag{5.10}$$

The channel is estimated by a ratio of the measured channel data to the measured reference data multiplied by a calibration factor of $X_{\mathrm{atten}}(f) = (A(f)/R(f)S(f))$ composed of the attenuator and cables R and S. The same attenuator and cables were consistent throughout the Conducted-Channel measurement campaign for all days, roundabouts, and waveforms.

The Direct-Pulse channel sounder measurement of the channel, $C(f)$, is an estimate with unknown experimental noise and potential modeling errors. Care must be taken to ensure we are not dividing by zero in (5.10). When the measurement approaches low SNR, additional post-processing, which is described below, is applied to obtain accurate path gain values. A low SNR did occur during the measurement campaign in the DirectPath_3 and DirectBouncePath_3 channels.

Unlike the frequency-domain post-processing used to analyze the measurements made by the Correlation-Based channel sounder, *time-domain* post-processing and noise reduction were applied to the Direct-Pulse channel sounder data. To reduce noise and improve SNR, we averaged over repeat measurements of $y_{\mathrm{ref}}(t)$. This reduces the broadband experimental noise. Moreover, since the RTO has an offset error, we adjusted both $x_{\mathrm{ref}}(t)$ and $y_{\mathrm{ch}}(t)$ so that they have zero mean. These were the only corrections we applied for errors in the RTO response function.

We also made use of the fact that both the back-to-back and measured data are pulses, meaning that the received signal has zero power over much of the measurement time and only experimental noise remains. Hence, only experimental noise remains significant for values of t in which the received signal has primarily decayed to zero. We multiplied the back-to-back and measured data by a window function. This window function is unity for time values corresponding to high SNR and smoothly decays to zero for time values corresponding to low SNR. We artificially replaced much of the noise by zeros and, hence, increased the SNR in the frequency domain. A visualization of the windowing post-processing is shown in Fig. 5-12. This post-processing drastically improves the similarity of Direct-Pulse measurements to VNA measurements. In the low SNR cases, the estimates are nearly 5 dB closer to VNA measurements than estimates produced without any windowing.

5.3.3 Path Gain using Direct-Pulse Channel Sounder

After the post-processing of the Direct-Pulse channel sounder measurements, we estimated the channel path gain. For easier comparison with VNA measurements, we used a discrete Fourier transform of the time domain data to compute the path gain as a function of frequency for discrete frequencies between 3.3 GHz and 3.7 GHz. Path gain is defined as $G(f) = |C(f)|^2$ for a fixed frequency, computed at the reference planes indicated in Fig. 2-2.

We then computed the median path gain over this frequency range which yielded a single estimate of the channel's path gain. Note that the median path gain is more robust to outliers in the frequency-dependent path gain than the mean. In the experiments reported here, the difference between the mean and median path gain was typically less than 1 dB.

Including all the post-processing steps, we estimated channel path gain G for each fixed waveform within a fixed roundabout and fixed day as

$$G = median\left|\frac{W(f)(Y_{\mathrm{ch}}(f) - \overline{Y_{\mathrm{ch}}})}{W(f)\left(X_{ref}(f) - \overline{X_{\mathrm{ref}}}\right)} X_{Atten}(f)\right|^2, \tag{5.10}$$

where $W(f)$ is the smoothed window, $\bar{\cdot}$ indicates the average over each time point and over each waveform within a roundabout, and $E\{\cdot\}$ indicates the average of the different reference waveforms measured on a given day. The calculation of path gains and calibration of the data benefits from a reduction of the effect of measurement noise.

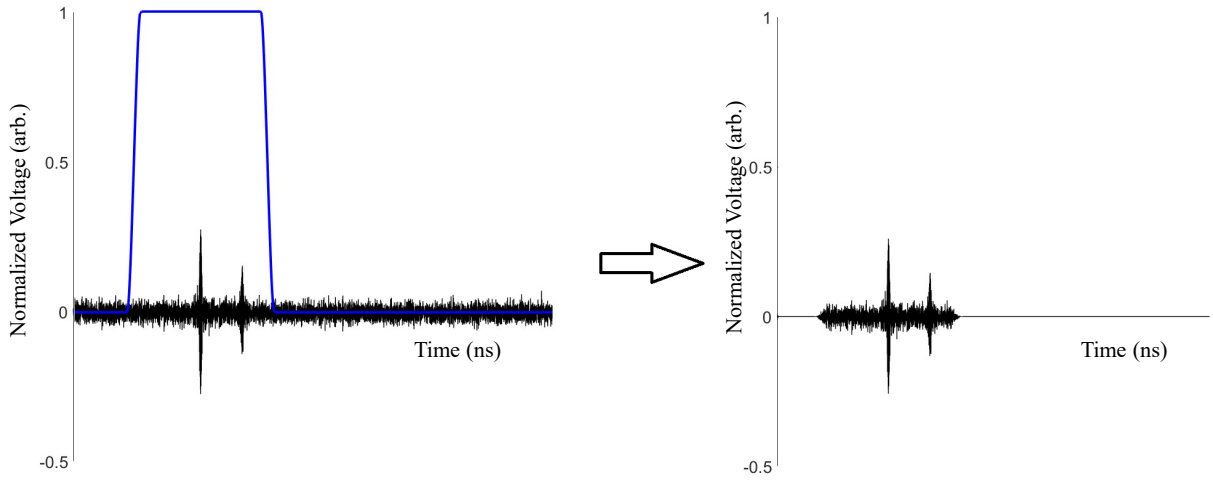

Fig. 5-12: Example of windowing procedure (blue curve) applied to a channel measurement (black curve) to reduce noise. The left figure shows the window and pre-modified measurement. The right figure shows the windowed measurement. The amplitude of the channel measurement was modified for visualization purposes.

The path gain values are shown in Table 5-12. Table 5-13 lists the variance components of the Direct-Pulse channel sounder for both the direct-only and direct-and-bounce channels. Here, $\hat{\sigma}_{dB}^2$ refers to the variability due to error and roundabout, and $\hat{\sigma}_{\mathrm{D,dB}}^2$ refers to the variability due to day. All variance components were less than 0.12 dB.

5.3.4 Direct-Pulse Channel Sounder Measurement Result

The Direct-Pulse channel sounder measurements of path gain are given in Table 5-12.

Table 5-12: Direct-Pulse channel sounder: channel comparison of path gain with VNA.

Direct Only Channel		Path Gain (dB) ± Std. Unc. (dB)	Difference
DirectPath_1	VNA	-53.48 ± 0.06	0.21 ± 0.06
	Direct Pulse CS	-53.27 ± 0.03	
DirectPath_2	VNA	-63.35 ± 0.03	0.17 ± 0.06
	Direct Pulse CS	-63.18 ± 0.05	
DirectPath_3	VNA	-73.39 ± 0.04	0.22 ± 0.06
	Direct Pulse CS	-73.17 ± 0.05	
Direct and Bounce Channel		**Path Gain (dB) ± Std. Unc. (dB)**	**Difference**
DirectBouncePath_1	VNA	-60.59 ± 0.05	0.11 ± 0.05
	Direct Pulse CS	-60.70 ± 0.02	
DirectBouncePath_2	VNA	-70.53 ± 0.06	0.16 ± 0.06
	Direct Pulse CS	-70.69 ± 0.03	
DirectBouncePath_3	VNA	-80.51 ± 0.04	0.58 ± 0.06
	Direct Pulse CS	-79.93 ± 0.04	

Table 5-13: Direct-Pulse channel sounder: variance components from Eq. E.19..

Direct Pulse CS	$\widehat{\sigma}^2_{dB}$	$\widehat{\sigma}^2_{D,dB}$
DirectPath_1	0.07	0.10
DirectPath_2	0.03	0.06
DirectPath_3	0.09	0.12
DirectBouncePath_1	0.02	0.04
DirectBouncePath_2	0.03	0.07
DirectBouncePath_3	0.02	0.06

6 Best Practices for Channel-Sounder Measurements

Accurate channel-sounder measurements require an understanding the capabilities and limitations of the channel-sounder hardware and post-processing methods. Verifying system performance using sound metrological foundations in a controlled environment provides an understanding of system operation and uncertainties. Sound metrological foundations are also part of a more general best measurement practices. These best practices ensure that measurements are repeatable, can be reproduced by other researchers to obtain accurate measurements, and can be used to better understand the processes used to make the measurement with a desired confidence level. The process used to establish these best practices is documented throughout this report and summarized here. Although these measurements were performed using three specific channel sounders and a reference VNA, these best practices can be used to establish system performance for any channel sounder.

The best practices gleaned from the conducted measurements are summarized below and explained in more detail in the remainder of this section:

1. Team involvement and coordination
2. Thorough documentation
3. Data file-name conventions and storage
4. Environmental and power parameters and requirements
5. Simple-to-complex system testing
6. Comparisons with reference measurements
7. Impact of RF connectors
8. Repeatable and stable channel
9. System parameter characterization
10. Measurement team coordination
11. Calibration of measurement equipment
12. Data verification and validation

Before beginning system verification testing, it is important to sit down with all personnel involved in the testing to design the test set-ups and procedures, decide on the measurement parameters of interest, determine a file-naming convention and the location of stored data, and coordinate the assembly of equipment at the measurement site. It is desirable to include personnel that may be providing statistical analysis from the beginning of the experimental design. The statistical analysis is a very important component in the design of the system test matrix. This procedure is the design of the experiment and leads directly to the development of a project test plan including care of the data.

As the team begins to design the experiment, it is important to provide clear documentation [40] of the system design and test procedures. These systems and procedures should be clearly communicated to all team members. Clear communication enables reproducible measurements, protection and safety of the personnel and measurement systems. Documentation should begin with a block diagram as shown in Fig. 2-1 and Fig. 2-2 of the system set-up so team members can review and avoid potential complications or missed items before testing begins. The test matrix documentation should include the expected measurement duration and order of testing. Strict file-naming conventions help to ensure accurate tracking, data storage, and data re-use over time. As the testing evolves, any support measurements, such as system losses or reflection coefficients, should be documented. It is also important to determine the power draw of the test equipment so electrical support can be properly evaluated for the measurement campaign. From the information in Table 2-3, we determined that a single 110 VAC, 20 A circuit breaker was sufficient for the measurements.

Measurement equipment can be vulnerable to fluctuations in the environment. We monitor these fluctuations in the measurement campaign environment via sensors. We document the results of our

findings in Appendix C. If an environmentally-controlled laboratory is not available, it is important to record environmental parameters during the measurements so that possible correlations can be drawn between aberrant measurements and environmental changes.

If the channel sounder has removable antennas, initial system testing should be completed in a conducted channel. The variability for a conducted channel should be smaller than in a radiated channel and any anomalies due to hardware can be more easily detected in a controlled channel. Measuring a conducted channel ensures that variation in measurements are more likely due to system variabilities as opposed to radiated channel variabilities. In addition, a switch matrix ensures a repeatable environment, especially with respect to variations in reflections due to connecting and disconnecting the RF cables.

It is important to design the conducted tests to emulate real-world scenarios that the measurement system will encounter. We designed our conducted tests to emulate the NIST open-area test site (OATS) on the NIST, Boulder campus. For this reason, the conducted channels simulated 1) path gains on the order of -50 to -80 dB by inserting a variable attenuator, 2) a second RF cable to simulate ground bounce, and 3) optional power amplifiers which are used with a given channel sounder to boost the output power of the system in a radiated environment. If a channel emulator is available, it can be used in a laboratory environment to emulate Rayleigh and Rician channels. This emulator can test the system under more complicated fading conditions, although the stability of this instrument must be included in the uncertainty analysis.

Comparisons of channel-sounder measurements to those of a reference system are valuable. If a switch matrix is not used, the VNA can be used to understand the variability due to the component connections and disconnections and due to reflections and due to losses. Next, the reference channel measurements can be shifted to the channel sounder reference planes in post-processing, as described in Section 3.1.3.

As the system is assembled prior to testing, it is important to clean all connectors and to use torque wrenches to tighten connections, especially when measuring at higher frequencies. It is important to use the appropriate torque wrench for each type of connector. This helps to ensure more accurate and repeatable measurements. Measurements of power amplifier linearity, as shown in Fig. 2-5, noise floor, and waveform characteristics as a function of detector and resolution bandwidth are also important to characterize prior to final assembly.

During testing, there should be a strong focus to direct the measurements. Having this focus leads to better testing efficiency and minimizes distractions and hazards in the testing environment. This focus will decide when measurements are to be made and the order of measurements. This focus should enable frequent discussion forums amongst team members to modify or streamline testing so that issues that arise can be addressed immediately.

After all measurements are complete, a statistical analysis should be performed on the collected data. The statistical analysis identifies and quantifies the intrinsic sources of error and variabilities due to random effects in the channel measurement equipment.

7 Next Steps

The NIST/NTIA verification of channel-sounder performance by use of a reference VNA will include other measurement environments. This report discusses conducted measurements. Next, we plan to extend this verification to short-range propagation measurements carried out on the NIST OATS located on the campus of the Department of Commerce, Boulder campus. The channel-sounding systems used in the conducted measurements described here will be used in the next phase of the project.

8 Conclusion

Laboratory verification of the NIST correlation-based channel sounder, ITS scanning-probe channel sounder, and NIST direct-pulse channel sounder was carried out using (1) a switch-matrix to switch among the systems without moving or disconnecting cables; (2) a conducted environment to study hardware-induced differences between the systems, and (3) measurements from a VNA with uncertainties due to both systematic and random effects to provide bounds of reference system performance. Best-practices are provided so channel-sounder users may perform similar verifications with their systems.

Modern waveform analysis tools such as the NIST Microwave Uncertainty Framework provided an uncertainty analysis for the VNA to establish it as the reference for comparisons to channel sounders of path gain or power delay profile. For improved comparison, the VNA reference planes were shifted to those of the channel sounder. And the VNA frequency range and filtering, if applicable, were matched to each of the channel sounders. Finally, by applying a two-tiered analysis of the random component of uncertainty, we could assess the channel sounders' variability due to random effects. In general, differences between the VNA and the channel sounders' measured path gains were less than 0.77 dB.

Appendix A — Detailed Schematic for Conducted Tests

The detailed schematic in Fig. A-1 contains component names and other attributes

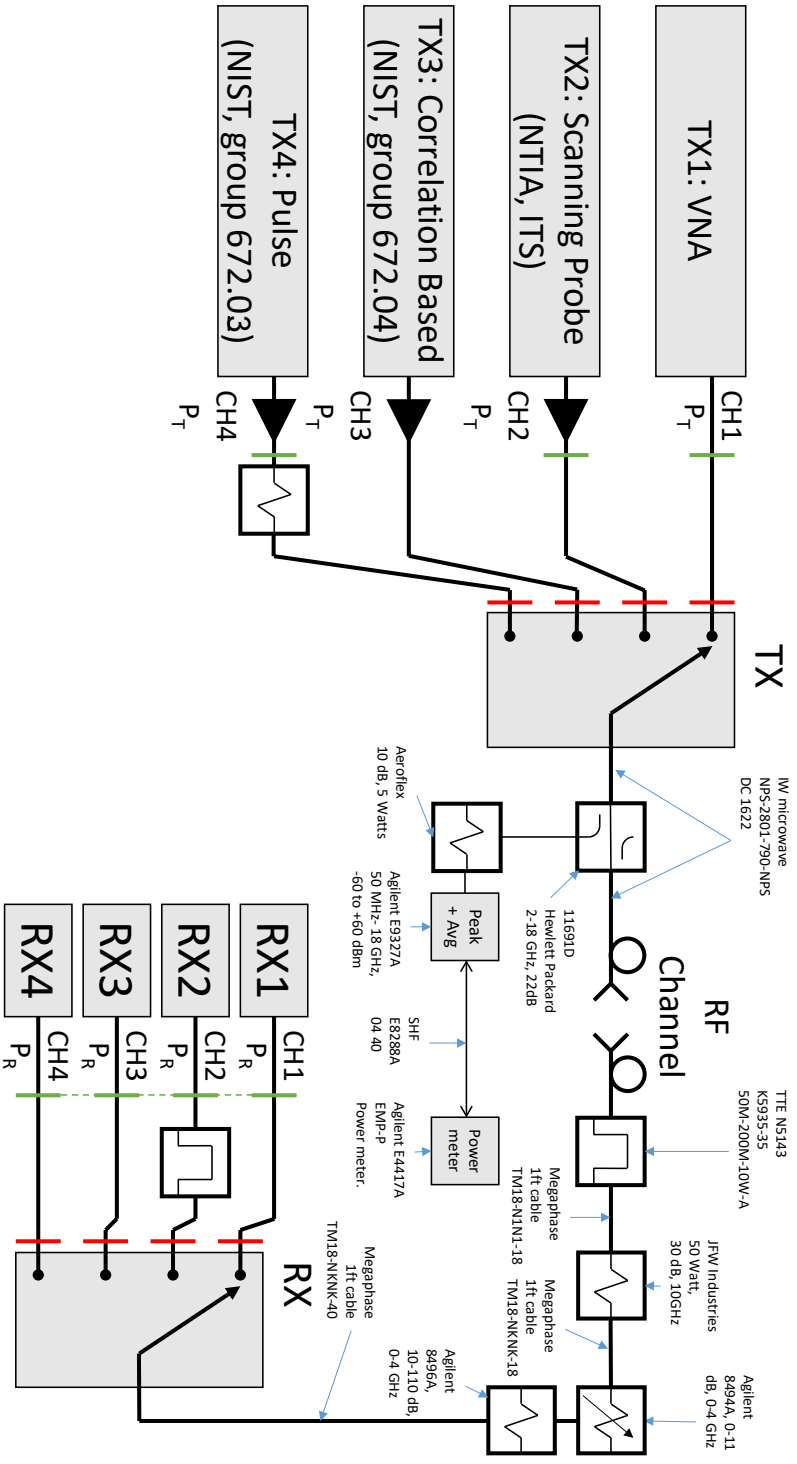

Fig. A-1: Detailed schematic for conducted tests.

Appendix B — Transmit and Receive Switch Matrices

Detailed information on the receive and transmit switch matrix components and configurations is provided here. The switch matrices' RF properties should both be derived from the measurement campaign requirements and verified through measurements prior to testing.

B.1 Transmit Switch Matrix

The switch matrix on the transmit side of the set-up consists of three double-pole, double-throw (DPDT) transfer switches and one single-pole, double-throw (SPDT) switch, all electronically controlled, as shown in Fig. B-1(a). The multiple-switch set-up was used to allow for switching of high-power signals and so that all inactive TX ports were switched to 10 W, 50 Ω loads. The photograph in B-1(b) illustrates the transmit switch matrix. Depressing various configurations of the color-lighted push-buttons connects the input of the various TX ports to the output port of the transmit switch matrix (and hence the input to the channel).

Table B-1 provides a summary of transmit switch matrix states describing the state of each switch required to connect each TX port to the channel input. The third row "Buttons to Press" shows the configuration of push buttons needed for each TX port. The "None" column connects all four TX ports to 50 Ω loads and serves to reset the switches prior to changing to another TX configuration.

In Fig. B-2(a), the coaxial-cable connections between the switch ports are diagrammed. In Fig. B-2(b), wiring diagrams with the power connections to the switches for each channel sounder configuration are provided. The wiring diagrams for the different TX switch states are shown in Figs. B-3 and B-4. Table B-2 provides a parts list for the switch matrix.

Table B-1: Transmit Switch Matrix States.

Output		None	TX1	TX2	TX3	TX4
Switch position	DPDT #1	1	1	2	1	1
	DPDT #2	1	1	1	2	2
	DPDT #3	1	1	1	1	2
	SPDT	1	2	2	2	2
Input is directed to	TX1	Load 2	Output	Load 1	Load 3	Load 3
	TX2	Load 1	Load 1	Output	Load 1	Load 1
	TX3	Load 3	Load 3	Load 3	Output	Load 4
	TX4	Load 4	Load 4	Load 4	Load 4	Output
Buttons to Press	White	X				
	Blue					X
	Green			X		
	Orange				X	X
	Red		X	X	X	X

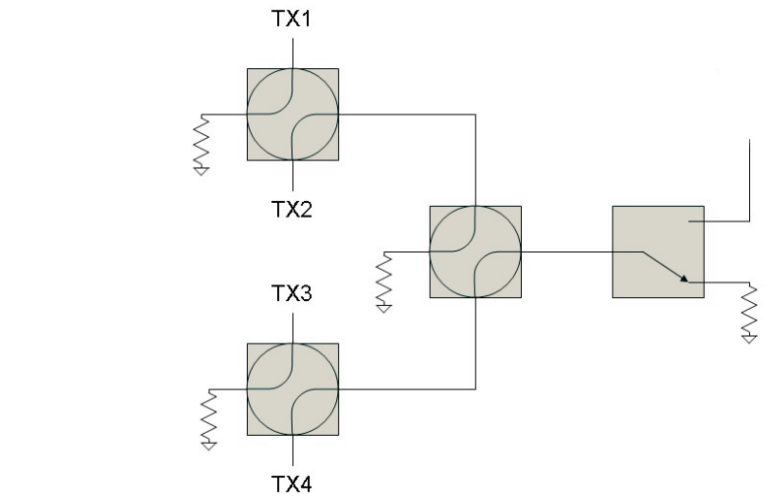

(a)

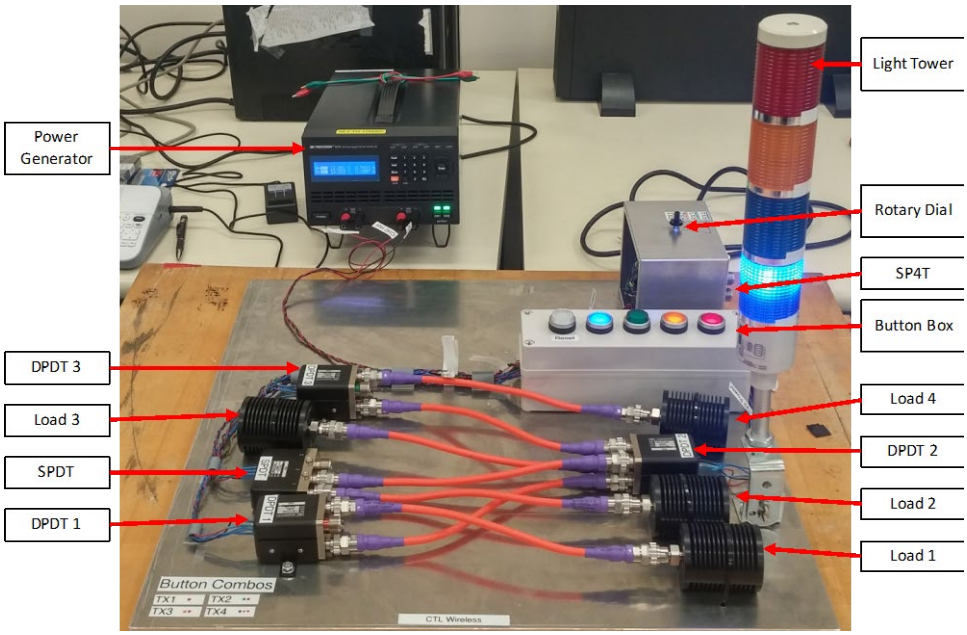

(b)

Fig. B-1: (a) Schematic of the TX switch assembly. (b) Transmit switch matrix showing the three DPDT and one SPDT transfer switches required to connect the various channel sounder TXs to the input of the channel. The TXs that are not connected to the channel are terminated in high-power 50 Ω loads.

Coaxial diagram for no output

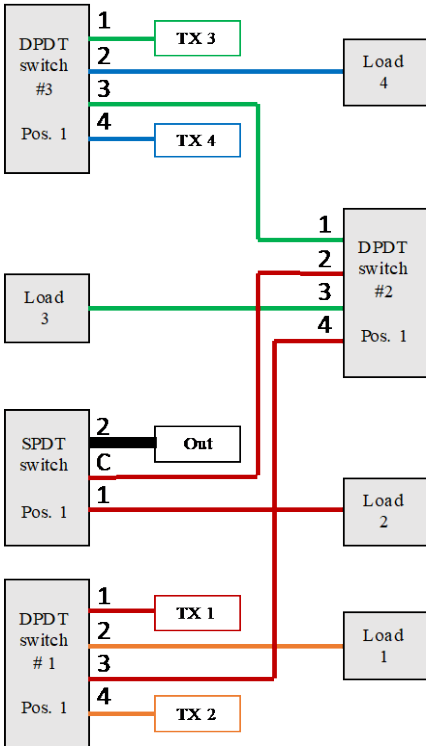

State Reset: No Output

DPDT switch #1:	Position 1
DPDT switch #2:	Position 1
DPDT switch #3:	Position 1
SPDT switch:	Position 1

Input	Directed to
TX1 (Red)	Load 2
TX2 (Orange)	Load 1
TX3 (Green)	Load 3
TX4 (Blue)	Load 4

Button(s) to press: White

(a)

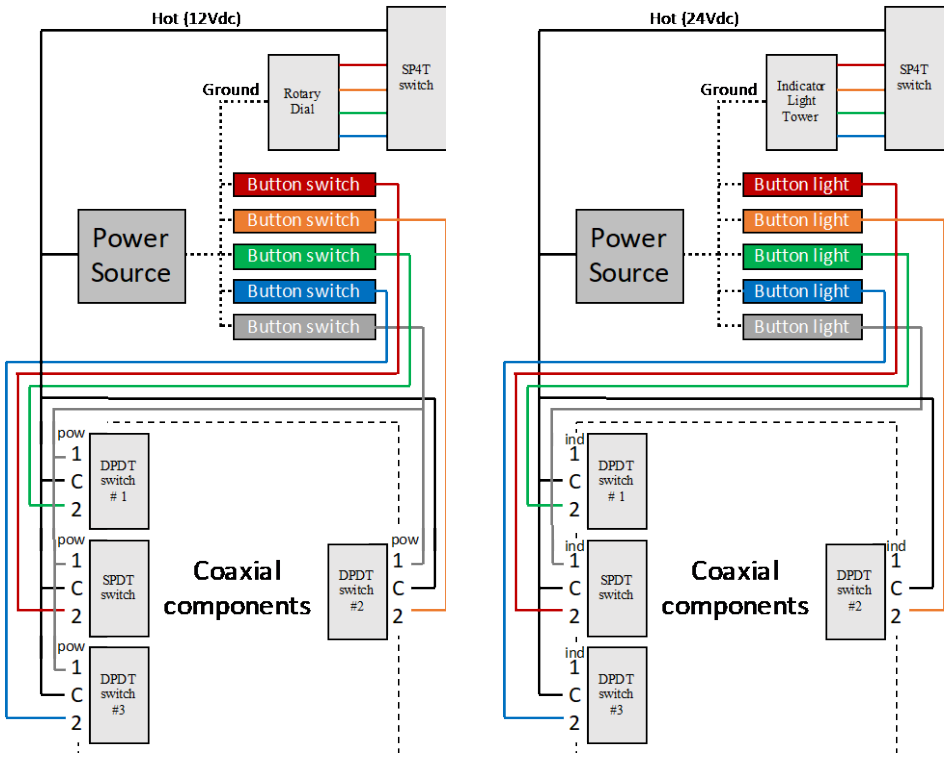

Switch power circuit

Indicator light circuit

(b)

Fig. B-2: (a) Coaxial cable connections and (b) wiring diagrams.

Coaxial diagram for TX1 out

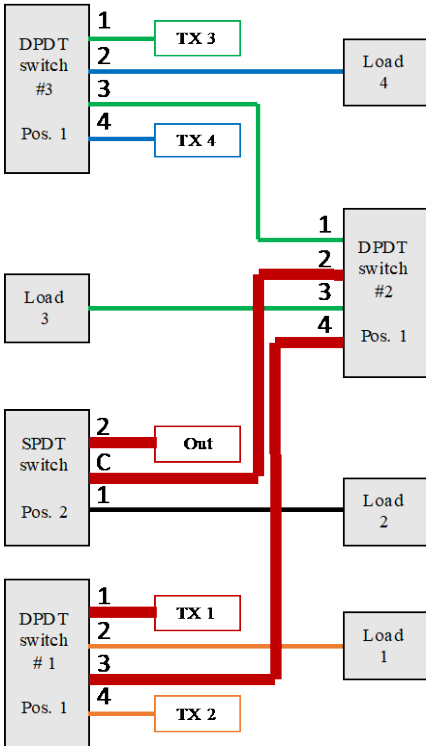

State 1: Output TX1

DPDT switch #1:	Position 1
DPDT switch #2:	Position 1
DPDT switch #3:	Position 1
SPDT switch:	Position 2

Input	Directed to
TX1 (Red)	Out
TX2 (Orange)	Load 1
TX3 (Green)	Load 3
TX4 (Blue)	Load 4

Button(s) to press: Red

Coaxial diagram for TX2 out

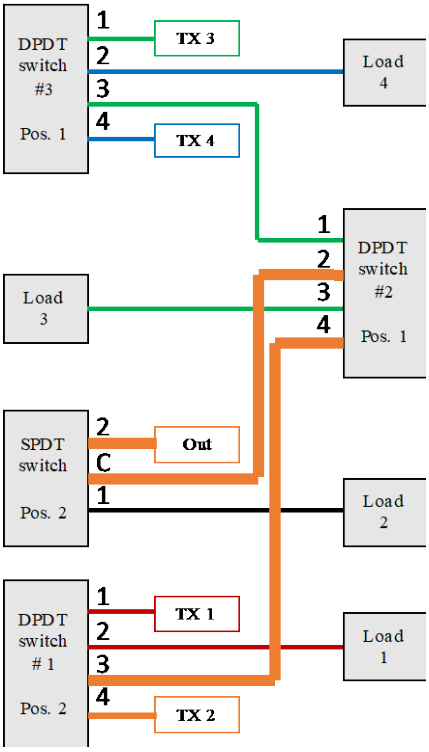

State 2: Output TX2

DPDT switch #1:	Position 2
DPDT switch #2:	Position 1
DPDT switch #3:	Position 1
SPDT switch:	Position 2

Input	Directed to
TX1 (Red)	Load 1
TX2 (Orange)	Out
TX3 (Green)	Load 3
TX4 (Blue)	Load 4

Button(s) to press: Red, Green

Fig. B-3: Coaxial cable connections.

Coaxial diagram for TX3 out

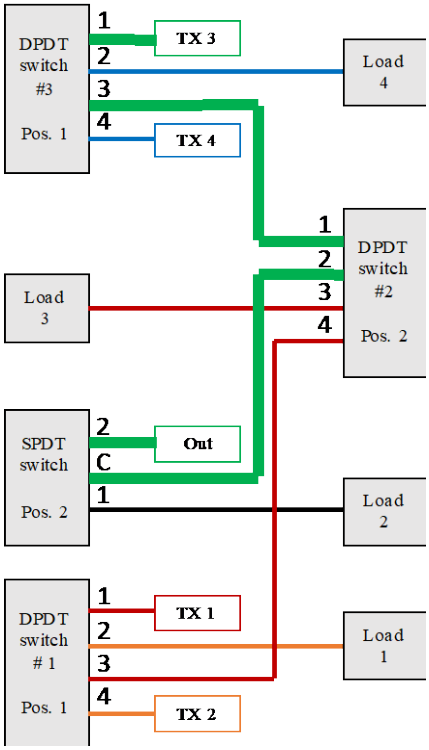

State 3: Output TX3

DPDT switch #1:	Position 1
DPDT switch #2:	Position 2
DPDT switch #3:	Position 1
SPDT switch:	Position 2

Input	Directed to
TX1 (Red)	Load 3
TX2 (Orange)	Load 1
TX3 (Green)	Out
TX4 (Blue)	Load 4

Button(s) to press: Red, Orange

Coaxial diagram for TX4 out

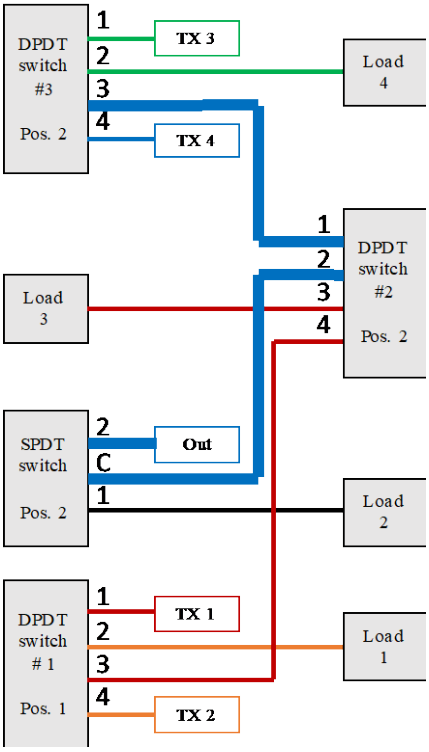

State 4: Output TX4

DPDT switch #1:	Position 1
DPDT switch #2:	Position 2
DPDT switch #3:	Position 2
SPDT switch:	Position 2

Input	Directed to
TX1 (Red)	Load 3
TX2 (Orange)	Load 1
TX3 (Green)	Load 4
TX4 (Blue)	Out

Button(s) to press: Red, Orange, Blue

Fig. B-4: Coaxial cable connections.

Table B-2: Part List for Switch Matrices. The mention of brand names does not imply an endorsement by NIST or NTIA. Other products may work as well or better.

Parts List	
Switch matrix quantities	Switch matrix description
1	LED-Andon five color, 24 Vdc Indicator Lamp Kit (KT-2224-000)
1	LED-Andon four color, 24Vdc LED Stack Light (LD-5224-100)
3	Charter Engineering DPDT mechanical switch (L2N-311100)
1	Charter Engineering SPDT mechanical switch (U4N-311100)
1	Charter Engineering SP4T mechanical switch (B5N-311100)
7	Megaphase RF Orange™ Test Cable
Channel hardware quantities	Channel hardware description
2	Meca 2-way N-Female Power Divider/Combiner (802-4-3.250WWP)
1	UtiFLEX Ultra Low Loss coaxial cable (UFB311A)
2	Federal Cable N Male LMR300 N Male 12" Cable Assembly (CA5905-12)
1	Federal Cable N Male LMR300 N Male 24" Cable Assembly (CA5905-24)

B.2 User Guide for Switch Matrices

Turn on the power supply. The voltage for the switches should be set at 12 VDC, and 24 VDC for the indicator lights. Both voltage supplies should have a current limit of 1 Amp.

To get the desired output, perform the following steps:

1. Turn the dial on the receiver switch matrix to match the desired output. This must be done before adjusting any of the buttons.
2. Press the combination of the blue, green, orange, and red on the TX Switch matrix for the desired input using Table B-3.
3. Check that the only buttons that are pressed down are specified in the table below. The indicator lights on the buttons should also match the table below, and the white light should be unlit.

After each channel sounder measurement, the system should be reset.

1. After the roundabout (defined in Section 2.5 of this report) is done, press the white reset button.
2. Check that none of the colored lights are on. If they are, make sure that the corresponding button is not pressed down.

To power off the system, simply turn off the power supply.

Table B-3: TX switch matrix configuration.

	Blue	Green	Orange	Red
TX1				X
TX2		X		X
TX3			X	X
TX4	X		X	X

B.3 Receive Switch Matrix

The receive switch matrix consists of one manually controlled single-pole, four throw (SP4T) switch and is shown in Fig. B-5. It is controlled by a rotary knob shown on the top of the metal box at the lower right. The “Light Tower” indicates which of the four RXs is connected to the channel.

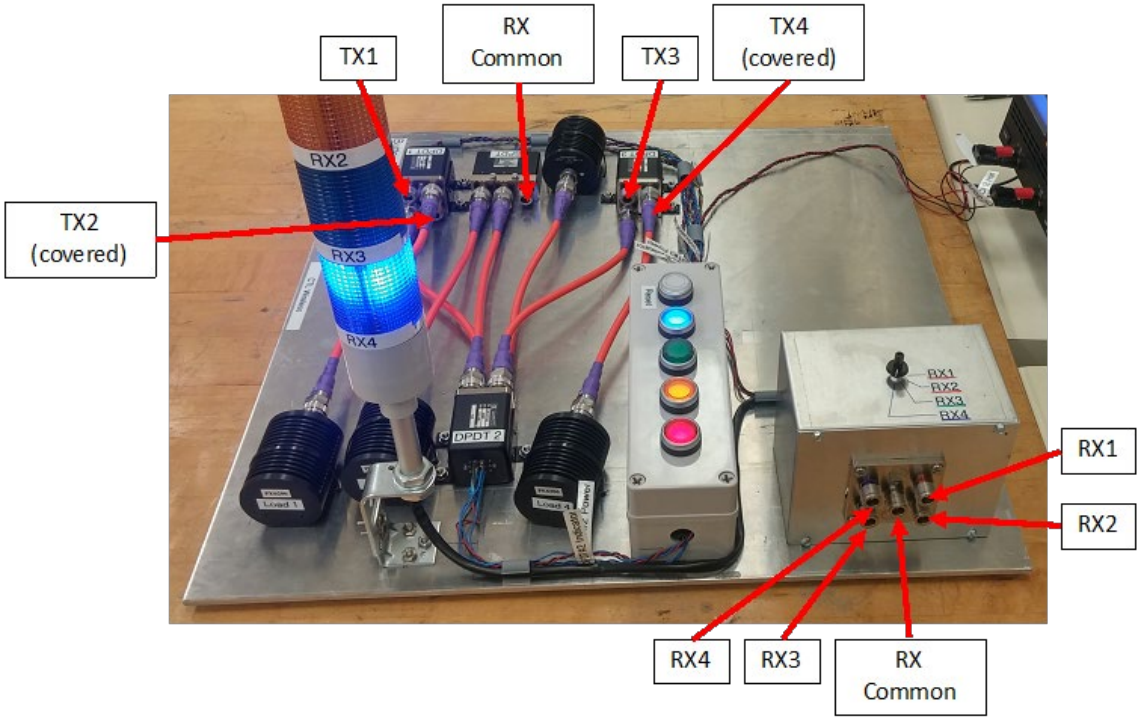

Fig. B-5: Receive switch matrix showing the SP4T switch that connects the output of the channel to the various channel sounder receivers.

Appendix C — Environmental Conditions During Measurements

We measured the environmental conditions of the laboratory. The statistical analysis should capture any measurement uncertainties due to environmental effects. The conditions measured were temperature, humidity, and atmospheric pressure as seen in Figs. C-1, C-2, and C-3, respectively. The NIST correlation-based channel sounder power amplifier was recorded at the start of its measurement during a roundabout in Fig. C-4.

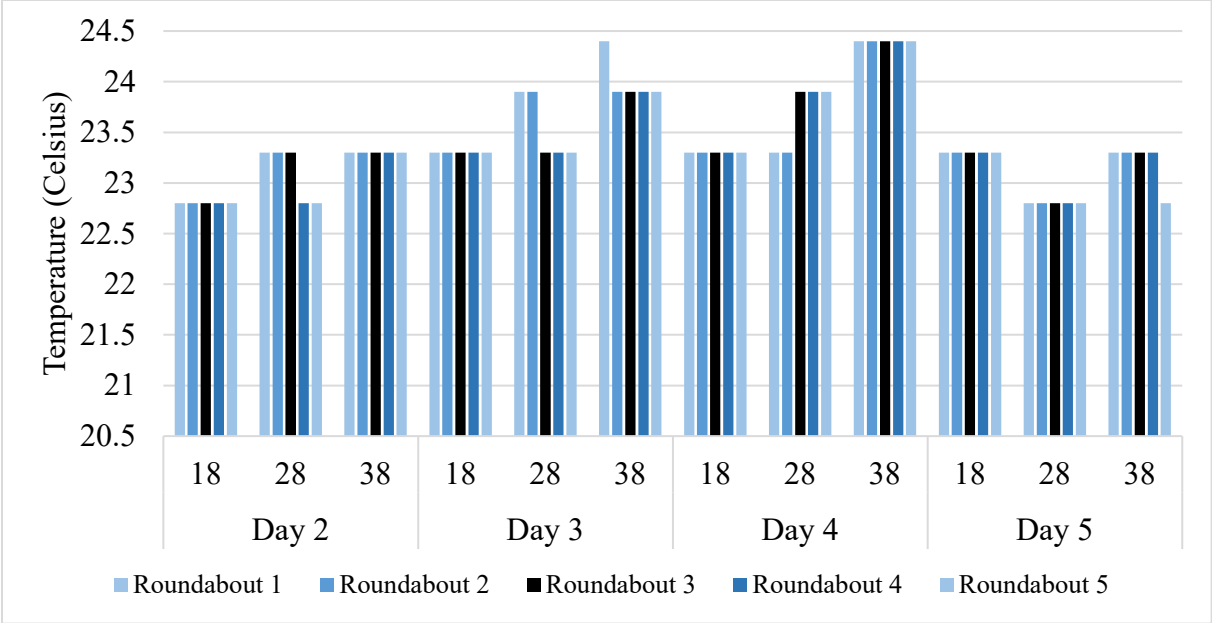

(a)

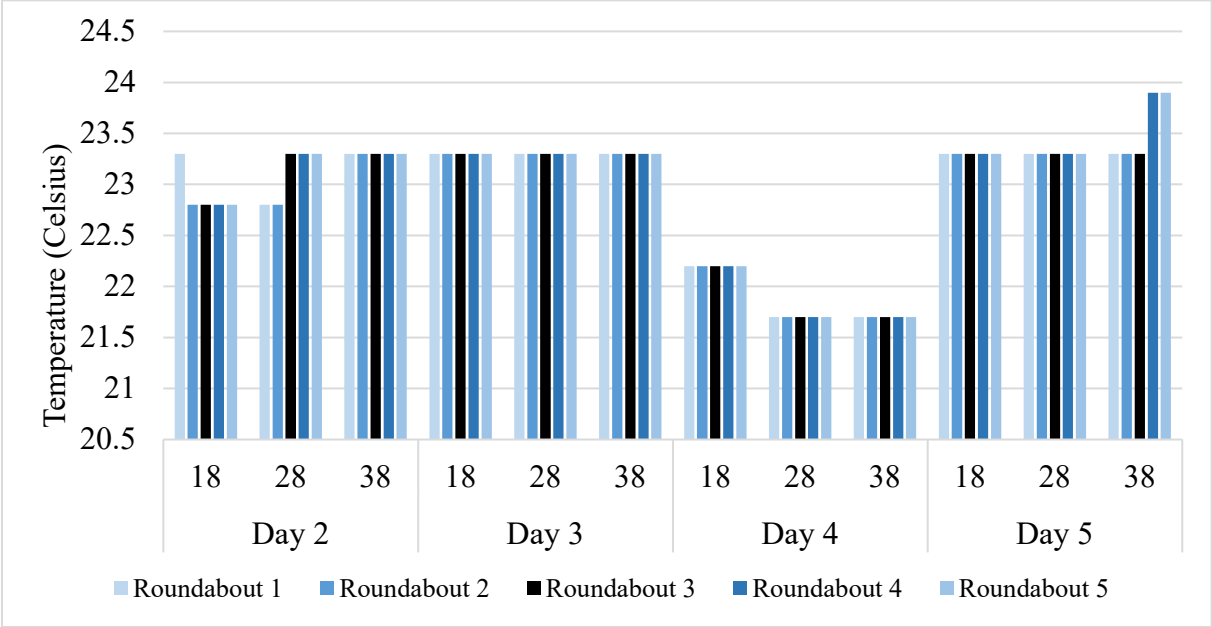

(b)

Fig. C-1: Temperature measurements of the laboratory test environment for the different set-ups, attenuations, roundabouts, and days for (a) direct-and-bounce-paths tests and (b) direct-path-only tests. 18, 28, and 38 refer to the attenuation setting for Attenuator 2 from Table 2-1 and Table 2-2, respectively.

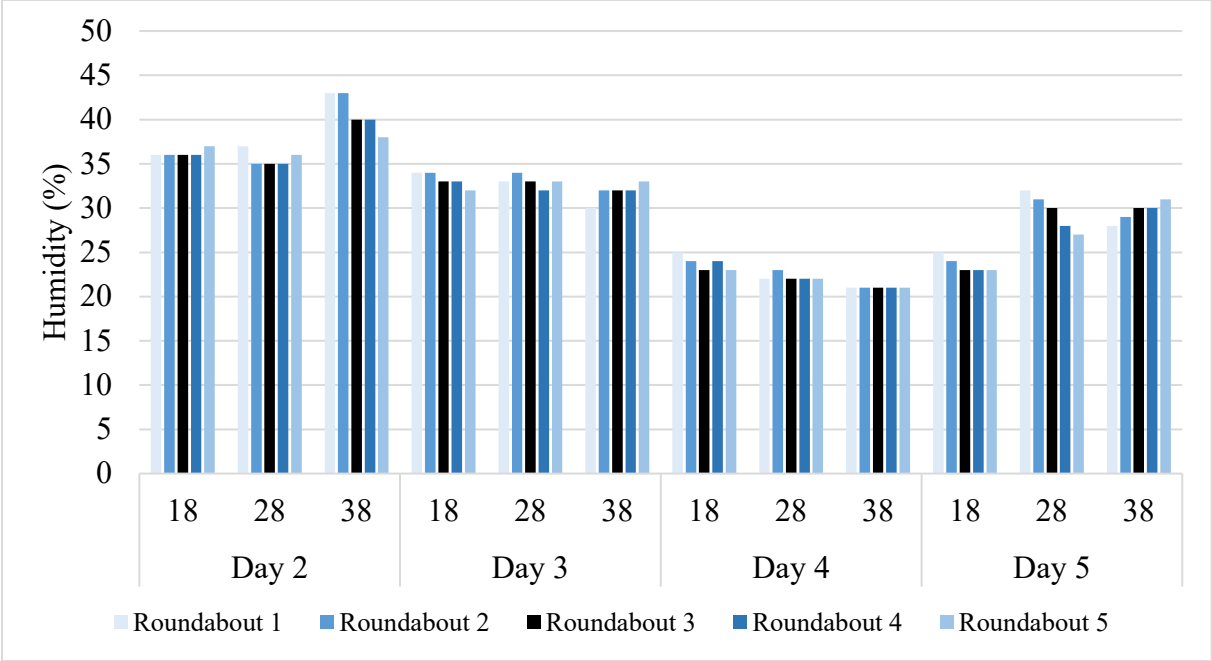

(a)

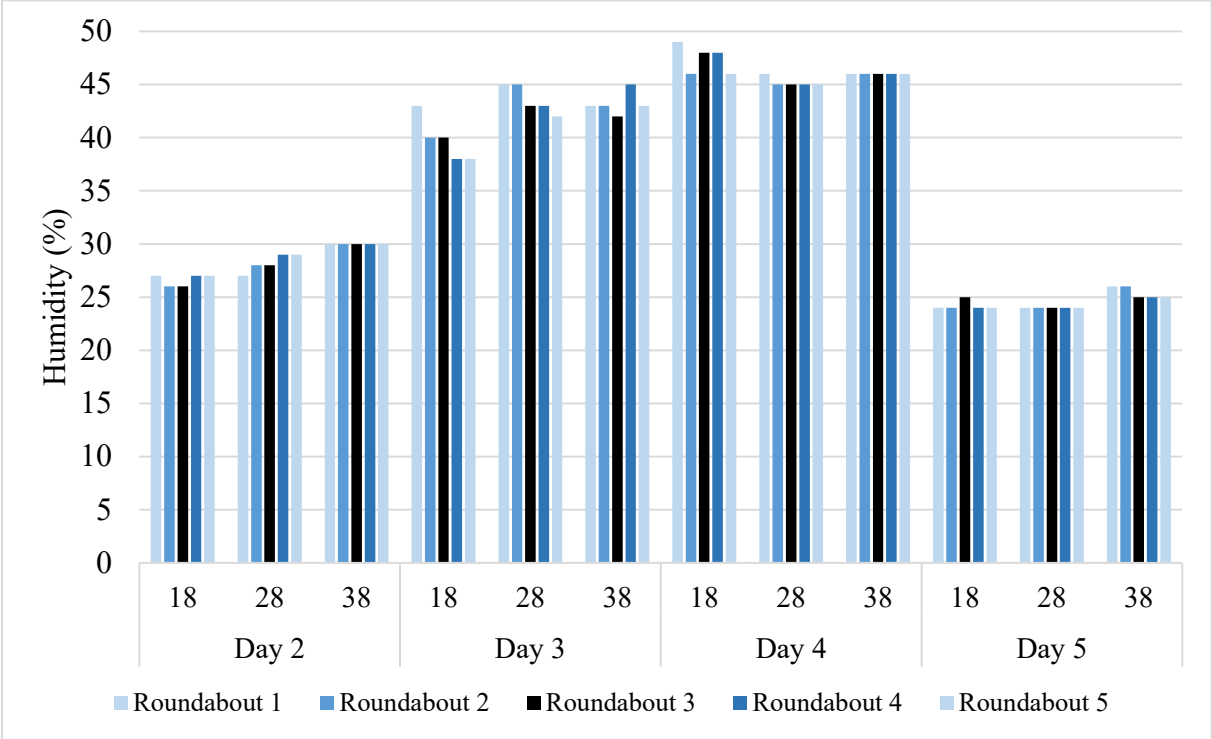

(b)

Fig. C-2: Humidity measurements of the laboratory test environment for the different set-ups, attenuations, roundabouts, and days for (a) direct-and-bounce-paths tests and (b) direct-path-only tests. 18, 28, and 38 refer to the attenuation setting for Attenuator 2 from Table 2-1 and Table 2-2, respectively.

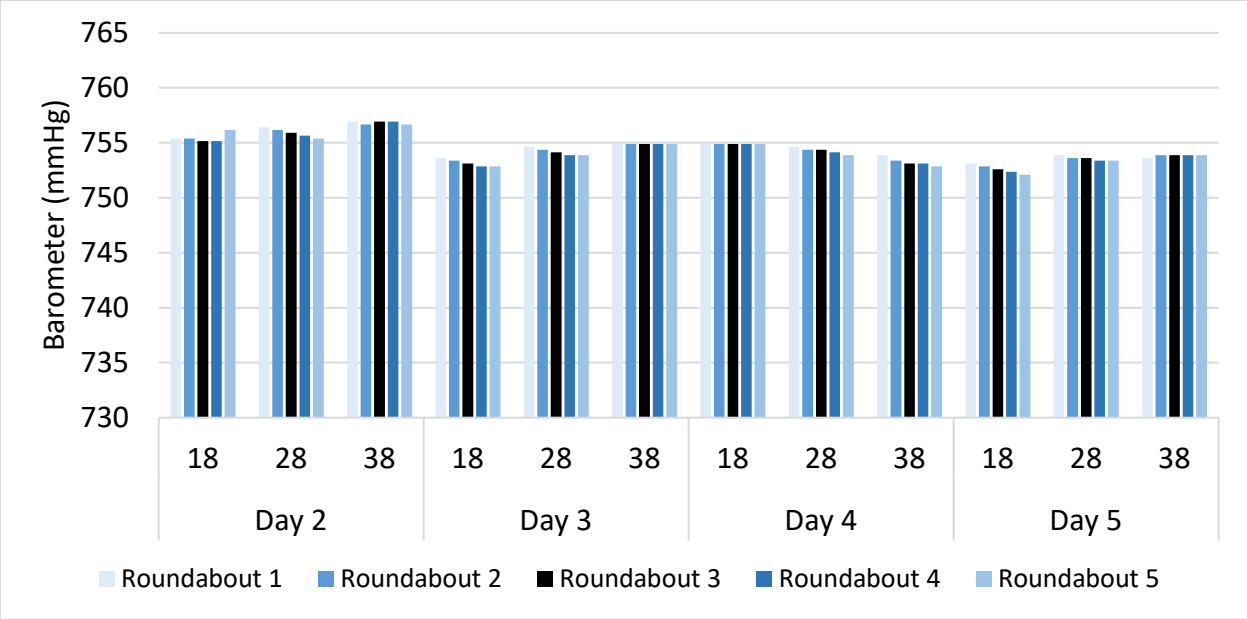

(a)

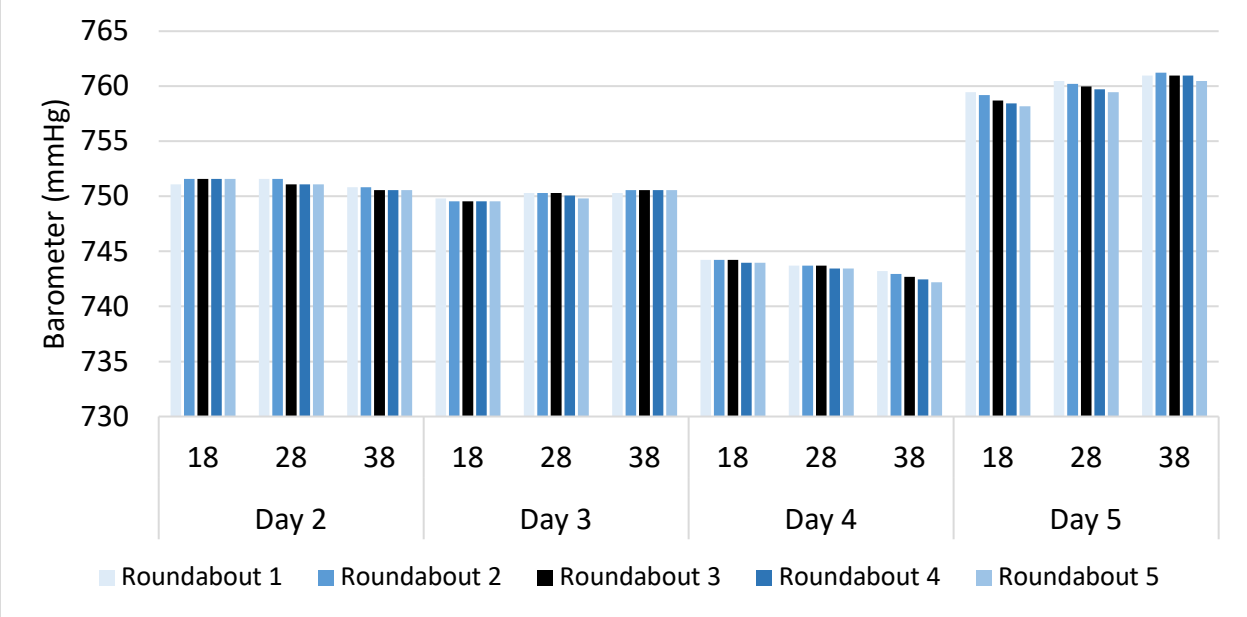

(b)

Fig. C-3: Pressure measurements of the laboratory test environment for the different set-ups, attenuations, roundabouts, and days for (a) direct-and-bounce-paths tests and (b) direct-path-only tests. 18, 28, and 38 refer to the attenuation setting for Attenuator 2 from Table 2-1 and Table 2-2, respectively.

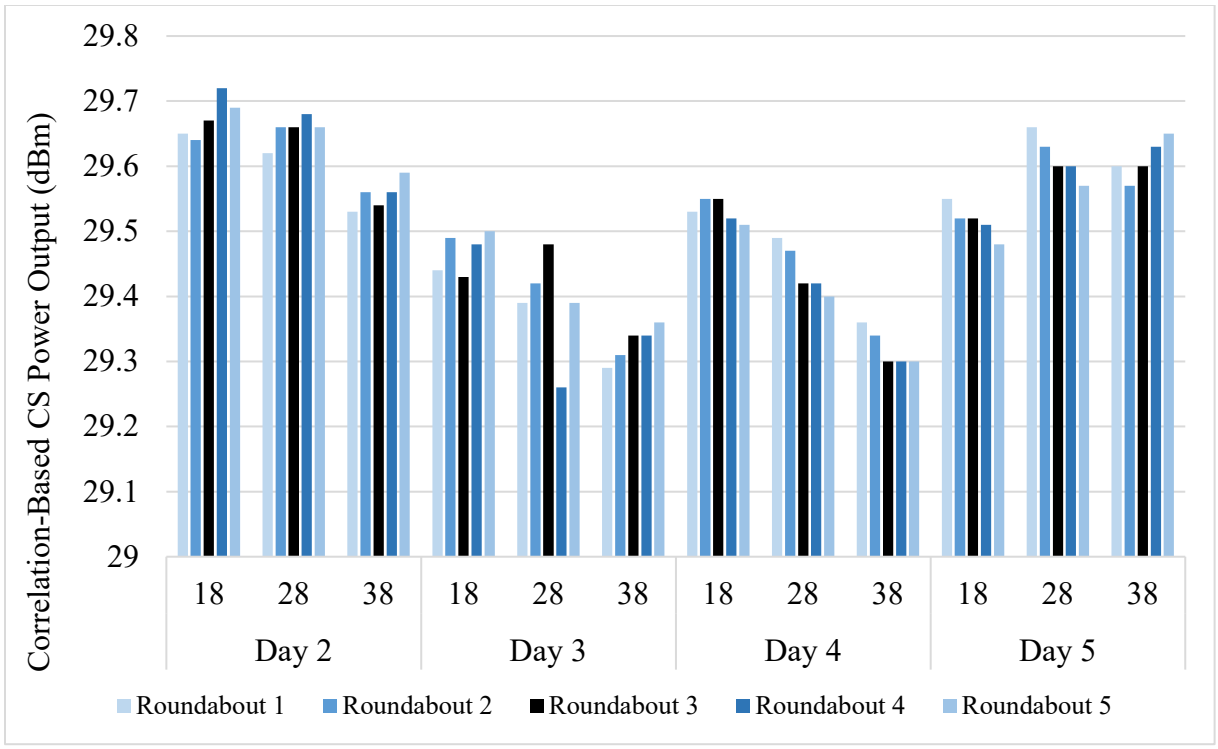

(a)

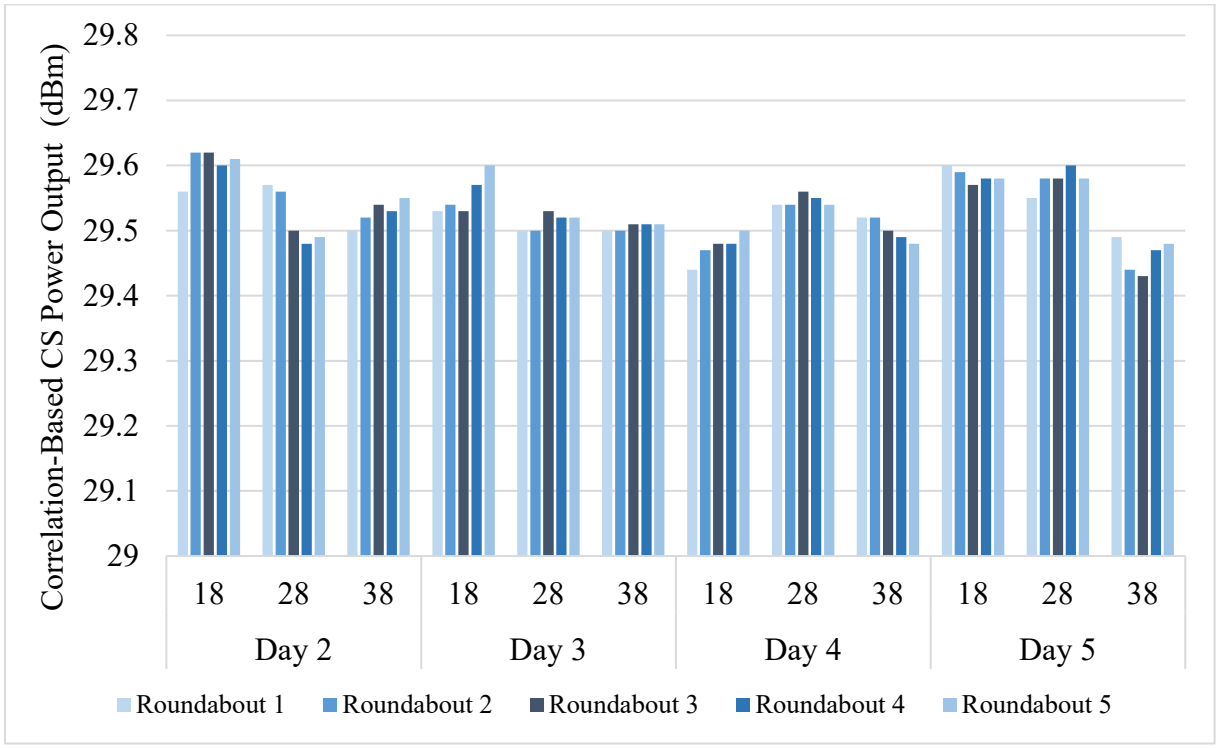

(b)

Fig. C-4: Correlation-based CS TX-amplifier power readings for the different set-ups, attenuations, roundabouts, and days for (a) direct-and-bounce-paths tests and (b) direct-path-only tests. 18, 28, and 38 refer to the attenuation setting for Attenuator 2 from Table 2-1 and Table 2-2, respectively.

Appendix D — Environmental Chamber Tests of 15.2 m Cable

The 15.2 m (50 foot) coaxial cable that was used in the direct-plus-bounce channel was subjected to environmental testing as shown in Fig. D-1. We expected the losses and phase-changes to be significant as the cable was measured with a vector network analyzer at four temperatures (6 ºC, 23 ºC, 40 ºC, and 49 ºC) and one humidity setting, 50 % relative humidity (RH). These temperatures were chosen because they were expected to simulate possible real-world testing temperatures both at the OATS and during mobile measurements.

During testing, the cable was placed in the temperature- and humidity-controlled environmental chamber from 8 to 24 hours before using the VNA to measure the S-parameters of the cable. Only one measurement was made at each temperature setting, except at 23 ºC. The measurement data were then input into the NIST MUF for an uncertainty analysis. The MUF generates uncertainties for the measurements, propagated from uncertainties due to systematic effects in the calibration standards.

The resultant data for the four temperature measurements are shown in Fig. D-2. The solid green line shows the cable loss magnitude, S_{21}, in decibels (dB) vs. frequency in gigahertz (GHz) at a temperature of 6 ºC. The solid red and black lines show the cable-loss for the room-temperature measurements (23 ºC). The solid blue and pink lines show the magnitude of the cable loss at a temperature of 40 ºC and 49 ºC, respectively. The cable loss difference from 6 ºC to 49 ºC at 1.5 GHz is approximately 0.06 dB, and at 3.5 GHz is approximately 0.19 dB.

The cable is optimized to operate at room temperature. Fig. D-2(b) shows the phase differences between room temperature (23 ºC) and 6 ºC (green), room temperature and 40 ºC (blue), and room temperature and 49 ºC (pink). The phase difference for the green line is approximately -1.5 degrees at 1.5 GHz and decreases to approximately -4.2 degrees at 3.5 GHz. The phase difference for the blue line is approximately -4.1 degrees at 1.5 GHz and increases to approximately -10.0 degrees at 3.5 GHz. And the phase difference for the pink line is approximately -7.3 degrees at 1.5 GHz and increases to approximately -17.4 degrees at 3.5 GHz.

The following figures show the manufacturer's specifications for maximum insertion loss (Fig. D-3(a)) and typical phase change vs. temperature (Fig. D-3(b)) for low-loss UTiFLEX® cables provided by Micro-coax [36].

(a) (b)

Fig. D-1: (a) NIST environmental chamber and (b) 15.2 m cable being tested within the chamber.

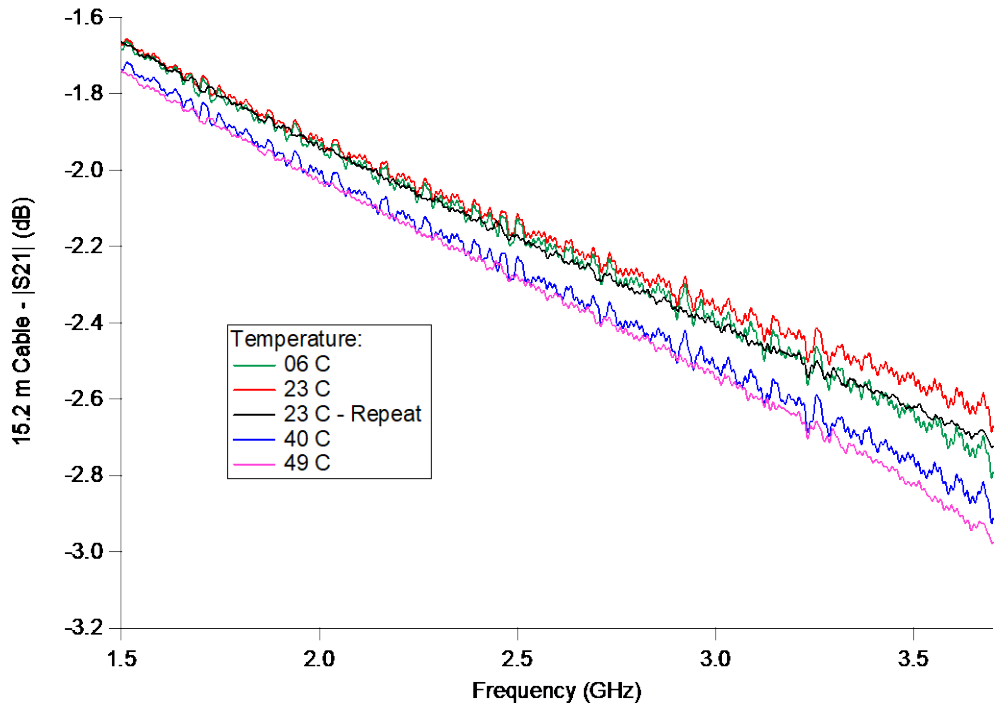

(a)

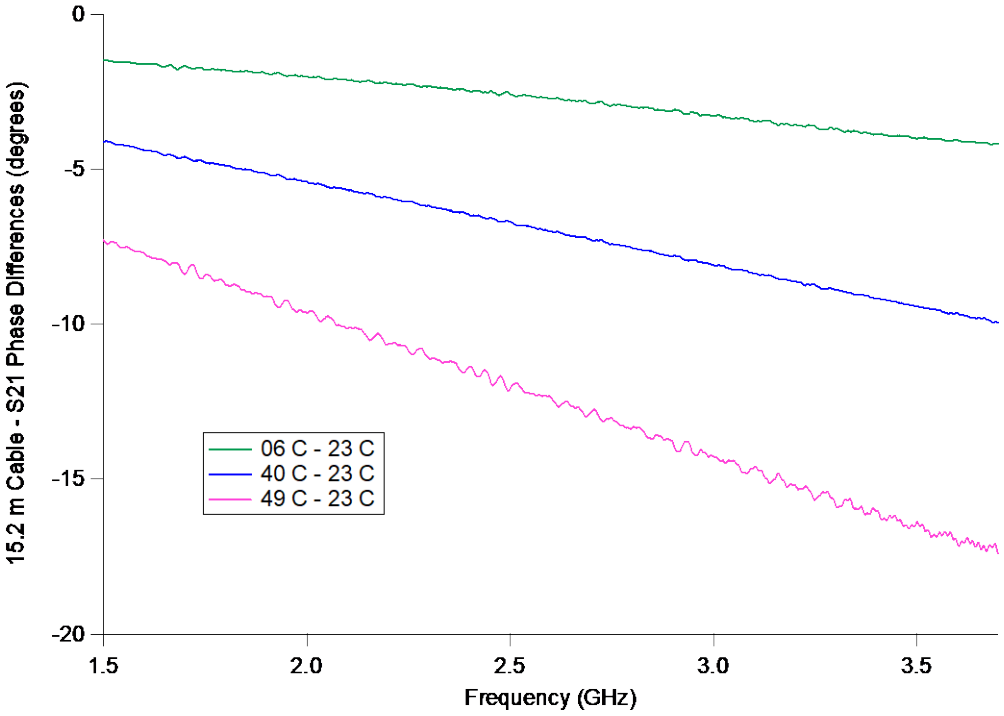

(b)

Fig. D-2: (a) Measurements for a 15.2 m RF cable at four temperatures. (b) Phase differences for a 15.2 m RF cable from 6 ºC to 23 ºC (green line), from 23 ºC to 40 ºC (blue line), and from 23 ºC to 49 ºC (pink line).

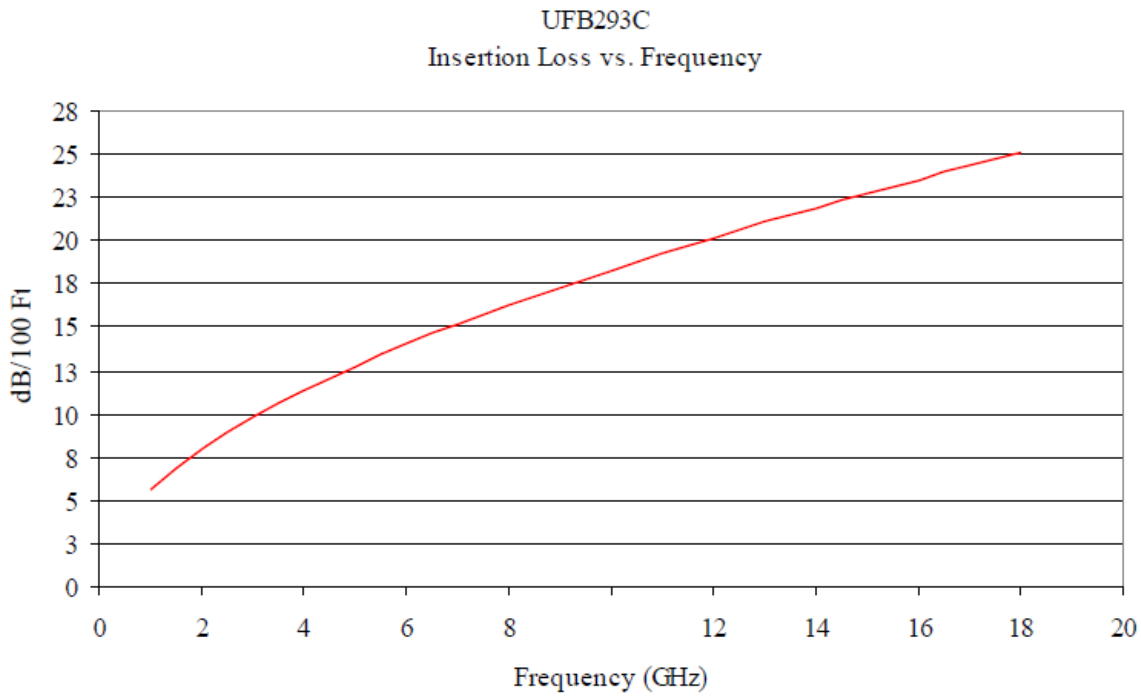

(a)

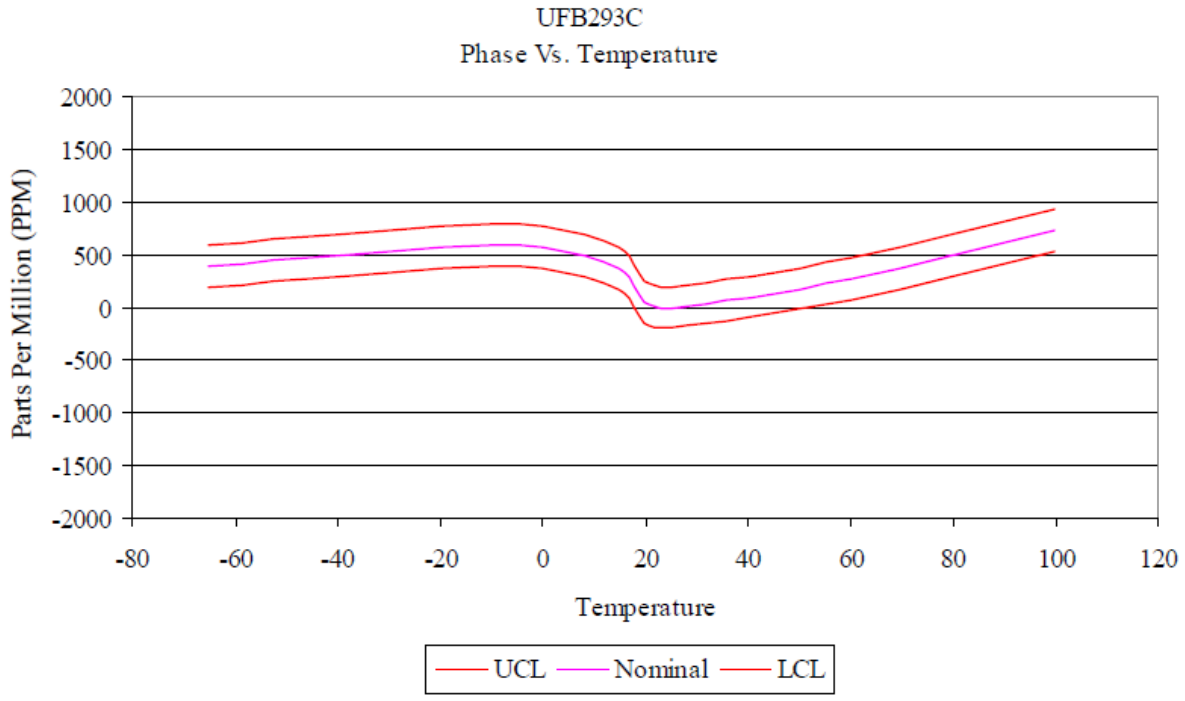

(b)

Fig. D-3: Manual specifications (a) Insertion loss vs. frequency specifications for UTiFLEX® UFB293C Micro-Coax, Inc. cables. (b) Typical phase change versus temperature for the same cable. UCL is the upper control limit and LCL is the lower control limit.

Appendix E — Random Effects Model Technical Approach

This Appendix provides a technical description of the random effects model. We also discuss the appropriateness of applying the model to data collected from the conducted-channel measurement campaign. The procedure used to implement a random effects model analysis includes exploratory data analysis using visual inspection and autocorrelation function plots. After completing the exploratory data analysis, a model that is suitable to be used with the measurement data is provided, and an analysis of variance (ANOVA) method is used to estimate model parameters [31]–[34].

Based on the conducted-cable measurement campaign procedure, we start by assuming the data follows the random effects Model 1

$$X_{ijk} = G + D_i + R_{j(i)} + \epsilon_{k(ij)}, \tag{E.1}$$

for $i = 1, \dots, I$ ($I =$ number of days), $j = 1, \dots, J$ ($J =$ number of roundabouts in a day), and $k = 1, \dots, K$ ($K =$ number of measurements within a roundabout). Here $D_i \sim N(0, \sigma_D^2)$ is an effect due to day, $R_{\mathrm{j}(i)} \sim N(0, \sigma_R^2)$ is an effect due to roundabout, and $\epsilon_{(ij)k} \sim N(0, \sigma^2)$. Under this model, we assume that our measurement channels are stable and that all repeat measurements are measuring the same quantity (G, path gain measured by the channel sounder under the same conditions) with some variability due to day, roundabout, and repeat measurement error. We also assume that the path gain measurements are independent. It is important to check these assumptions before we proceed with the analysis using this model.

E.1 Exploratory Data Analysis

E.1.1 Visual Inspection

The first step is to visually inspect time series of all the data. Here we are looking for evidence that the measurement process is not stable, and we are looking for possible outliers. The visual inspection allows us to flag and assess measurements that look out of place. We do not advocate simply removing outliers, but we do recommend investigating why they occur. If, after investigation, it is determined that the outlier is erroneous, it can be removed to avoid letting a bad data point unduly influence results [37].

Fig. E-1 shows an example of an outlier discovered during exploratory data analysis of the Direct-Pulse channel sounder measurements. In two roundabouts (of the 150 total for this system), the very first measurement was very far from all other repeat measurements in the time series. These points were flagged as suspicious, and further investigation revealed an issue in the post-processing of the data. This post-processing error was corrected before the analysis proceeded.

Fig. E-2 shows time series of repeat measurements taken with the Correlation-Based channel sounder during three different roundabouts. The first series of repeat measurements displays the behavior we are looking for. The measurement system looks stable and the repeat measurements appear to be measuring the same quantity, with random noise. The second plot shows evidence that the measurement process was not stable in the first 200 measurements. The third plot suggests that the repeat measurements may come from two different distributions. Further investigation revealed that the amplifier had not been turned on at the beginning of this set of measurements. Since this is an example of bad data, it would be prudent to remove these measurements before continuing with the analysis.

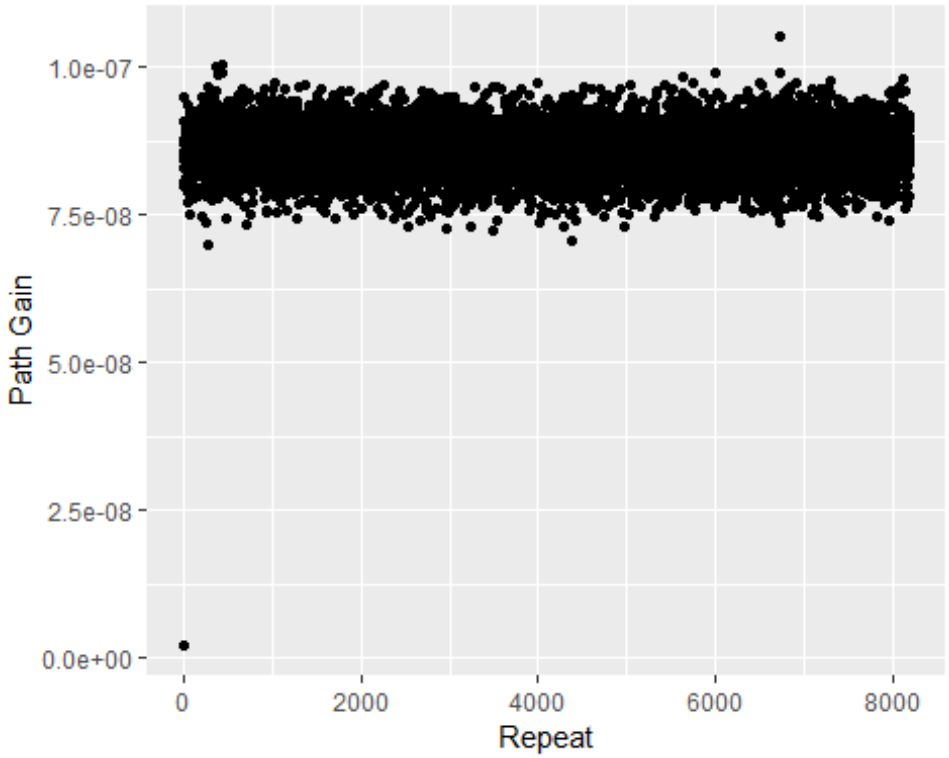

Fig. E-1: Outlier from Direct-Pulse channel sounder at lower left of the chart. This point (and another just like it on a different roundabout) is flagged as suspicious because it is the very first measurement and it is very far from all other measurements.

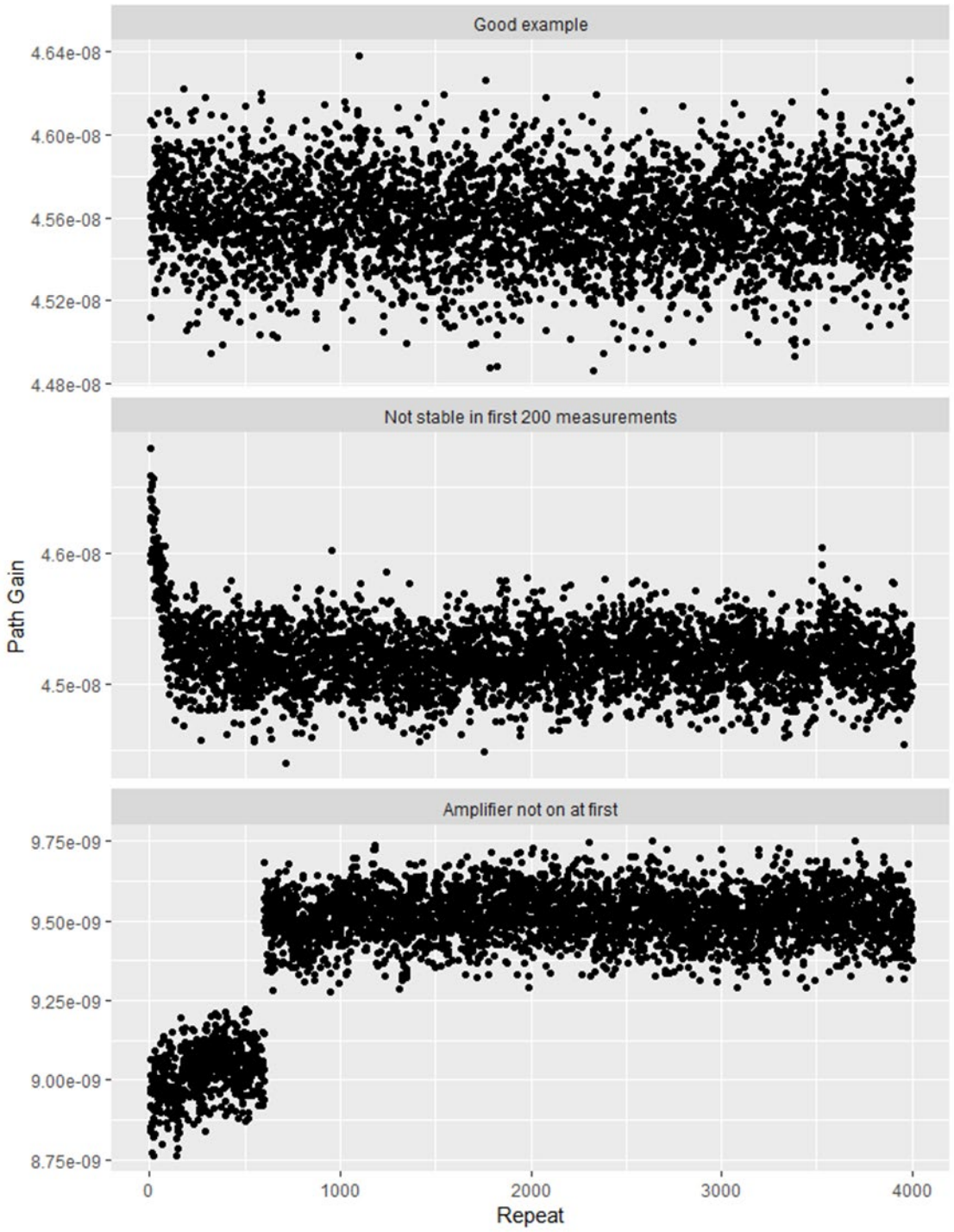

Fig. E-2: Time series of repeat measurements taken with the Correlation-Based channel sounder during three different roundabouts. The first figure shows behavior acceptable for Model 1 (see description of Model 1 in Section 4.1.2). The other figures show violated assumptions for Model 1.

Fig. E-3 shows all measurements of path gain for one channel configuration (direct bounce and 38 dB attenuation) taken with the Correlation-Based channel sounder during five roundabouts on one day. Measurements from different roundabouts are denoted by different colors. From this plot, the measurements from Roundabout 1 are different than the measurements from the other four roundabouts.

Possible sources of the difference may be due to a poor coaxial connection to the switch matrix. This is a possible violation of the assumption that all repeat measurements are measuring the same quantity (G, path gain measured by the channel sounder under the same conditions). These measurements are flagged and assessed as well using the analysis provide here.

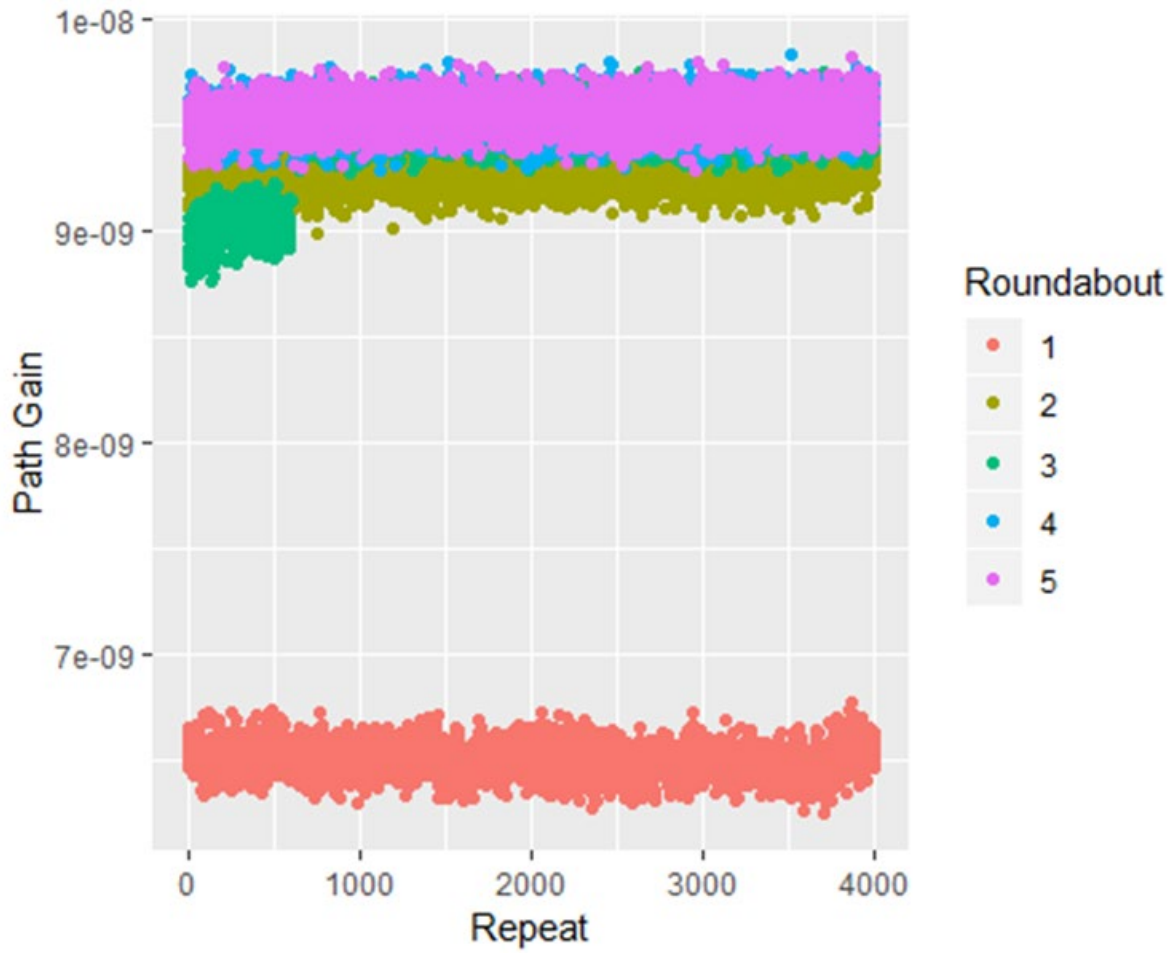

Fig. E-3: Time series of repeat measurements of path gain taken with the Correlation-Based channel sounder during five roundabouts on one day. Measurements from the first roundabout appear to be very different than repeat measurements from the other four roundabouts on this day.

E.1.2 Autocorrelation Function Plots

Next, we look at autocorrelation function (ACF) plots to check for evidence that our data are not independent. For a series of observations x_t for $t = 1,2,\ldots,T$, the autocorrelation function is the collection of autocorrelation coefficients, ρ_h, at lag h (h= 0,1,2, ...), where

$$\rho_h = \frac{\mathrm{Cov}(x_t, x_{t+h})}{\mathrm{Var}(x_t)}. \tag{E.2}$$

This is estimated from the data as

$$\hat{\rho}_h = \frac{\sum_{t=1}^{T-h}(x_t-\overline{x})(x_{t+h}-\overline{x})}{\sum_{t=1}^{T}(x_t-\overline{x})^2}, \quad \text{(E.3)}$$

for $h = 0,1,\ldots,H$. In practice, T should be greater than 50 and $H \leq T/4$ [38]. We plot one autocorrelation function in Fig. E-4, for $T = 8192$ and $H = 400$.

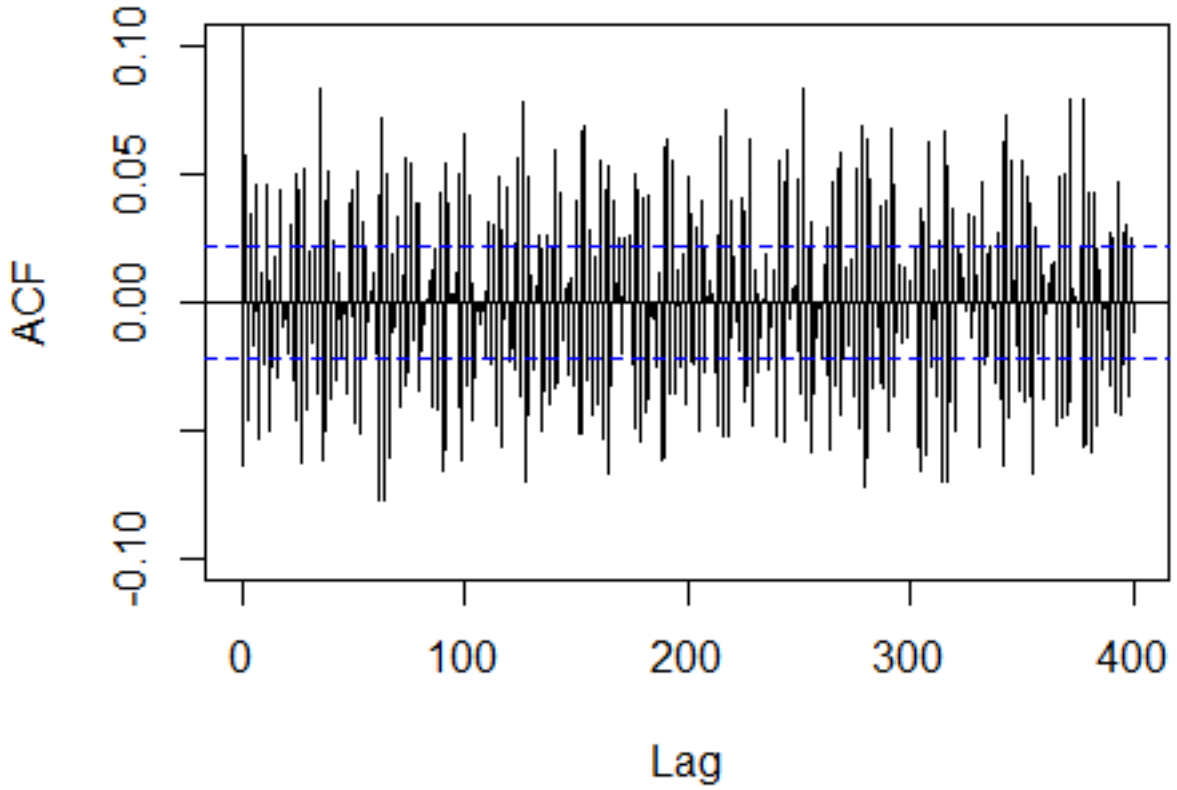

Fig. E-4: ACF plot for 8192 repeat measurements of path gain measured by the Direct-Pulse channel sounder on day 1, roundabout 2, attenuation of 18 dB, and under the direct channel configuration. The dashed blue lines are 95% confidence bands.

Under the assumption that the autocorrelation coefficient at lag h, ρ_h, is 0, the standard error of ρ_h, $se(\rho_h) \approx 1/\sqrt{T}$. Therefore, 95% confidence bands for the ACF plot are calculated as $\pm {}^{1.96}/_{\sqrt{T}}$ [39]. These bounds are plotted in Fig. E-4 as dashed blue lines. Autocorrelation coefficients outside of these bounds are evidence against the hypothesis that these coefficients are zero.

The ACF plot in Fig. E-4 and others indicate that the repeat measurements are not time independent, since many of the autocorrelation coefficients are significantly non-zero. One way to deal with this is to thin the data until we have independent repeats. We do this for the Direct-Pulse channel sounder data, thinning the repeat measurements by keeping only every 100th observation (leaving 82 repeat measurements). The ACF plot for this thinned data is shown in Fig. E-5. However, for some of the sets of measurements from other channel sounders no amount of thinning eliminated the significantly non-zero autocorrelation coefficients.

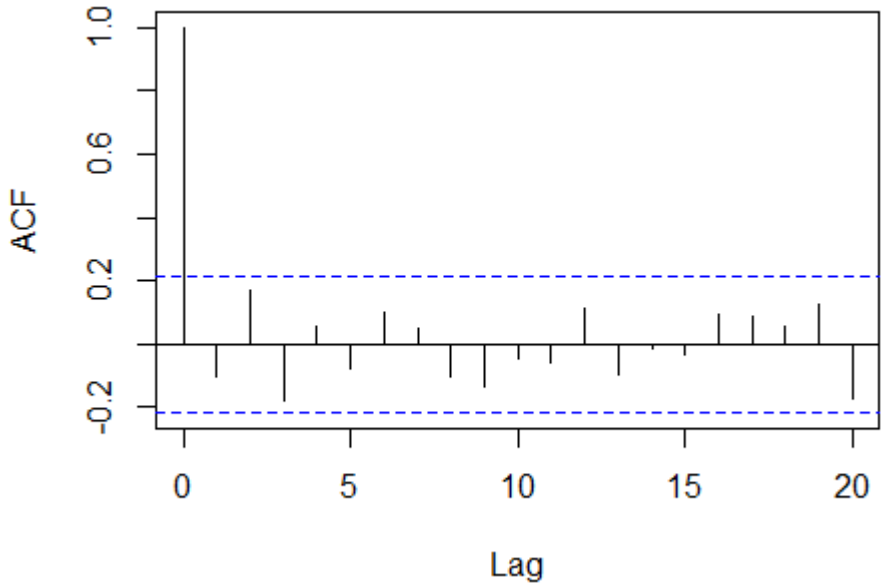

Fig. E-5: ACF plot for 82 thinned repeat measurements of path gain measured by the Direct-Pulse channel sounder on day 1, roundabout 2, attenuation of 18 dB, and under the direct channel configuration. The dashed blue lines are 95% confidence bands.

E.2 Alternative Model, ANOVA Method, and Model Diagnostics

Since exploratory data analysis revealed violations of the Model 1 assumptions, we must assume a different model for our data. We decided to reduce our repeat measurements within each roundabout to one value (the mean over the repeats, $\overline{X}_{ij\cdot} = \frac{1}{n}\sum_{k=1}^{n} X_{ijk}$ for $i = 1, \ldots, I$ and $j = 1, \ldots, J$) and use Model 2

$$Y_{ij} = G + D_i + \epsilon_{ij}, \tag{E.4}$$

where $Y_{ij} = \overline{X}_{ij\cdot}$, $D_i \sim N(0, \sigma_D^2)$ is an effect due to day, and $\epsilon_{ij} \sim N(0, \sigma^2)$. Now we have variability within each day and between the days. The variability within each day now includes variation due to both roundabout and measurement error. We use an Analysis of Variance (ANOVA) method to estimate the parameters in this random effects model. We repeated the above analysis on the aggregated data and found that the correlation between the different days was not significant. This criteria was met for all the channel sounders' data.

E.2.1 Detailed Two-Tiered Analysis of Random Component of Uncertainty

A description of the ANOVA results for Model 2 starts with the path gain measurements Y_{ij} in terms of a linear scale calculated individually for each channel sounder.

1. Calculate

$$\overline{Y}_{i\cdot} = \frac{1}{J}\sum_{j=1}^{J} Y_{ij}\,, \qquad i = 1,2, \ldots, I \tag{E.5}$$

and

$$\overline{Y}_{..} = \frac{1}{I}\sum_{i=1}^{I}\overline{Y}_{i\cdot}. \tag{E.6}$$

2. Calculate the Sums of Squares due to error within a day (SSE).

$$SSE = \sum_{i=1}^{I}\sum_{j=1}^{J}\left(Y_{ij} - \overline{Y}_{i\cdot}\right)^2 \tag{E.7}$$

The associated Mean-Squared error (MS_e) is:

$$MS_e = \frac{SSE}{I(J-1)} \tag{E.8}$$

3. Calculate the Sums of Squares between days (SSD).

$$SSD = J\sum_{i=1}^{I}\left(\overline{Y}_{i\cdot} - \overline{Y}_{..}\right)^2 \tag{E.8}$$

The associated Mean-Squared error (MS_D) is:

$$MS_D = \frac{SSD}{I-1} \tag{E.9}$$

It is a well-known result from ANOVA [31] that the expected values of the mean squares given by Eqs. E.10 and E.11 are

$$E(MS_D) = \sigma^2 + J\sigma_D^2 \tag{E.10}$$

and

$$E(MS_e) = \sigma^2 \tag{E.11}$$

where σ^2 represents the variability due to different roundabouts and σ_D^2 the variability due to different days. Note that the expected mean-square term for Day includes variation within a day (σ^2) and variation between days (σ_D^2).

The variables σ^2 and σ_D^2 are called variance components and can be estimated from the mean-squared errors above. Specifically, $\hat{\sigma}^2 = MS_e$ and $\hat{\sigma}_D^2 = \frac{MS_D - MS_e}{J}$. This allows us to estimate the impact of day on the overall uncertainty. In theory, the variance components are non-negative and $E(MS_D) \geq E(MS_e)$. Note that if there is no variability due to day, $E(MS_D) = \sigma^2$. Since $E(MS_D)$ and $E(MS_e)$ are estimated from data, it is possible that the inequality does not hold for the estimated quantities when there is no variability due to day. If the estimate of a variance component is negative, it should be set equal to zero [33].

4. The variance associated with the jth measurement from day i is

$$\hat{Var}\left(Y_{ij}\right) = \hat{\sigma}^2 + \hat{\sigma}_D^2 \tag{E.12}$$

and the covariance between two measurements is

$$Cov(Y_{ij}, Y_{i'j'}) = \begin{cases} \sigma_D^2 & i = i', j \neq j' \\ 0 & i \neq i' \end{cases} \tag{E.13}$$

Thus,

$$\begin{aligned} Var\left(\sum_{i=1}^{I}\sum_{j=1}^{J} Y_{ij}\right) &= \sum_{i=1}^{I}\sum_{j=1}^{J} Var(Y_{ij}) + \sum_{i\neq i' \cup j\neq j'} Cov(Y_{ij}, Y_{i'j'}) \\ &= IJ(\sigma^2 + \sigma_D^2) + IJ(J-1)\sigma_D^2 \\ &= IJ\sigma^2 + (IJ + IJ(J-1))\sigma_D^2 \\ &= IJ(\sigma^2 + J\sigma_D^2) \end{aligned} \tag{E.14}$$

From which it follows that

$$Var(\overline{Y}_{..}) = \frac{1}{(IJ)^2} Var\left(\sum_{i=1}^{I}\sum_{j=1}^{J} Y_{ij}\right) = \frac{\sigma^2 + J\sigma_D^2}{IJ} \tag{E.15}$$

so that

$$\hat{Var}(\overline{Y}_{..}) = \frac{\hat{\sigma}^2 + J\hat{\sigma}_D^2}{IJ} = \frac{MS_D}{IJ}. \tag{E.16}$$

To present our results on a dB scale, the transformation

$$\overline{Y}_{..,dB} = 10\log_{10}\overline{Y}_{..} \tag{E.17}$$

is made. The variance of $\overline{Y}_{..,dB}$ can then be approximated as

$$\hat{Var}(\overline{Y}_{..,dB}) = \frac{\hat{\sigma}_{dB}^2 + J\hat{\sigma}_{D,dB}^2}{IJ} \tag{E.18}$$

where the variance components on a dB scale are estimated using propagation of errors for the functional relationship given in Eqn. E.17 as follows:

$$\begin{aligned} \hat{\sigma}_{dB}^2 &= \left(\frac{10}{\ln(10)\cdot\overline{Y}_{..}}\right)^2 \hat{\sigma}^2 \\ \hat{\sigma}_{D,dB}^2 &= \left(\frac{10}{\ln(10)\cdot\overline{Y}_{..}}\right)^2 \hat{\sigma}_D^2 . \end{aligned} \tag{E.19}$$

E.2.2 Model Diagnostics

Before reporting the variance components, it is important to check the remaining model assumptions. Specifically, we want to check for nonlinearities, outliers, and that the within-day variability is the same across the five days. We do this with residual analysis. For this model, the residuals are

$$e_{ij} = Y_{ij} - \hat{Y}_{ij}, \tag{E.20}$$

where $\hat{Y}_{ij}$ is the predicted value of Y_{ij}. For this random effects model, the predicted value $\hat{Y}_{ij} = \hat{G} + \hat{D}_i$ with $\hat{G} = \overline{Y}_{..}$ and $\hat{D}_i = \overline{Y}_{i.} - \overline{Y}_{..}$, so the predicted value is the mean for each day, $\overline{Y}_{i.}$, and the residuals reduce to $e_{ij} = Y_{ij} - \overline{Y}_{i.}$.

To check the assumption that the within-day variability is the same across the five days, we plot the residuals by day. The range and distribution of points within day looks reasonably similar between the days, based on statistical expectations, so this assumption does not appear to be violated for this system configuration. As an example, Fig. E-6 shows the residuals in measurements of the direct-path-only channel performed with the Correlation-Based channel sounder.

Next, we look at plots of the residuals (e_{ij}) vs. the predicted values ($\overline{Y}_{i.}$), looking for patterns that suggest non-linearity or outliers. In these plots you want to see a random cloud of points with no apparent structure, such as larger variance in the residuals for larger predicted values. The residuals vs. predicted values plot in Fig. E-7 reveals no structure.

We repeated these model diagnostics for all channel sounders and channel configurations and found no serious violations of the model assumptions, so we report the variance components estimated using the ANOVA method in Section 5.

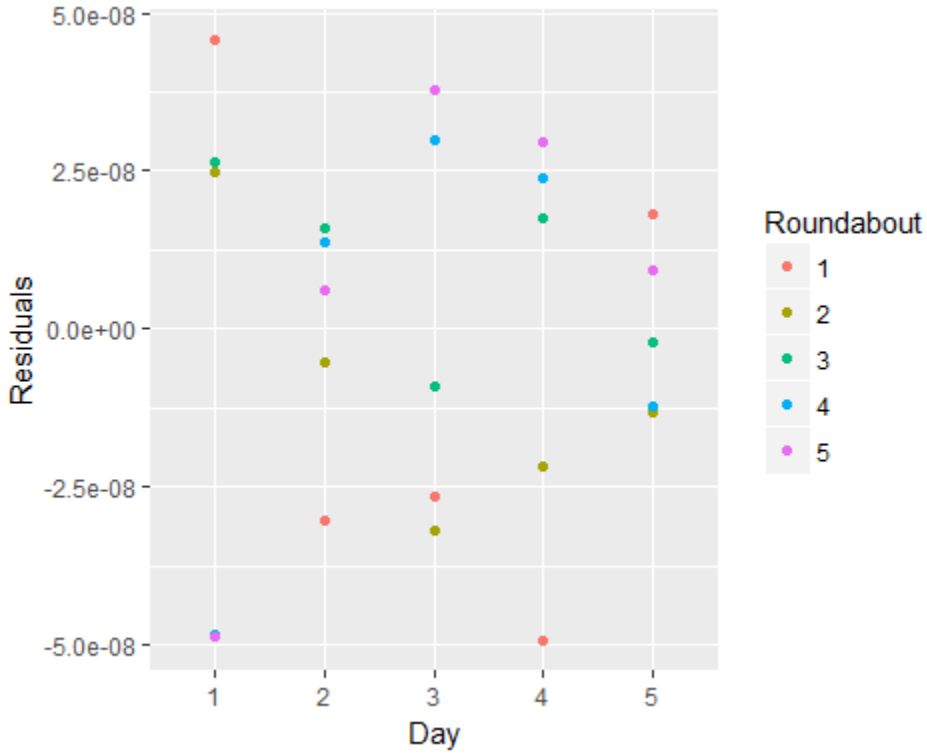

Fig. E-6: Residuals plotted by day for path gain (average over the repeat measurements) measured by the Correlation-Based channel sounder under the direct-path-only channel configuration with 18 dB attenuation.

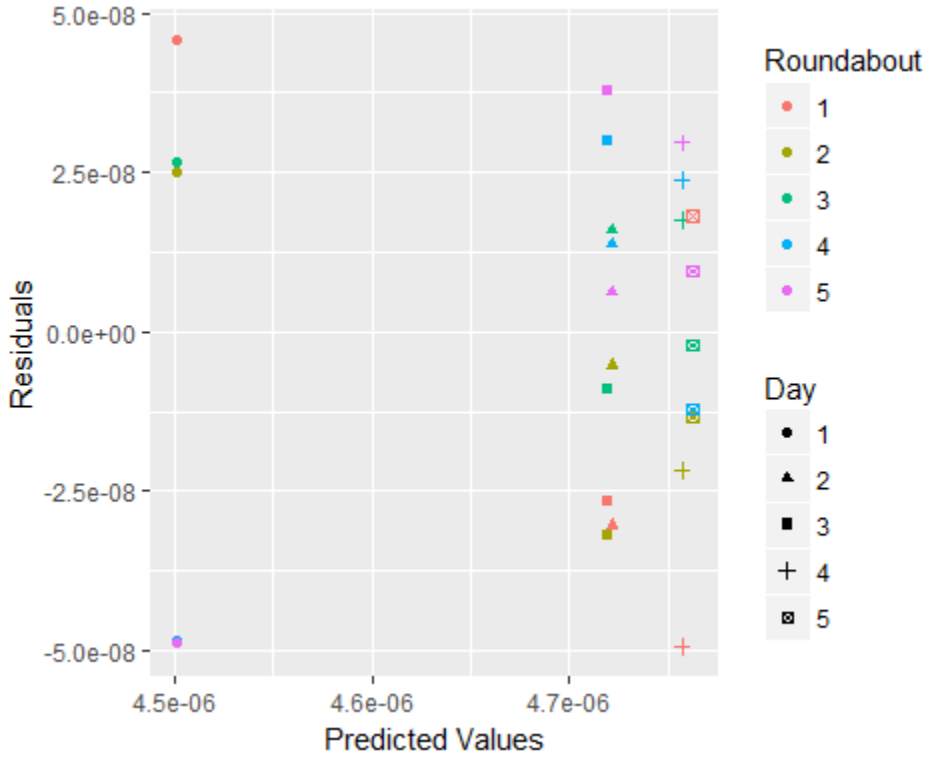

Fig. E-7 Residuals vs. predicted values for path gain (average over the repeat measurements) measured by the correlation-based channel sounder under the direct-path-only channel configuration with 18 dB attenuation. This plot reveals no apparent outliers or patterns that would suggest non-linearity.

Appendix F — Software Script for Two-Tiered ANOVA

For user convenience, we provide the software code for two-tiered ANOVA approached used in this report.

```
%-------------------------------------------------------------------------
%-------------------------------------------------------------------------
%This function computes the uncertainty using the recipe.
t.
% Function: Function_uncert_multitiered
% Author: Jeanne Quimby and Amanda Koepke - 12/12/2016
%-------------------------------------------------------------------------
%Inputs and Outputs for Function_uncert
%Inputs:
%   str_title:
%       string, title for plots
%   Axis_limit:
%       4 numerical value, puts limits on the plots
%   CS_data:
%       Structural Array
%       CSdata.PathType_char -> PathType_str = 'D' or 'DB'
%       CSdata.Xtype_char -> string of xaxis label
%       CSdata.Xtype_num -> single numerical array for plotting CS_data PDP or CS_data Path Gain
%       CSdata.Day#.roundabout## -> structural array containing the
%           channel sounder (CS) data.  Day# -> Day1, Day2, Day3, ...,
%          roundabout## -> roundabout1, roundabout2, roundabout3, ...,
%           This array contains all the power (PDP or Path Gain) values
%           computed for the number of roundabouts and number of days.
%Outputs
%   uncertfig
%       Matlab figure handle, figure handle to save uncertainty plot
%   Ypp
%       numerical array [1 number of records]
%       This numerical array returns the mean over the number of
%       roundabouts and number of days.  It is assumed that the number of records will
%       equal the number of records for power delay profile or 1 for path gain.
%   Var_method1 -> from formula 5.a. In reporting use maximum of
%   Var_method1 or Var_method2
%       numerical array [1 number of records]
%       This numerical array returns the Variance which is the diagonal entries from
%       the covariance matrix using formula 5.a.  The results shown in the
%       graphs may be computed using 10.*log10((sqrt(Var_method1) + Ypp)./Ypp);
%   Var_method2 -> from formula 5.b
%       numerical array [1 number of records]
%       This numerical array returns the Variance which is the diagonal entries from
%       the covariance matrix using formula 5.b.  The results shown in the
%       graphs may be computed using 10.*log10((sqrt(Var_method2) + Ypp)./Ypp);
%   sigma
%       numerical array [1 number of records]
%       This numerical array return the expected mean square term for error
%       only included within a roundabout
%   sigma_r
%       numerical array [1 number of records]
%       This numerical array return the expected mean square term for error
%       only included within a roundabout and variation between roundabouts.
%        It is the expect mean square term for roundabouts
%   sigma_d
```

```
%       numerical array [1 number of records]
%       This numerical array return the expected mean square term for error
%       only included within a roundabout, variation between roundabouts,
%       and variation between days.  It is the expected mean square term
%       for day.
%-------------------------------------------------------------------------
%Function calls
%    none
%-------------------------------------------------------------------------
%-------------------------------------------------------------------------
function [uncertfig,Ypp,Var_method1,sigma_e,sigma_d] = Function_uncert_twotiered(str_title,axis_limit,CSdata)
set(groot,'defaultAxesColorOrder',[0 255 255; 0 0 255; 0 0 255; 0 255 0; 0 255 0; 255 0 0;  255 0 0; 0 0 0; 0 0 0; 255
255 0; 255 255 0]/255,'defaultAxesLineStyleOrder','-|--|:|-.|-')

%1. Quality Check
CS_fieldnames_cll = fieldnames(CSdata);
J = size(fieldnames(CSdata.(CS_fieldnames_cll{4})),1); %Number of Roundabouts, The cell location is 4 due to the
below previous structure format
I = size(CS_fieldnames_cll,1) - 3;  %The number of Days, The 3 is due to structure files: PathType_char,
XType_char, and XType_num
N = size((CSdata.(CS_fieldnames_cll{4}).roundabout1),2);  %The number of records in a single roundabout
M = size((CSdata.(CS_fieldnames_cll{4}).roundabout1),1);  %The of PDP or Path Gains in a single roundabout
r = CSdata.Xtype_num;
if (M > 1); str_y = 'PDP'; else str_y = 'Path Gain'; end;
ndx_i = 1;
for i = 4:I+3
   CS_roundabout_fieldnames = fieldnames(CSdata.(CS_fieldnames_cll{i}));
   for j = 1:size(CS_roundabout_fieldnames,1)
       Yij_tmp = CSdata.(CS_fieldnames_cll{i}).(CS_roundabout_fieldnames{j});
       Yij(:,ndx_i) = sum(Yij_tmp,2)./N;
      ndx_i = ndx_i + 1;
   end
end

%2. Compute Yip over a roundabout for the number of days
%This assumes the roundabouts are sequential in the ttl_mnPDP, meaning the
%day 1 has all roundabouts 1-5, day 2 has 5 - 10.
for i = 1:I  %Compute mean over a roundabout
   Yip_tmp = Yij(:,J.*(i-1) + 1:J.*(i-1) + J);
   Yip(:,i) = sum(Yip_tmp,2)./J;
end

%2. Compute Y.. (Ypp) over days
Ypp = sum(Yip,2)./I; Ypp_dB = 10.*log10(Ypp);

%3.1 Compute MSR - Due to Roundabouts
Yip_tmp1 = 0; Yip_tmp2 = 0;
for i = 4:I+3
   for j = 1:J
      Yip_tmp1 = sum(Yij(:,J.*(i-4)+j).*Yij(:,J.*(i-4)+j),2) + Yip_tmp1;
   end
   Yip_tmp2 = sum(Yip(:,(i-3)).*Yip(:,(i-3)),2) + Yip_tmp2;
end
SSe = Yip_tmp1 - J.*Yip_tmp2;
MSe = SSe./(I.*(J - 1));
```

```
%3.2 Computes SSD for the day
Ypp_tmp1 = 0;
for i = 4:I+3
   Ypp_tmp1 = sum(Yip(:,(i-3)).*Yip(:,(i-3)),2) + Ypp_tmp1;
end
SSd = J.*Ypp_tmp1 - I.*J.*Ypp.*Ypp;
MSd = SSd./(I-1);

%3.3 Compute the Covariance for the overall mean two ways
Var_method1 = MSd./(I.*J);
std_method1_dB = 10.*log10((sqrt(Var_method1) + Ypp)./Ypp)

%3.3 Compute Variance Components
if (MSd < MSe)
   sigma_d = 0;
   sigma_e = ((I-1).*MSd + I.*(J-1).*MSe)./((I-1) + I.*(J-1));
else
   sigma_d = (MSd - MSe)./(J);  %Variance between days
   sigma_e = MSe;
end

sigmae_dB = sqrt(sigma_e).*(10./(log(10).*Ypp));
sigmad_dB = sqrt(sigma_d).*(10./(log(10).*Ypp));

std_method2_dB = sqrt((sigmae_dB.^2 + J.*sigmad_dB.^2)./(I.*J))

%4 Plot
uncertfig = figure;
if (M > 1)
   plot(r.*1e9,Ypp_dB, ...
       r.*1e9,Ypp_dB+std_method1_dB,r.*1e9,Ypp_dB-std_method1_dB, ...
       r.*1e9, Ypp_dB+std_method2_dB, r.*1e9, Ypp_dB-std_method2_dB, ...
       r.*1e9, Ypp_dB+sigmae_dB, r.*1e9, Ypp_dB-sigmae_dB, ...
       r.*1e9, Ypp_dB+sigmad_dB, r.*1e9, Ypp_dB-sigmad_dB, ...
   'linewidth', 2);
   ylabel('PDP (dB)'); xlabel(CSdata.Xtype_char); axis(axis_limit);

else
   plot(1:length(Ypp),Ypp_dB,'*', ...
      1:length(Ypp),Ypp_dB+std_method1_dB,'o',1:length(Ypp),Ypp_dB-std_method1_dB,'o', ...
      1:length(Ypp), Ypp_dB+sigmae_dB,'o', 1:length(Ypp), Ypp_dB-sigmae_dB, 'o', ...
      1:length(Ypp), Ypp_dB+sigmad_dB,'o', 1:length(Ypp), Ypp_dB-sigmad_dB, 'o', ...
   'linewidth', 2);
   ylabel('Path Gain (dB)');    xlabel(CSdata.Xtype_char); title(strrep(str_title,'_',' '));
   axis([0 2 axis_limit(3) axis_limit(4)]);
end
grid on; set(gca,'FontSize',20); set(gca,'FontName','arial') ;
legend('Nominal', 'Nominal + overall Uncert.','Nominal - Overall Uncert',...
   'Nominal + SigmaE', 'Nominal - SigmaE', ...
   'Nominal + SigmaD', 'Nominal - SigmaD');
return
%--------------------------------------------------------------------------
%--------------------------------------------------------------------------
```

Appendix G — Test Schedule for Roundabouts

Table G-1 provides the specific test schedule used during the measurements.

Table G-1: Test Schedule.

Measurement Steps	
1	Variable Attenuator set to 18 dB (repeat 5x)
1a	Correlation-based CS reference measurement (their system is unhooked from switch matrices)
1b	VNA measurement: 1 sweep from 3300 MHz to 3700 MHz
1c	Scanning Probe CS measurement
1d	Correlation-based CS measurement: 40 records/sweep, 100 sweeps, 8188 waveforms
1e	Direct Pulse CS measurement: 8192 waveforms
2	Variable Attenuator set to 28 dB (repeat 5x)
2a	Correlation-based CS reference measurement (their system is unhooked from switch matrices)
2b	VNA measurement: 1 sweep from 3300 MHz to 3700 MHz
2c	Scanning Probe CS measurement
2d	Correlation-based CS measurement: 40 records/sweep, 100 sweeps, 8188 waveforms
2e	Direct Pulse CS measurement: 8192 waveforms
3	Variable Attenuator set to 38 dB (repeat 5x)
3a	Correlation-based CS reference measurement (their system is unhooked from switch matrices)
3b	VNA measurement: 1 sweep from 3300 MHz to 3700 MHz
3c	Scanning Probe CS measurement
3d	Correlation-based CS measurement: 40 records/sweep, 100 sweeps, 8188 waveforms
3e	Direct Pulse CS measurement: 8192 waveforms
3f	Correlation-based CS reference measurement (their system is unhooked from switch matrices)

References

[1] P. Hale, J. Jargon, P. Jeavons, M. Lofquist, M. Souryal, and A. Wunderlich, "3.5 GHz radar waveform capture at Fort Story: Final test report," NIST Technical Note 1967 (2017).

[2] P. Hale, J. Jargon, P. Jeavons, M. Lofquist, M. Souryal, and A. Wunderlich, "3.5 GHz radar waveform capture at Point Loma: Final test report," NIST Technical Note 1954 (2017).

[3] "Amendment of the commission's rules with regard to commercial operations in the 3550–3650 MHz band," FCC Report and Order and Second Further Notice of Proposed Rulemaking, GN Docket No. 12-354, April 2015. [Online]. Available: https://apps.fcc.gov/edocs_public/attachmatch/FCC-15-47A1_Rcd.pdf

[4] "Citizens broadband radio service," Code of Federal Regulations. Title 47, Part 96, June 2015.

[5] A. Molisch, *Wireless Communications*, J. Wiley & Sons Ltd., 2011.

[6] S. Sun, T. Rappaport, T. Thomas, A. Ghosh, H. Nguyen, I. Kovac, I. Rodriguez, O. Koymen, and A. i, "Investigation of Prediction Accuracy, Sensitivity, and Parameter Stability of Large-Scale Propagation Path Loss Models for 5G Wireless Communications," *IEEE Trans. Antennas and Prop*., vol. 65, no. 5, May 2016

[7] S. Salous, *Radio Propagation Measurement and Channel Modeling*, Chichester, U. K., 2013

[8] ITU-R Recommendation P. 1407-5: Multipath propagation and parameterization of its characteristics, Geneva, Switzerland, 2013.

[9] D. F. Williams, J. C-. M. Wang, and U. Arz, "An Optimal Vector-Network-Analyzer Calibration Algorithm," *IEEE Trans. MTT*, vol. 51, no. 12, pp. 2391–2401, Dec. 2003.

[10] J. A. Jargon, D. F. Williams, and P. D. Hale, "Developing Models for Type-N Coaxial VNA Calibration Kits within the NIST Microwave Uncertainty Framework," *87th ARFTG Microwave Measurement Conference*, San Francisco, CA, May 2016.

[11] IEEE 287:2007 Precision Coaxial Connectors (dc to 110 GHz), Institute of Electrical and Electronics Engineers, 2007.

[12] D. Frickey, "Conversions Between S, Z, Y, *h*, T, *ABCD*, and Parameters which are Valid for Complex Source and Load Impedances," *IEEE Trans. Microw. Theory and Tech*, vol. 42, no. 2, pp. 205 – 211, February 1993

[13] J. T. Quimby, R. Candell, K. A. Remley, D. R. Novotny, J. Diener, P. B. Papazian, A. E. Curtin, and G. H. Koepke, "NIST Channel Sounder Overview and Channel Measurements in Manufacturing Facilities " Technical Note (NIST TN) 1979 (2017).

[14] R. Candell, K.A. Remley, J. T. Quimby, D. R. Novotny, A. E. Curtin, P. B. Papazian, G. H. Koepke, J. E. Diener, M. T. Hany, "Industrial Wireless Systems: Radio Propagation Measurements" Technical Note (NIST TN) 1951 (2017).

[15] D. Novotny, A. Curtin, J. Quimby, K. Remley, P. Papazian, and R. Candell, “A Tetherless, Absolute-Time Channel Sounder; Processing Results for a Complex Environment,” *AMTA*, 2016, pg. 1-6.

[16] C. A. Hammerschmidt and R. T. Johnk, “Understanding the Impact of Terrain Databases on the Irregular Terrain Model,” *Proceedings of the 2017 IEEE International Symposium on Electromagnetic Compatibility & Signal/Power Integrity (EMCSI)*, Washington DC, 7-11 Aug. 2017.

[17] E. F. Drocella Jr., J. C. Richards, R. L. Sole, F. Najmy, A. Lundy, and P. M. McKenna, “3.5 GHz Exclusion Zone Analyses and Methodology,” NTIA Technical Report TR-15-517, June 2015.

[18] R. Johnk, C. Hammerschmidt, M. McFarland, and J. Lemmon, “A fast-fading measurement system,” *IEEE Int. Symp. EMC*, August 6-10, 2012 pp. 584-589.

[19] C. Hammerschmidt and R. Johnk, “Extracting clutter metrics in the 1755-1780 MHz band, *Proc. of the IEEE Military Communications Conf.*, Baltimore, MD, Nov. 1-3, 2016.

[20] R. T. Johnk, C. A. Hammerschmidt, and I. Stange, “A High-Performance CW Mobile Channel Sounder," *Proceedings of the 2017 IEEE International Symposium on Electromagnetic Compatibility & Signal/Power Integrity (EMCSI)*, Washington DC, 7-11 Aug. 2017.

[21] N. P. Yoza, Narrowband 5 GHz Mobile Channel Characterization, M.S. Thesis, Interdisciplinary Telecommunications Program, University of Colorado at Boulder, 2015.

[22] J. D. Parsons, *The Mobile Radio Propagation Channel*, John Wiley & Sons, New York, New York, 2000.

[23] F. P. Fontan and P. M. Espineira, *Modelling the Wireless Propagation Channel: A Simulation Approach with MATLAB*, John Wiley & Sons, New York, New York, 2008.

[24] S. Saunders and A. Aragon-Zavala, *Antennas and Propagation for Wireless Communication Systems*, John Wiley & Sons, New York, New York, 2007.

[25] G. Matz, A. F. Molisch, M. Steinbauer, F. Hlawatsch, I. Gaspard and H. Artes, "Bounds on the systematic measurement errors of channel sounders for time-varying mobile radio channels," *Gateway to 21st Century Communications Village. VTC 1999-Fall. IEEE VTS 50th Vehicular Technology Conference (Cat. No.99CH36324)*, Amsterdam, The Netherlands, 1999, pp. 1465-1470 vol.3.

[26] G. Matz, A. F. Molisch, F. Hlawatsch, M. Steinbauer and I. Gaspard, "On the systematic measurement errors of correlative mobile radio channel sounders," in *IEEE Transactions on Communications*, vol. 50, no. 5, pp. 808-821, May 2002.

[27] P. Almers, S. Wyne, F. Tufvesson and A. F. Molisch, "Effect of random walk phase noise on MIMO measurements," *2005 IEEE 61st Vehicular Technology Conference*, Stockholm, 2005, pp. 141-145 Vol. 1.

[28] D.F Williams, W. Zhao, R. A. Chamberlin, J. Cheron, and M. Urteaga, “Verification of a foundry-developed transistor model including measurement uncertainty,” *87th ARFTG Microw. Meas. Conf. Dig.*, San Francisco, CA, USA, May 2016, pp. 1-4.

[29] J. Quimby, D. G. Michelson, M. Bennai, K. A. Remley, J. Kast and A. Weiss, "Interlaboratory Millimeter-Wave Channel Sounder Verification," *2019 13th European Conference on Antennas and Propagation (EuCAP)*, Krakow, Poland, 2019, pp. 1-5.

[30] Joint Committee for Guides in Metrology 2012. International Vocabulary of Metrology—Basic and General Concepts and Associated Terms (VIM). 3rd edn (Sèvres: BIPM) (JCGM 200:2012 (2008 version with minor corrections) www.bipm.org/en/publications/guides/vim.html.

[31] F. A. Graybill, *Theory and Application of the Linear Model*. North Scituate, MA: Duxbury Press, 1976.

[32] D. C. Montgomery, *Design and Analysis of Experiments*, 8th ed. New York: Wiley, 2013.

[33] S. R. Searle, *Linear Models*. New York: Wiley, 1971.

[34] A. Koepke and J. A. Jargon, "Quantifying Variance Components for Repeated Scattering-Parameter Measurements," *90th ARFTG Microwave Measurement Conference*, Boulder, CO, Nov. 2017.

[35] Joint Committee for Guides in Metrology. Evaluation of measurement data — Guide to the expression of uncertainty in measurement. International Bureau of Weights and Measures (BIPM), Sèvres, France, 2008a. URL www.bipm.org/en/publications/guides/gum.html. BIPM, IEC, IFCC, ILAC, ISO, IUPAC, IUPAP and OIML, JCGM 100:2008, GUM 1995 with minor corrections.

[36] Micro-Coax, Inc., "Source Control Drawing Cable Assemblies, UFB293C Ultra Los Loss, 18.0 GHz," page 10 and page 15.

[37] NIST/SEMATECH e-Handbook of Statistical Methods, https://www.itl.nist.gov/div898/handbook/eda/section3/eda35h.htm, May 23, 2018.

[38] D. C. Montgomery, C. L. Jennings, and M. Kulahci. *Introduction to Time Series Analysis and Forecasting*. John Wiley & Sons, 2015.

[39] NIST/SEMATECH e-Handbook of Statistical Methods, https://www.itl.nist.gov/div898/handbook/eda/section3/autocopl.htm, May 23, 2018.

[40] A. Goodman, A. Pepe, A.W. Blocker, C.L. Borgman, K. Cranmer K, et al, Ten Simple Rules for the Care and Feeding of Scientific Data. PLOS Computational Biology 10(4), 2014, https://doi.org/10.1371/journal.pcbi.1003542

REPORT DOCUMENTATION PAGE

Form Approved
OMB No. 0704-0188

1. REPORT DATE *(DD-MM-YYYY)*	**2. REPORT TYPE**	**3. DATES COVERED** *(From - To)*
April 2020	Technical Report	N/A

4. TITLE AND SUBTITLE
Channel Sounder Measurement Verification: Conducted Tests

5a. CONTRACT NUMBER

5b. GRANT NUMBER

5c. PROGRAM ELEMENT NUMBER

6. AUTHOR(S)
Jeanne Quimby, Jeffrey A. Jargon, Rod Leonhardt, Paul D. Hale, Kate A. Remley, Amanda Koepke, Sarah Streett, Robert T. Johnk, Chriss Hammerschmidt, Paul McKenna, Irena Stange, Mike Chang, Nicholas DeMinco, Joseph E. Diener, Jacob D. Rezac, Richard Chad Smith, Christopher Hoyt, Sofia Springer

5d. PROJECT NUMBER
3111012-300

5e. TASK NUMBER

5f. WORK UNIT NUMBER

7. PERFORMING ORGANIZATION NAME(S) AND ADDRESS(ES)
National Telecommunications and Information Administration, Institute for Telecommunication Sciences
325 Broadway, MS NTIA/ITS.D
Boulder, CO 80305
National Institute for Standards and Technology, Communications Technology Laboratory
325 Broadway
Boulder, CO 80305

8. PERFORMING ORGANIZATION REPORT NUMBER
NIST Technical Note 2076
NTIA Joint Report JR-20-549
DOI: https://doi.org/10.6028/NIST.TN.2076

9. SPONSORING/MONITORING AGENCY NAME(S) AND ADDRESS(ES)
National Telecommunications and Information Administration, Institute for Telecommunication Sciences
325 Broadway, MS NTIA/ITS.D
Boulder, CO 80305
National Institute for Standards and Technology, Communications Technology Laboratory
325 Broadway
Boulder, CO 80305

10. SPONSOR/MONITOR'S ACRONYM(S)

11. SPONSOR/MONITOR'S REPORT NUMBER(S)

12. DISTRIBUTION/AVAILABILITY STATEMENT
Approved for Public Release. Distribution Unlimited.

13. SUPPLEMENTARY NOTES

14. ABSTRACT
Channel modeling often provides a basis for the design and deployment of wireless technology. Engineers design systems to operate under certain expected channel conditions. Channel models are typically based on the statistics of a collection of many measurements performed by channel sounders in nominally similar radio-propagation environments. In 2016, researchers at the US Department of Commerce National Institute of Standards and Technology (NIST) and the National Telecommunications and Information Administration Institute for Telecommunication Sciences (ITS) began a collaboration to conduct a series of channel sounder verifications to identify sources of uncertainty due to systematic and random effects in a channel sounder hardware. This report describes conducted-channel measurements designed to focus on errors within the channel sounding hardware as a base-line test of the channel sounder's performance. Repeat measurements and an analysis of the random components of uncertainty were performed. Sample results are reported and analyzed. The work concludes with guidance and best-practice procedures with the intent of allowing users to perform similar verifications of their channel sounders.

15. SUBJECT TERMS
channel modeling, channel sounder, propagation measurement, metrology, path gain measurements, conducted channel measurements, measurement uncertainty analysis, propagation measurement best practices

16. SECURITY CLASSIFICATION OF:			**17. LIMITATION OF ABSTRACT**	**18. NUMBER OF PAGES**	**19a. NAME OF RESPONSIBLE PERSON**
a. REPORT	**b. ABSTRACT**	**c. THIS PAGE**			Jeanne Quimby
Unclassified	Unclassified	Unclassified	Same as Report	84	**19b. TELEPHONE NUMBER** *(Include area code)* 303-497-4217